SYSTEM BIOLOGY ANALYSIS OF THE ROLE OF DNA REPAIR IN CANCER TREATMENT OUTCOME

by

MENGDI QIAN

Submitted in partial fulfillment of the requirements

for the degree of Doctor of Philosophy

Department of Electrical Engineering and Computer Science

CASE WESTERN RESERVE UNIVERSITY

August 2019

CASE WESTERN RESERVE UNIVERSITY

SCHOOL OF GRADUATE STUDIES

We hereby approve the dissertation of

Mengdi Qian

candidate for the degree of **Doctor of Philosophy***.

Committee Chair

Dr. Evren Gurkan-Cavusoglu

Committee Member

Dr. Alexandru Almasan

Committee Member

Dr. Vira Chankong

Committee Member

Dr. Christian A. Zorman

Committee Member

Dr. M. Cenk Cavusoglu

Date of Defense

April 24, 2019

*We also certify that written approval has been obtained

for any proprietary material contained therein.

Contents

List of Tables **iv**

List of Figures **vi**

Acknowledgments **ix**

Nomenclature **xi**

Abstract **xiii**

1 Introduction **1**

1.1 Role of Damage Response in Cancer Treatment 1

1.2 Problem Formation and Objectives 4

1.3 Dissertation Contributions and Organization 8

2 Modeling and Quantitative Analysis of Major DNA Double Strand Break Repair Pathways **10**

2.1 Introduction 10

2.2 *In Silico* NHEJ Models of Radiotherapy for Prostate Cancer 15

2.2.1 NHEJ Pathway Mechanism 17

2.2.2 Mathematical Model of NHEJ 17

2.2.3 Sensitivity and Identifiability Test 22

2.2.4 Results for Mechanism of Radiosensitization 23

2.2.5 Quantitative Analysis of the Treatment Outcome 27
2.3 *In Silico* HR Models of Radiotherapy for Prostate Cancer 30
2.3.1 HR Pathway Mechanism 33
2.3.2 Mathematical Model of HR 36
2.3.3 Sensitivity and Identifiability Analysis 38
2.3.4 Quantitative Analysis of the Role of HR in Response to IR for Prostate Cancer 39
2.4 Detailed Identifiability Analysis 43
2.4.1 Strategy I: Data Sampling Technique 43
2.4.2 Strategy II : Model Re-structure Technique 45
2.5 Conclusion 46

3 Cell Cycle Dependent Modeling of DSB Repair 48
3.1 Cell Cycle Dependent Mathematical Modeling of DSB Repair 49
3.1.1 Cell Cycle Modeling Background Review 49
3.1.2 Modeling Cell Cycle Progression after IR Treatment 52
3.2 Detailed Study of DSB Repair by NHEJ During Cell Cycle Post IR . 58
3.2.1 Model Setup and Data Processing 59
3.2.2 NHEJ Model Parameters for Different Cell Cycle Phases . . . 61

4 Computational Modeling of Base Excision Repair 66
4.1 Introduction 67
4.2 Quantitative Base Excision Repair Model 71
4.2.1 Mathematical Model of BER 71
4.2.2 Sensitivity Analysis 74
4.2.3 Identifiability Analysis 75
4.3 Role of Base Excision Repair in Sensitization of Cancer Cells to Chemotherapy 75

4.3.1 BER Parameters in the Modeling Results 75
4.3.2 DNA Glycosylase Depletion Enhances 5-FU Effect 76
4.3.3 APC Mutation Decreases 5-FU Cytotoxicity 78
4.3.4 PARPi and Ligase Enzyme Deficiency Inhibit BER 79
4.3.5 Sensitivity Analysis Results 82
4.3.6 Identifiability Test Results 84
4.4 Conclusion on BER and 5-FU Chemotoxicity 85

5 Conclusions **87**

6 Suggested Future Work **90**

List of Tables

2.1 Experimental Measurements for NHEJ Proteins Kinetic Constants . . 21
2.2 Experimental Data on γH2AX Foci per Cell 22
2.3 NHEJ Parameter Optimization for PCa 25
2.4 Sensitivity Analysis and Identifiability Test Results for NHEJ Parameters for PCa Models 25
2.5 HR Model Parameters 41
2.6 Sensitivity Analysis and Identifiability Test Result for Parameters of HR Gene 43

3.1 C4-2 PCa Cell Doubling Time 54
3.2 Parameter Used in Cell Proliferation Models 58
3.3 γH2AX Foci With/Without HR Inhibition under 0.5/5Gy IR 60
3.4 Estimated Protein Kinetics for NHEJ When HR Inhibited 61
3.5 NHEJ Parameter Sensitivity and Identifiability Results in G1, S, G2 . 65

4.1 Number of Repaired FU:G Lesions in Percentage 74
4.2 Enzyme Concentrations Used in the Model 74
4.3 Parameters Fitted in Experimental Data: the unit of k_i is s^{-1} and the unit of K_m is nM 77
4.4 APC Mutation's Effect on Enzymes 79
4.5 Intermediates Accumulating +PARPi 81

4.6 Altered Parameters in BER with PARPi (I: identifiable SGain: Sensitivity Gain) 83
4.7 Sensitivity and Identifiability Test Results 84

List of Figures

1.1 DNA Damage and DNA Damage Response in Cancer Treatment . . . 3

2.1 Major DSB Repair Mechanisms: the major proteins such as Ku, DNA-PKcs, Artemis and ligase in NHEJ and MRN complex, RPA, BRCA and Rad551 in HR that are involved in the pathways attach to the broken DSB end successively after DSB end recognition. 12

2.2 NHEJ Mechanism: NHEJ is initiated by Ku70-80 and DNA-PKcs is recruited after Ku; DNA-PKcs phosphorylates several substrates, including XRCC4 and Ligase IV; XRCC4 forms a complex with Ligase IV; other proteins involved in the pathway are Artemis, Polymerase λ, and Polymerase μ 16

2.3 Modeling Result Compared to Experimental Data: the modeling results are in good agreements with he experimental data under both IR and IR+ADT cases. 24

2.4 Weekly IR Treatment Plan 27

2.5 Averaged DSB per Cell in the Weekly Schedule Treatment Plan . . . 28

2.6 Individual Patient Response to ADT: the Y axis represent relative Ku levels and the X axis indicate patients numbering, different patients have different responses to ADT and the differences are reflected in changes of Ku levels 29

2.7 Patients Group Sensitive to ADT 30
2.8 Patients Group Less Sensitive to ADT 31
2.9 Patients Group not Sensitive to ADT 32
2.10 Homologous Recombination Mechanism [73]: MRN complex interacts with DSB ends and initiates end resection; RPA binds to DNA damage ends for protection; BRCA binding for facilitating the exchange of RPA off and addition of Rad51 to the single strand overhang; Rad51 filament invades the sister chromatid and starts strand invasion; Rad54 binds, D-loop formation and end capturing; DSBR pathway: second end capturing,Holliday junction formation and resolution, and crossover repaired DNA; and SDSA pathway: dissociation, DNA synthesis, ligation, and non-crossover repaired DNA. 35
2.11 HR Model Results with Optimized Parameters for IR and IR+ADT Treatment 40
2.12 HR Efficiency for varying BRCA Protein Concentrations 42
2.13 Two Sampling Strategies: Panel one has samples every hour, panel two has only six samples. Modeling results show that sampling frequency did not effect model results. 44
2.14 Data Sampling Strategies: Sampling with every half hour for IR and IR+ADT models 44

3.1 DSB Repair Flow in Separate Cell Cycle Phases (G1, S and G2/M) . 52
3.2 Cell Cycle Arrest and Cell Proliferation Timeline 55
3.3 Rate of Cell Survival in Cell Cycle 56
3.4 PCa Cell Proliferation 57
3.5 Curve Fitting for NHEJ When Inhibiting HR in G1, S and G2 Phase 62

4.1 5-FU Cytotoxicity to DNA 69

4.2 BER Pathway Mechanism 73
4.3 BER Model Results compared with Experimental Data for SW480 and HeLa Cell Lines 76
4.4 DNA Glycosylase Depletion and BER Outcome 78
4.5 Repaired Damage for Different APC Expression Cells 80
4.6 Repair in Cells with Different APC Levels for Varying 5-Fu Doses . . 80
4.7 a. Experimental data without PARPi and the data set generated from this experimental data with PARPi effects included; b.BER kinetics change after PARPi; c. BER kinetics change after inhibition of ligase; d. PARPi and ligase inhibition on BER kinetics. 82
6.1 Synthetic Lethality of PARPi and BRCA Mutation 91

Acknowledgments

First of all, I would like to give special thanks to my advisor, Dr. Evren Gurkan-Cavusoglu, who has led me into the door of computational system biology and provided me guidance and help during my Ph.D. studies in Case Western Reserve University in the past 5 years. I have known Dr. Evren Gurkan-Cavusoglu since 2013 when I was an undergraduate student at CWRU and I am proudly grateful to have her as my advisor for my graduate studies. I would also like to thank her for the countless time that she spent to teach and inspire me as well as her support and encourage.

Then I would like to thank Prof. Vira Chankong, Prof. Christian A. Zorman and Prof. M. Cenk Cavusoglu for serving as my committee, who have spent valuable time and offering me helpful suggestions. I would also like to thank Dr. Alexandru Almasan, who serves as my committee and offering me help from the biology perspective.

Then I would like to express sincere thanks to my dearest friends I met at CWRU: Wanyun Zhong, for all her enlightenment and care like a sister which makes me feel warm even if being thousands miles away from home; Fan Zhang and Jingsong Wang, for the unforgettable time we shared together. I would like to extend my thanks to Huiying Zhao, Yihao Zhang and those who has helped me during my Ph.D. studies. Our friendship is the treasure of my life.

Last but most importantly, I am deeply grateful to my beloved parents who gave

me endless unconditional love, support and understandings. They are my role models and they made me who I am today. Their spiritual and financial support make it possible for me to start this adventurous journey and being fearless. I cannot tell how much I love them. I am so proud of my parents and now I hope they are proud of their big girl.

The past five years is the best marathon in my life, and I believe there will be more challenges in the future. I will try my best to forge ahead and make further progress.

Nomenclature

5-FdU 5-fluorodeoxyuridine

5-FU 5-fluorouracil

ADT androgen deprivation therapy

AP apurinic/apyrimidinic

APC adenomatous polyposis coli

AR androgen receptor

BER base excision repair

DDR DNA damage response

DSB double strand break

DSBR double strand break repair

HR homologous recombination

IR ionizing radiation

IUdR iododeoxyuridine

LET low linear energy transfer

MMR DNA mismatch repair

NHEJ non-homologous end joining

ODE ordinary differential equation

PARP poly ADP ribose polymerase

PARPi poly ADP ribose polymerase inhibitor

PCa prostate cancer

SDSA synthesis-dependent strand annealing

SSB single strand break

SSBR single strand break repair

UDG uracil DNA glycosylase

UNG uracil-Nglycosylase

System Biology Analysis of the Role of DNA Repair in Cancer Treatment Outcome

Abstract

by

MENGDI QIAN

Cancer is one of the most lethal and hard to cure diseases. The common treatments for cancer include surgery, radiation therapy, chemotherapy, immunotherapy, and hormone therapy. Ionizing radiation (IR) is one of the main clinical treatments for cancer and it works by inducing DNA double strand breaks (DSBs), which are the most toxic DNA lesions that can lead to cell death. The effectiveness of IR treatment depends on the amount of induced damage and the DNA damage repair status of the cancer cells. DSBs are repaired by multiple DNA repair pathways and this repair reduces the effectiveness of the treatment leading to resistance to IR. It has been shown in the literature that by targeting the DNA repair pathways the treatment efficacy can be modulated.

In this work, a systems biology approach is used to quantitatively study the role of DNA repair pathways in determining and improving the radiation treatment outcome. Specifically, the mathematical models of DNA repair pathways, non-homologous end joining (NHEJ) and homologous recombination (HR), are developed for analyzing the role of DNA repair in enhancing the treatment sensitivity for prostate cancer (PCa) when a combination of radiation and hormone deprivation therapies is used. DSBs are repaired by one of the two DNA repair pathways: NHEJ and homologous recombination (HR). NHEJ is the major pathway, whereas HR is restricted to S- or G2-phases of the cell cycle after DNA replication has been completed. The cell cycle specific contribution of the repair pathways are incorporated into the computational models. A comprehensive identifiability analysis is carried out to determine the factors affecting parameter identifiability and strategies to increase identifiability are

developed. In parallel to the NHEJ and HR models, a computational model of the base excision repair (BER) pathway is developed to analyze its role in response to chemotherapy under different treatment scenarios.

Combination treatment strategies that aim to inhibit the functional DNA repair pathways for the cancer cells that are defective in other repair pathways achieve synthetic lethality. One such strategy is the use of poly ADP ribose polymerase inhibitors (PARPi) in addition to the combination treatment with IR and androgen deprivation therapy (ADT). The experimental data in the literature show that AR promotes both NHEJ and HR following IR, and inhibition of androgen receptor by ADT impairs both of these pathways in PCa cells leading to either increased radiosensitivity or sensitization to PARP inhibitors. The effect of using PARPi in this scenario has been computationally analyzed in this work by extending the modeling efforts to include the effect of PARP inhibitors on the treatment outcome. The inhibition of BER by PARPi is also quantitatively studied. The models and findings in this work can then be extended to other cancers, such as lung cancer and ovarian cancer that benefit from similar synthetic lethality.

Chapter 1

Introduction

1.1 Role of Damage Response in Cancer Treatment

Cancer is one of the top leading causes of death. According to the global cancer statistics in [1], only in 2018, there are approximately 18.1 million new cancer cases and 9.6 million cancer deaths. Lung cancer has been the most common and mortal cancer regardless of gender with 18.4% of total cancer death and the second highest incidence of cancer is prostate cancer for men and breast cancer for women. Traditional and novel treatments have been developed to increase the overall survival of cancer patients. At present, the common treatment approaches for cancers (tumors) include surgery, chemotherapy, radiotherapy, biological immunotherapy, molecular targeted therapy, and particularly, hormone therapy for specific cancers, such as breast cancer, ovarian cancer and prostate cancer (PCa). The major treatment approaches in modern cancer therapies are the first three types: surgery, chemotherapy, and radiotherapy.

Surgery is the preferred method for treating most early malignancies. For patients with advanced cancer, surgery is only used as an adjunct treatment. Chemotherapy is a systemic treatment, and its effect is rapid, but it also kills normal cells together with

tumor cells. Radiation therapy is available for most cancer types and can be delivered to patients as a single treatment or in combination with surgery or chemotherapy as part of a comprehensive treatment to improve the effectiveness. Except for surgeries which remove the tumor directly, radiation and chemotherapy work by inducing damages to the DNA and this damage leads to cell death. The DNA damages caused in cancer treatment include the single strand break, the most common lesion; the double strand breaks, the most lethal lesion; base mismatch, bulky adducts, nucleotide mutations, and so on [2].

As summarized in Figure 1.1 [2, 3, 4], single strand breaks (SSBs) are repaired by base excision repair (BER), which is the pathway for the repair of base damages caused by ionizing radiation (IR) and cancer therapy drugs. Double strand breaks (DSBs), known as the most lethal lesions that cause cell death are repaired through the non-homologous end joining (NHEJ) and homologous recombination (HR) pathways. The combination of NHEJ and HR to DSB repair is cell cycle phase dependent and their efficiencies also depend on the cell cycle phase [5]. DNA damage is the direct cause of cell death, making the DNA damage response (DDR) a target for enhancing treatment efficacy. The DDR mechanism is a complex process that includes the DNA repair pathways mentioned above, but also damage tolerance process and cell cycle checkpoints that safeguard genomic integrity [6].

DNA damage induced by different treatments are repaired by multiple pathways and the amount of unrepaired damage determines treatment outcome. It has been shown in the literature that by targeting the DNA repair pathways, the treatment efficacy can be modulated [7, 8]. Therefore, the study of leading DNA repair mechanisms is particularly important in the understanding of cancer treatment effects.

In addition to the direct effect of DNA damage repair pathways in the damage response mechanisms of cell cycle checkpoint in the cell cycle play an important role as well. When abnormal events such as DNA damage or DNA replication blocking occur

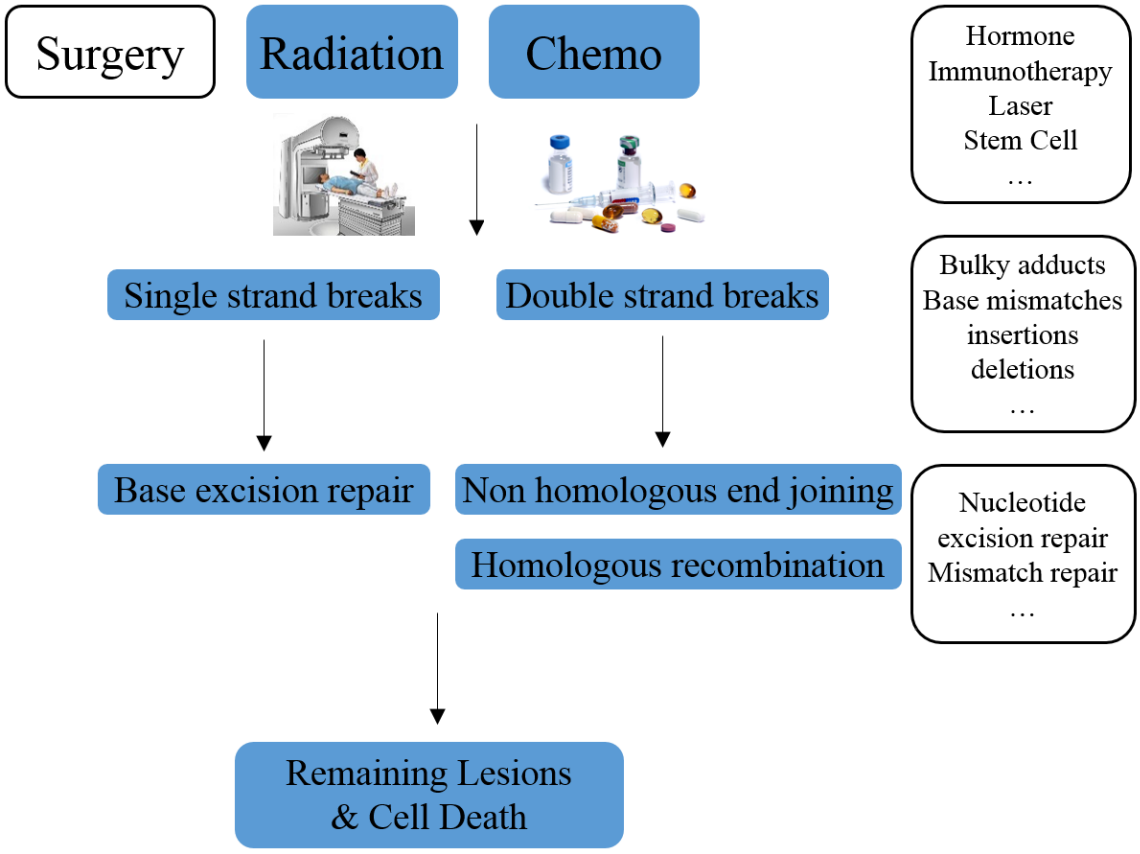

Figure 1.1: DNA Damage and DNA Damage Response in Cancer Treatment

during cell cycle progression, such regulatory mechanisms are activated to interrupt the cell cycle in a timely manner. After the damage is repaired, cell cycle progression can resume. Cell cycle checkpoints coordinate various functions in the cells with DNA damage [9].

In this work, the focus will be on the role of DNA repair in the treatment outcome for prostate cancer. Prostate cancer is selected as a model system, and the models and findings in this work can be extended to other cancers. Prostate cancer, a most frequently diagnosed cancer in men is generally treated with IR accompanied with androgen deprivation therapy (ADT). ADT enhances the response to IR by hormone suppression, which leads to reduced androgen receptor activities that then down-regulate HR and NHEJ repair proteins [10, 11]. The down-regulation of the proteins involved in the repair pathways result in reduced damage repair of DSBs.

In addition to ADT, it is also reported that when used in combination with IR and ADT, poly (ADP-ribose) polymerase inhibitors (PARPi) increase the effectiveness of IR and ADT for PCa patients due to synthetic lethality [11].

1.2 Problem Formation and Objectives

In this work, a systems biology approach is used to quantitatively study the role of DNA repair pathways in determining and improving the radiation treatment outcome. Specifically, the mathematical models of DNA repair pathways, non-homologous end joining (NHEJ) and homologous recombination (HR), are developed for analyzing the role of DNA repair in enhancing the treatment sensitivity for prostate cancer (PCa) when a combination of radiation and hormone deprivation therapies is used. DSBs are repaired by one of the two DNA repair pathways: NHEJ and homologous recombination (HR). NHEJ is the major pathway, whereas HR is restricted to S- or G2-phases of the cell cycle after DNA replication has been completed. The cell cycle specific contribution of the repair pathways are incorporated into the computational models. A comprehensive identifiability analysis is carried out to determine the factors affecting parameter identifiability and strategies to increase identifiability are developed. In parallel to the NHEJ and HR models, a computational model of the base excision repair (BER) pathway is developed to analyze its role in response to chemotherapy under different treatment scenarios.

Combination treatment strategies that aim to inhibit the functional DNA repair pathways for the cancer cells that are defective in other repair pathways achieve synthetic lethality. One such strategy is the use of poly ADP ribose polymerase inhibitors (PARPi) in addition to the combination treatment with IR and androgen deprivation therapy (ADT). The experimental data in the literature show that AR promotes both NHEJ and HR following IR, and inhibition of androgen receptor by ADT im-

pairs both of these pathways in PCa cells leading to either increased radiosensitivity or sensitization to PARP inhibitors. The effect of using PARPi in this scenario has been computationally analyzed in this work by extending the modeling efforts to include the effect of PARP inhibitors on the treatment outcome. The inhibition of BER by PARPi is also quantitatively studied. The models and findings in this work can then be extended to other cancers, such as lung cancer and ovarian cancer that benefit from similar synthetic lethality.

Mathematical models of NHEJ have been developed in the literature using both deterministic and stochastic approaches [12, 13, 14, 15, 16, 17]. Biochemical kinetics of NHEJ is modeled using deterministic nonlinear ordinary differential equations in [12] and repair dynamics after exposure to low-energy transfer (LET) radiation is analyzed for fibroblast cells. In [15], the model developed in [14] is modified to study the effect of protein recruitment order on the DNA repair outcome. The models in [16, 17] employ a stochastic Monte Carlo approach using first order reaction kinetics to simulate the DSB repair after low- and high-linear energy transfer irradiation in human fibroblast cells. Mathematical models of HR and HR sub-pathways have been developed in [18, 19, 20] by applying law of mass action for individual proteins mathematically using ordinary differential equations (ODE). It is also important to study the relationship between BRCA, PARP and HR and BER. For this purpose, BER models are developed in this work. In the literature, BER models have been developed in [21, 22, 23, 24, 25] using Michealis-Menten kinetics.

Most of the current research as reviewed above is focused on modeling a single DNA repair pathway. However, the repair pathways do not function independent of each other. The analysis of the overall repair efficiency of DNA damage requires the combination of these models, especially considering the important role of the cell cycle. In DSB repair, the efficiency of NHEJ and HR determines the remaining DSB amount that leads to cell cycle arrest and ultimately cell death. In [18], although

multiple repair pathways are combined, only the cell cycle employs cell cycle distribution at the beginning for allocation for DSBs in each pathway as starting points is considered. The quantitative model in [18] is developed for human skin fibroblast cells before and after LET.

The repair kinetics are different in each cell type and DNA repair models for PCa cells were not developed before in the literature. There is experimental data on the DSB repair kinetics for PCa, but there are no prior modeling efforts. The experimental data in the literature for PCa includes the repair kinetics after treatment with IR, combination treatment with IR+ADT as well as combining IR+ADT with PARPi.

The research on the role of DNA repair in treatment outcome has lead to development of treatment strategies that target cancers with DNA repair defects [7]. The research also shows the variability among patients in their responses to combination treatment with IR+ADT [26].

One important step in the model development is the identifiability analysis in addition to sensitivity analysis. Even though the model outcome is in good agreement with the experimental data, not all the model parameters might be identifiable. In order to be able to drive conclusions from the modeling effort, it is important to determine the identifiable parameters. The non-identifiability of the parameters may be due to the structure of the model [27], where some parameters are multiplied together making them structurally non-identifiable. Apart from non-identifiability, the parameters need to be examined for their identifiability to be able to drive biologically relevant conclusions.

To overcome the limitations stated above, a modeling framework is proposed in this work with the integration of the major pathways in DNA damage repair after IR treatment in a cell cycle dependent manner. Specifically, HR and NHEJ pathways are combined in a cell cycle dependent manner to study the treatment outcome of radiation treatment for prostate cancer. BER models are developed in parallel

to study chemotherapy outcome. Both modeling efforts are extended to incorporate synthetic lethality treatment approaches. There are three novel aspects to be examined in this work. Based on the developed modeling framework, analysis will be carried out to quantify the role of DNA damage repair pathways in determining and improving IR treatment outcome; to analyze the role of DNA repair in enhancing treatment sensitivity; and to study the benefits of combination treatment strategies quantitatively.

This dissertation aims at developing computational models of NHEJ, HR, and BER pathways, respectively for DNA damage repair regarding different damage types and integrating these on a cell phase dependent manner to quantitatively study the DDR in cancer therapies. Specifically, the models of DNA double strand repair are developed for PCa under IR and ADT, where the changes in the dynamics due to enhancement or inhibition of the pathways are represented by kinetics changes in repair proteins. Double strand break repair models developed in this work take into account the NHEJ and HR efficiency variation through the cell cycle. The model application uses PCa experimental data, therefore all the parameters need to be estimated optimally for the cells lines that are used for the data collection. In order to make the biological relevance of optimized parameters, the sensitivity test together with the identifiability test need to be conducted in this study.

The models are to be quantitatively studied for the following scenarios that were observed in literature: ADT enhance the effect of IR by down regulating Ku and DNA-PKcs in NHEJ and MRE11 and Rad51 proteins in HR through inhibiting androgen receptor (AR) activities; PARPi is another combination treatment that is studied here and PARPi increases IR or chemotherapy toxicity to cancer cells; variable patient response to chemotherapy or IR.

1.3 Dissertation Contributions and Organization

In this dissertation, a comprehensive computational model of DNA double strand break repair is developed in a cell cycle phase dependent manner which allows examining the repair dynamics in detail for G1, S, and G2 phases. As the major pathways for DNA double strand break repair, mathematical models of non-homologous end joining and homologous recombination repair pathways are developed using nonlinear ordinary differential equations and the models are parameterized using experimental and clinical data from the literature. The specific values of some of these parameters are hard to measure in the experiments while our model performs parameter estimation and optimization, which provides a reliable data range for these parameters for PCa. The DSB repair models based on cell cycle dynamics for prostate cancer develop in this work form a novel modeling framework to study the effectiveness if IR and combination treatments for PCa.

A cancer cell proliferation model is developed for the cancer treatment combining IR and ADT. Repair pathways selections are based on the cell cycle phase and for cell cycle dependent accuracy. The integration of modeling of NHEJ, HR, and cell cycle is performed to obtain a full picture of DSB repair. This is an important step to obtain a comprehensive perspective on the therapeutic efficacy of radiation treatment for PCa quantitatively.

Base damage is a common DNA damage in cancer treatment. We also study the base excision repair in the base damage repair mechanism and specifically its role in enhancing the sensitivity to the chemotherapy.

The computational models developed in this work successfully capture the following: radiation therapy enhancement by ADT through AR signaling by down regulating key proteins in both non-homologous end joining pathway and homologous recombination pathway; PARPi as an adjuvant treatment strengthening the outcome for IR and chemotherapy; how to untilize a special gene mutation that lead to defi-

ciency in DNA damage repair to enhance treatment outcome; cell cycle arrest; profiles for repair efficiency based on patient to patient variability.

The mathematical models forms the basis for an approach to quantitatively optimize dose and timing for radiation and chemotherapy.

The dissertation is organized as follows:

Chapter 2 provides an review on existing DSB repair pathway modeling method and experimental and clinical research findings on both NHEJ and HR. Mathematical models are developed and parameterized under the scenario of IR combined with ADT in PCa. A detailed identifiability analysis is also conducted in this chapter.

Chapter 3 describes a detailed study for NHEJ efficiency variation of different cell cycle phases, and an integrated model that contains HR, NHEJ, and cell cycle to quantitatively analyze cell proliferation after radiation treatment.

In Chapter 4, a computational model of base excision repair is built and validated using multiple data sets.

A conclusion of this dissertation is made in Chapter 5.

Finally, Chapter 6 provides a discussion on possible future work based on this dissertation.

Chapter 2

Modeling and Quantitative Analysis of Major DNA Double Strand Break Repair Pathways

2.1 Introduction

Cancer has long been the most fatal and hard to cure disease. Ionizing radiation (IR) is one of the major treatment approaches for cancer patients. IR induces double strand breaks (DSBs), which are known as the most lethal DNA lesion that causes cell death leading to slower tumor growth[7]. The effectiveness of IR treatment depends on the amount of induced damage and the DNA damage repair status of the cancer cells. DSB can be repaired by multiple DNA repair pathways that reduce the effectiveness of the treatment leading to resistance to IR. It has been shown in the literature that by targeting the DNA repair pathways the treatment efficacy can be modulated (see [7] for review). DSBs are repaired by one of the two DNA repair pathways: non-homologous end joining (NHEJ) and homologous recombination (HR). NHEJ is always active through the whole cell cycle, while HR is active during S- or G2-phases

of the cell cycle, which makes NHEJ the dominant pathway for DSB repair. A brief description of the mechanisms of both pathways are shown in Figure 2.1 [28]. The figure shows a simplified process of the DSB repair where the major proteins that are involved in the pathways attach to the broken DSB end successively after DSB end recognition. The components in the NHEJ pathway are the Ku70-80 heterodimer, DNA-PK catalytic subunit (DNA-PKcs), XRCC4, Ligase IV, and certain accessory factors such as 53BP1 [14]. Like Ku and DNA-PKcs in NHEJ, Rad51 is the key protein indicating HR activation. HR process is summarized as a repair process that includes end-resection step, strand invasion step and ligation step mediated by proteins such as MRN complex, RPA, BRCA and Rad51. The difference between NHEJ repair and HR is that, HR requires a template DNA to complete the repair whereas NHEJ does not.[29]. This is why HR is restricted to cell cycle phases after DNA replication, but compared to NHEJ, it is error free. Although NHEJ and HR are distinct repair pathways for DNA DSBs, it is shown in the literature that these two pathways might influence each other [30]. When NHEJ is impaired by inhibiting NHEJ repair proteins, Rad51 is also affected in the process, which means HR activity can be influenced by NHEJ. In the same study [30], it is shown that when HR is restricted, NHEJ effectiveness is also influenced. IR dose is also a factor that influences repair pathway efficiency on some scale. Therefore, it is important to develop a comprehensive modeling framework that simulate the DSB repair by both NHEJ and HR pathways to analyze the dynamics under different treatment scenarios.

Mathematical models of NHEJ have been developed in the literature using both deterministic and stochastic approaches. Biochemical kinetics of NHEJ is modeled using deterministic nonlinear ordinary differential equations in [14] to analyze repair dynamics after exposure to LET radiation in fibroblast cells. It is also reported on NHEJ modeling in [15] for the repair of DSB caused by ultrasoft X-ray and low-energy electrons instead of IR. In [16], the authors develop a Monte Carlo simulation

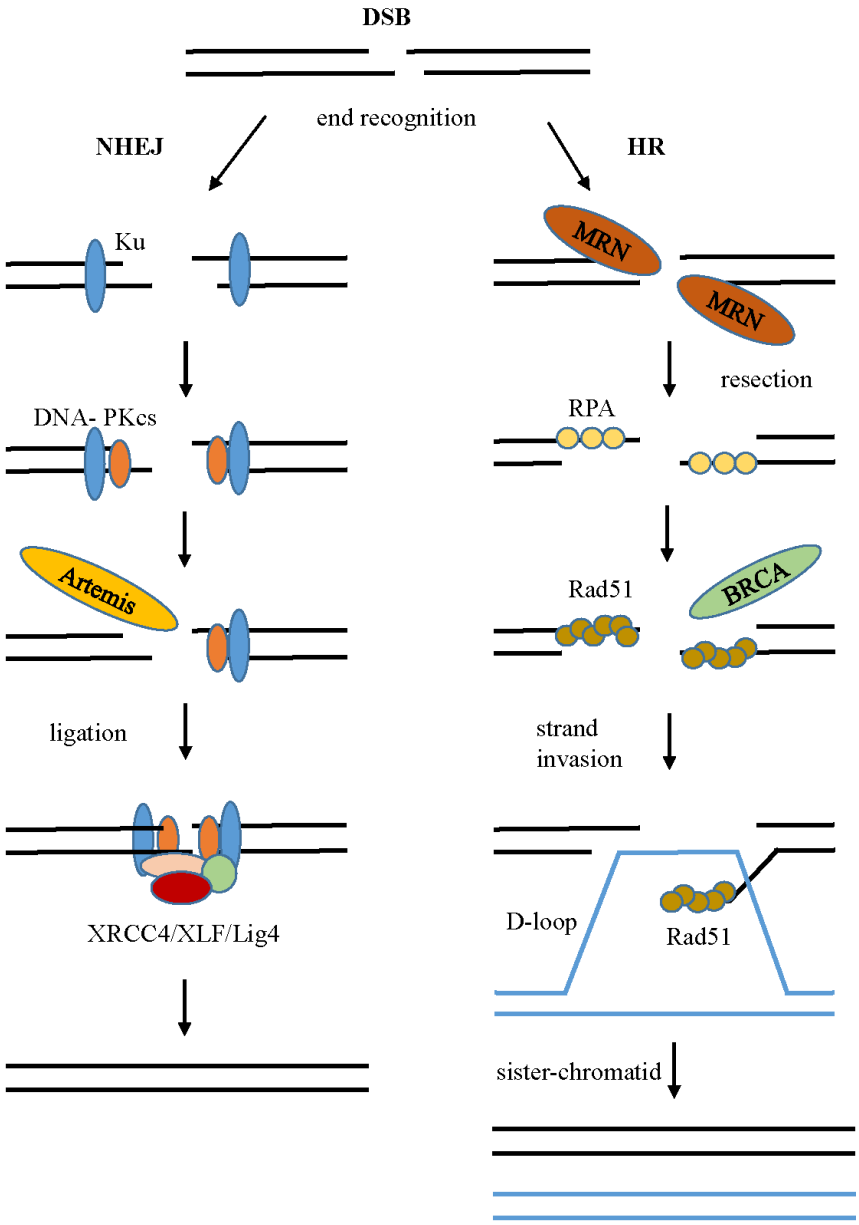

Figure 2.1: Major DSB Repair Mechanisms: the major proteins such as Ku, DNA-PKcs, Artemis and ligase in NHEJ and MRN complex, RPA, BRCA and Rad551 in HR that are involved in the pathways attach to the broken DSB end successively after DSB end recognition.

model for NHEJ. They estimate several parameters like Ku attachment kinetics to predict system dynamics post IR treatment. Following [16], Friedland also uses the same model in [17] to estimate kinetics for differential radiation types. In [31], an

integrated model that combines NHEJ and DNA signaling is created to fulfill the completeness required for combining separate simulations on DNA NHEJ repair and DNA signaling together. The model is used to predict cellular senescence after IR treatment.

Modeling approach in [12] compares the differences between a sequential model and a two phase model when simulating NHEJ. Sequential model is a widely used model for NHEJ since in this model actions are taken step by step according to the order in which proteins bind to the DSB end. On the other hand, in a two phase model, protein order is not a determinant. These two models share the same modeling framework using the law of mass action and the only differences are in the definitions of intermediates. It is also shown that the results from these two models are the same when there are sufficient repair proteins in the substrates. The same group also studied how NHEJ depends on damage complexity in [13] using ODEs that correspond to the biological reactions in NHEJ. It is shown that there are different repair efficiencies due to DSB complexity that a simple DSB can be repaired quicker without DNA-PKcs than a complex DSB.

In [29], a mechanism of HR is reviewed. A classic model called Holliday Model identifies four major steps of HR recombination: two homologous chromosomes are arranged in order; a strand of DNA breaks and links with another DNA to form a Holliday intermediate; a heterologous double stranded DNA is produced by branching; Holliday intermediates are cut and repaired to form two double strand recombinants. There are varieties of proteins that involved in HR such as MRN complex, BRCA1/2, Rad52, Rad59, Rad54, Rad51, XRCC. Due to the complexity of this biological mechanism, HR repair is studied in most cases indirectly by evaluating Rad51 activities.

Biochemical kinetics of HR is modeled using deterministic nonlinear ordinary differential equations in [18] and repair dynamics after exposure to both high and low energy transfer radiation is analyzed for human fibroblast and Chinese hamster lung

fibroblast cells. In [19], a mathematical model using differential equations that contains a simplified HR mechanism in G1 and early S phase is developed to study DSB repair in the specified cell cycle phases. The model of single strand annealing (SSA) is developed in [20] as a compensation for NHEJ and HR pathways. Instead of Rad51 binding, Rad52 conducts annealing function for DSB resolution. SSA and HR share the same initial steps but SSA is non conservative compared to HR [32]. In [33], it is pointed out that Rad51, the protein that is used as a marker protein for HR activities, inhibits SSA process mediated by Rad52. It is discussed that the modulation of HR by inhibiting Rad51 promotes Rad52 for mediating SSA, which is a compensating DSB repair pathway.

NHEJ and HR are separate DNA repair pathways but they both contribute to DSB repair post IR treatment in a cell cycle dependent manner. NHEJ is active through the whole cell cycle, and HR is only active in S/G2/M phase. While NHEJ repairs about 75% of cells faster and more efficiently, HR repairs the rest about 25% more accurately [34]. In this chapter, mathematical models of NHEJ and HR are developed and the experimental data for PCa is used to estimate the model parameters. Because of the close relationship of NHEJ, HR, and their cell cycle dependent efficiencies, approaches to combine these dynamics are described in Chapter 3. It is necessary to complete the DSB repair model including dose-related DSB formation; NHEJ modeling; HR modeling and cell cycle modeling to study DSB repair efficiencies under different scenarios. The long-term goal is to develop IR treatment plans (dosing and timing) that are optimized for an individual cancer patient to maximize treatment efficacy.

2.2 *In Silico* NHEJ Models of Radiotherapy for Prostate Cancer

One of the most commonly used cancer treatments is radiotherapy. Its effectiveness depends on the capacity of the cells to repair the DNA damage caused by the ionizing radiation (IR). Majority of the IR induced damage is repaired by non-homologous end joining (NHEJ) repair pathway. It is shown that impaired NHEJ improves the therapeutic outcome of radiotherapy. In this section, the role of NHEJ in the improved radiosensitivity is computationally studied. The focus is on the prostate cancer because of the availability of both experimental and clinical data on the repair dynamics and the variability in patient response to treatment. The presented methods can be generalized to other cancer types and treatments. The mathematical model of NHEJ is developed to study the interaction between the androgen deprivation therapy (ADT) and improved radiosensitivity for PCa. Sensitivity and identifiability analyses are applied to determine the reliably estimated parameters. A strategy is developed to increase the identifiability of the initially unidentifiable parameters. The model is used to study the effect of conventional, fractionated radiation treatment among patients with different levels of radiosensitivity. The model presented here is the first step to develop treatment scenarios to find the optimal strategies using the combination treatment with NHEJ inhibitors and IR.

It has been shown in the literature that the increased levels of NHEJ components result in poor treatment response to IR and cancer has progressed even after the IR treatment [10]. For PCa, the hormone level is also a key element that influences the treatment effectiveness. Generally, in most clinical treatment approaches, a combination of ADT and IR is widely used in order to improve patients overall survival probability and it is proved to have positive results for PCa patients [26]. The studies in literature [10, 26] show that androgen receptor (AR) is activated by IR and that

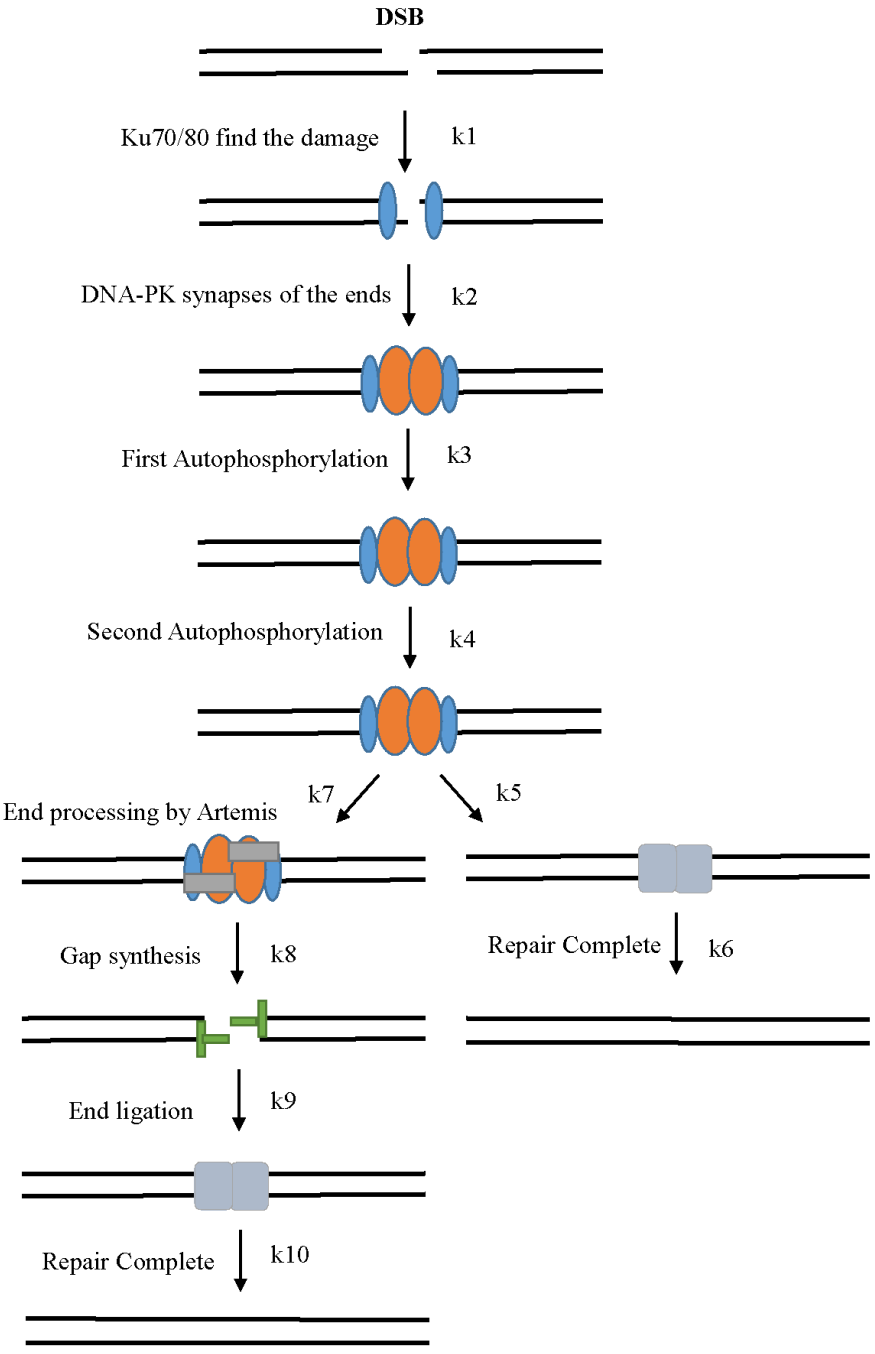

Figure 2.2: NHEJ Mechanism: NHEJ is initiated by Ku70-80 and DNA-PKcs is recruited after Ku; DNA-PKcs phosphorylates several substrates, including XRCC4 and Ligase IV; XRCC4 forms a complex with Ligase IV; other proteins involved in the pathway are Artemis, Polymerase λ, and Polymerase μ

increased AR activity promotes NHEJ repair and increases the radioresistance of the cancer cells.

In this section, we study the effect of AR in promoting DNA repair by developing a quantitative model of the NHEJ using the experimental data from [10]. Understanding this mechanism is important for possible enhancement of the treatment of PCa where the tumor growth and progression is AR activity dependent. Here, we quantify the effect of AR on the NHEJ pathway. This is an important step in quantitatively analyzing possible treatment scenarios to find the optimal treatment strategies for PCa using the combination treatment with ADT, NHEJ inhibitors, and IR.

2.2.1 NHEJ Pathway Mechanism

As presented in Figure 2.2 [14], the mechanism of NHEJ is described as follows: NHEJ is initiated by Ku70-80 heterodimers that bind to the free ends of DSBs [35] and they recruit DNA-PKcs [36]. DNA-PKcs phosphorylates several substrates, including XRCC4 and Ligase IV [37]. Ku70-Ku80 and DNA-PKcs promote synapsis of the broken DNA ends and act as a molecular scaffold for the recruitment of other NHEJ proteins. When activated, DNA-PKcs undergoes autophosphorylation, which results in loss of its kinase activity and disassembly from the DNA repair complex [38]. XRCC4 forms a complex with Ligase IV [39, 40] and Ligase IV is the essential enzyme that completes the last step in the NHEJ pathway. The other proteins involved in the pathway are Artemis, Polymerase λ, and Polymerase μ [14].

2.2.2 Mathematical Model of NHEJ

IR Dose Dependent DSB Induction

There are various reasons that could lead to DSBs in human cells. The reasons include endogenous DNA damage and exogenous agents causing DSBs where IR is the most

direct and effective way for generating DSBs during cancer treatment [41]. The base damages that are repaired by base excision repair and DNA mismatch repair could end up with improperly repaired intermediates. The intermediates could become SSBs and finally become DSBs. Besides IR dose variations, the number of radiation induced DSBs also depends on cell cycle phases. In [42], it is shown that G2 cells have more DSBs than G1 cells because they have double amount of DNA. It is also reported in [43] that there is a high level of γH2AX foci in S phase cells as a background. In [44], a more detailed model is developed studying simple and complex DSB as components for DNA damages with nonlinear dose validations. In the experiments that were designed for DSB related studies, measurements of histone H2AX phosphorylation as the DNA damage marker is widely used as it closely correlates with DSB [45, 46].

The DSB generation has been modeled in [41, 47, 48] stochastically and deterministically. In these studies, the formation of initial DSB is summarized in the following equation:

$$\frac{dDSB}{dt} = \alpha \frac{dDose}{dt} \tag{2.1}$$

and with DSB detected, RIF is calculated as:

$$C_c(t) = \alpha * D(1 - e^{-kt}) \tag{2.2}$$

where C is RIF formed by DSB, α is a factor that relates to the IR dose D. In [49, 50, 51], the number of DSBs is considered proportional to dose thus α has values corresponding to dose intensity. k is the rate of discovering a single DSB. As expected, with the increase in IR intensity, there will be more DSBs detected. However, the DSB formation process takes only minutes but the DNA repair process takes more than 20 hours. Comparing the time scales, we model the DSB formation mechanism as an impulse function, and use the maximum value of DSBs as the initial value in model simulations.

Mathematical Model of NHEJ

Every reaction in the NHEJ pathway is modeled using mass-action kinetics as in [14, 52]. DSBs form very rapidly within minutes after IR exposure [48], however the NHEJ repair takes place in hours. Because of this time scale difference, the DSB formation is not explicitly modeled but assumed to be an impulse at time zero and the number of DSBs are used as the initial condition in the simulations. The model consists of ODEs for each reaction as follows:

$$\frac{dY_1}{dt} = \alpha \frac{dDose}{dt} - k_1 e_{Ku}[Y_1] \tag{2.3}$$

$$\frac{dY_2}{dt} = k_1 e_{Ku}[Y_1] - k_2 e_{DNA-Pkcs}[Y_2] \tag{2.4}$$

$$\frac{dY_3}{dt} = k_2 e_{DNA-Pkcs}[Y_2] - k_3[Y_3] \tag{2.5}$$

$$\frac{dY_4}{dt} = k_3[Y_3] - k_4[Y_4] \tag{2.6}$$

$$\frac{dY_5}{dt} = k_4[Y_4] - k_5 e_{XLF,XRCC4,LIGIV}[Y_5] - k_7 e_{Artemis}[Y_5] \tag{2.7}$$

$$\frac{dY_6}{dt} = k_5 e_{XLF,XRCC4,LIGIV}[Y_5] - k_6[Y_6] \tag{2.8}$$

$$\frac{dY_7}{dt} = k_7 e_{Artemis}[Y_5] - k_8 e_{polymerase\lambda-\mu}[Y_7] \tag{2.9}$$

$$\frac{dY_8}{dt} = k_8 e_{polymerase\lambda-\mu}[Y_7] - k_9 e_{XLF,XRCC4,LIGIV}[Y_8] \tag{2.10}$$

$$\frac{dY_9}{dt} = k_9 e_{XLF,XRCC4,LIGIV}[Y_8] - k_{10}[Y_9] \tag{2.11}$$

$$\frac{dY_{10}}{dt} = k_{10}[Y_9] + k_6[Y_6] \tag{2.12}$$

In the above equations, Y_i represents the protein and DSB complex, k_i is the reaction rate constant, and e represents the concentration of the protein. Y_1 is the concentration of the DSBs and Y_{10} is the amount of repaired DSBs. The model has

the protein concentrations and the rate constants as the parameters to be estimated. The form of the model only allows estimating either the protein concentrations or the rate constants for some of the proteins such as Ku70/80 in equation 2.3 because the rate constants and the protein concentrations are multiplied with each other. Only the product terms in such cases are structurally identifiable, but the individual parameters are not [53]. Because of this structural non-identifiability, the protein concentrations are assumed constant and only the rate constants are estimated. The protein Ku70-Ku80 is abundant in the cell with 4×10^5 molecules per cell [35]. NHEJ protein concentrations are shown to be similar to Ku70-Ku80 in [54] and based on this reference, all concentrations are assumed to be equal to each other in the simulations.

The least squares parameter estimation is used to identify the rate constants of the model. The initial values for the rate constants are chosen from the literature to have a biologically relevant starting point. Table 2.1 summarizes the values used as an initial point. The units for k_1, k_2, k_5, k_7, k_8, k_9 are $molecule^{-1}s^{-1}$, for k_3, k_4, k_6, k_{10}, units are s^{-1} in Table 2.1. The parameters are constrained in the estimation such that they all have positive values. The error function in equation 2.13 is used as the objective function for parameter estimation where Y_m is the model output and Y_e is the experimental measurement at a particular experimental time point and the squared errors are summed over all the time points:

$$Error = \sum_k (Y_m(k) - Y_e(k))^2 \tag{2.13}$$

The experimental data on the time course of repair dynamics measured in the form of γH2AX foci are from [10]. The formation of DSBs in response to IR leads to the phosphorylation of histone H2A variant H2AX (γH2AX), which is the most sensitive marker used to measure the amount of DNA damage produced and the subsequent repair time course [46].

Table 2.1: Experimental Measurements for NHEJ Proteins Kinetic Constants

Name	Description	Value
k_1	attachment of Ku	$2.985 * 10^{-6}$ [16]
k_2	attachment of DNA-PKcs	$5.572 * 10^{-5}$ [16]
k_3	autophosphorylation	0.5 [55]
k_4	autophosphorylation	0.3 [55]
k_5	XLF/XRCC4/Ligase IV end ligation	$2 * 10^{-4}$ [56, 57]
k_6	repaired DNA release	$6 * 10^{-4}$ [58]
k_7	artemis end processing	$2.8 * 10^{-14}$ [13]
k_8	gap synthesis	$6.94 * 10^{-5}$ [13]
k_9	XLF/XRCC4/Ligase IV end ligation	$2 * 10^{-4}$ [56, 57]
k_{10}	gap synthesis	$8 * 10^{-4}$ [59]

Two repair time course data sets corresponding to two different treatment scenarios from [10] are used in the model development. In both set of experiments, AR-positive, castrate-resistant C4-2 prostate cancer cells were used. The cells were first exposed to IR (2 Gy) and the induced DSBs and the repair time course were measured by enumerating γH2AX foci. The second data set was the repair time course for the combination treatment of IR and ADT. In [10], the authors have evaluated the proficiency of castration resistant PCa cells (C4-2) in repairing DSBs in the presence and absence of androgen. They have observed rapid induction of γH2AX foci (about 11.5 foci/cell) at 2 hrs post IR treatment. The DSBs were repaired by 22 hrs post-treatment for hormone proficient conditions (IR without ADT) and the DSBs persisted up to 72 hrs for cells that were deprived of androgen. By combining these results with the other experimental results in their paper, they have concluded that AR promotes DSB repair through NHEJ. It should be noted that these experimental data show the repair dynamics of the combined DSB repair by NHEJ and HR. In order to take into account the percentage of the DSBs repaired by NHEJ only, the data were scaled by 80% based on the data presented in [60]. The experimental data used in the parameter estimations are given in Table 2.2. Two sets of models are

Table 2.2: Experimental Data on γH2AX Foci per Cell

Time(Hr)	0	2	8	22	48
IR only	x	9.2	4.14	3	x
IR+ ADT	x	9.2	5.75	5.06	4.14

developed corresponding to each treatment scenario, namely for the IR only case and for the IR combined with ADT (IR + ADT).

There are two different but closely related mechanisms of interaction between AR and NHEJ presented in the literature. The authors in [10] hypothesize that the mechanism is through the enhanced expression and activity of DNA-PKcs by androgen, and AR reduction by ADT inhibits NHEJ repair through reducing DNA-PKcs activity. The other hypothesis presented in [26] is based on the patient data collected after castration therapy combined with IR that show that AR inhibition by ADT reduces the Ku70 protein levels and as a result improves the radiosensitivity of the PCa cells. The Ku70 protein levels were reduced by two-fold on average among 14 patient samples. This fact is used in the models developed in this work for IR+ADT case by keeping the rate constant k_1 at a fixed value as half of the k_1 value that is estimated for IR only case and the rest of the parameters are estimated for this second model. The models developed in this work are used to test the plausibility of both mechanisms and provide recommendations for further experiments to understand this mechanism better.

2.2.3 Sensitivity and Identifiability Test

Sensitivity Analysis

In order to be able to analyze the mechanism of the interaction between AR and NHEJ, it is important to determine the rate constants in the model that the model is sensitive to. If the model is not sensitive to a particular rate constant, its change from

IR model to IR + ADT model will not be conclusive. The hypothesized mechanisms would cause k_1 or k_2 (rate constants for Ku and DNA-PKcs) to change, when ADT is added to the treatment. The changes in the parameters in response to different treatments can be considered biologically relevant only for those parameters for which the model is sensitive. The sensitivity gain is calculated using the following equation [61]:

$$S_P^M = \frac{\frac{\partial M}{M}}{\frac{\partial P}{P}} \tag{2.14}$$

In equation 2.14, M is the system output and P is the parameter to be analyzed for its sensitivity. In the analysis for this work, the numerator is the percent change in error function and the denominator is the percent change for the parameter itself. All the rate constants are both increased and decreased by 20 percent and the average value of percentage change in M is calculated to determine the sensitivity gain S for a particular rate constant.

Identifiability Analysis

An identifiability analysis is conducted as described in [62] for all the parameters to determine whether the parameters are identifiable in the model. In order to check the identifiability of a specific rate constant, the estimated value of this parameter is kept constant and all the rest of the parameters are re-estimated by changing the chosen parameter by 15 percent up or down. If the objective function becomes greater, the parameter is said to be identifiable, otherwise, the parameter is non-identifiable when the objective function remains the same.

2.2.4 Results for Mechanism of Radiosensitization

Two different models are developed in this work. The first model represents the repair kinetics for the androgen proficient PCa cells with fully functional NHEJ that were

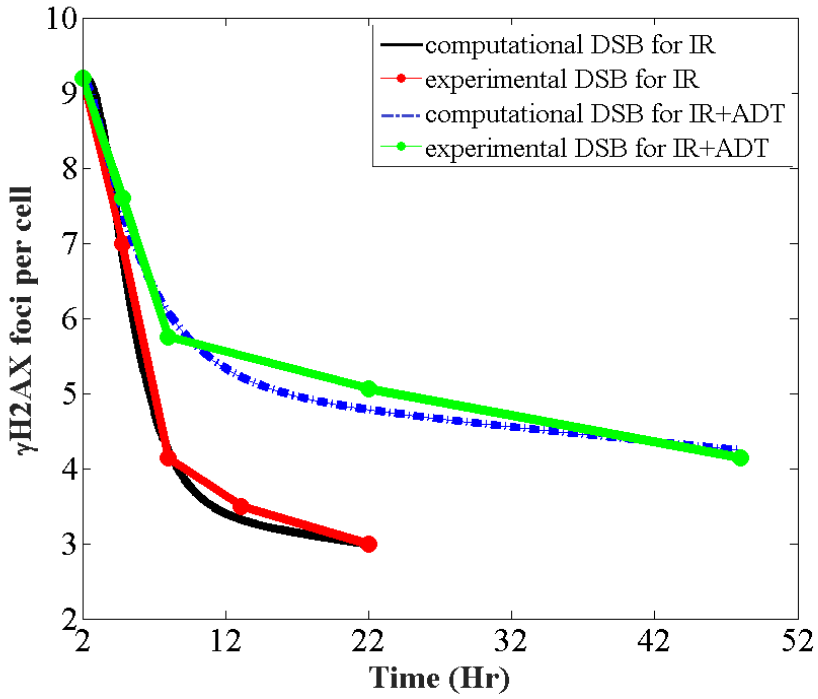

Figure 2.3: Modeling Result Compared to Experimental Data: the modeling results are in good agreements with he experimental data under both IR and IR+ADT cases.

only treated with IR. The second model has impaired NHEJ following ADT and IR treatment. Both models successfully captured the repair dynamics as seen in Figure 2.3. The estimated model parameters corresponding to these two models are given in Table 2.3.

In order to be able to understand the parameters that are affected by ADT, it is important to determine to which of the rate constants the model is sensitive as well as which of these constants are identifiable. The sensitivity gains for each parameter are presented in Table 2.4 together with identifiability results.

The parameters that are sensitive are k_1, k_2, k_5, and k_7 in both models. The parameters k_6 is sensitive in IR model and can be considered marginally sensitive for IR+ADT case. k_8 is only sensitive for IR only model In terms of identifiability, there is a similar trend to sensitivity with the parameters k_1, k_2, k_5, k_6, and k_7 being identifiable in both models. When sensitivity and identifiability results are compared

Table 2.3: NHEJ Parameter Optimization for PCa

Name	Description	Value (IR)	Value (IR+ADT)
k_1	attachment of Ku	$7.24 * 10^{-10}$	$3.62 * 10^{-10}$
k_2	attachment of DNA-PKcs	$4.72 * 10^{-10}$	$4.19 * 10^{-10}$
k_3	DNA-PKcs autophosphorylation	0.077	0.085
k_4	DNA-PKcs autophosphorylation	0.38	2.99
k_5	XLF/XRCC4/Ligase IV end ligation	0.05	0.07
k_6	repaired DNA release	$3.41 * 10^{-6}$	$1.75 * 10^{-6}$
k_7	artemis end processing	0.07	0.05
k_8	gap synthesis	$5.95 * 10^{-10}$	$5.95 * 10^{-7}$
k_9	XLF/XRCC4/Ligase IV end ligation	0.01	$3.21 * 10^{-8}$
k_{10}	gap synthesis	0.69	1.65

Table 2.4: Sensitivity Analysis and Identifiability Test Results for NHEJ Parameters for PCa Models

	IR		IR+ADT	
Name	Sensitivity Gain	Identifiability	Sensitivity Gain	Identifiability
k_1	11.01	+	3.55	+
k_2	20.80	+	2.54	+
k_3	0.0	-	0.0	-
k_4	0.0	-	0.0	-
k_5	31.13	+	44.22	+
k_6	5.64	+	0.33	+
k_7	73.46	+	19.48	+
k_8	13.65	+	0.0	-
k_9	0.0	-	0.0	-
k_{10}	0.0	-	0.0	-

for both models, it can be concluded that the reactions that are affected by ADT are the binding of Ku70-Ku80 (k_1) to the DSB to initiate the NHEJ repair, binding of DNA-PKcs (k_2)the ligation by XLF/XRCC4/Ligase IV complex (k_5), repaired DNA release (k_6) and Artemis end processing (k_7).

The mechanisms presented in the literature focus on the decrease in Ku70-Ku80 protein level or the reduced activity for DNA-PKcs following ADT. In the presented models, the effect of protein concentration change or kinetic constant change results in the same effect, because they appear in the form of $k_1 e_{Ku}$, so a two-fold change in k_1 between the two models can also be considered as a change in protein concentration of the same ratio. This change in k_1 can be used to explain the mechanism of interaction between NHEJ and AR, because k_1 is both a sensitive and identifiable parameter in both models. The modeling results show that the hypothesized effect of ADT on the NHEJ dynamics through Ku70 is a plausible mechanism. It should be noted that k_5, k_6 and k_7 are also identifiable and especially k_5 (XLF/XRCC4/Ligase IV end ligation) and k_7 (Artemis end processing) have very different values in both models, so they require further experimental investigation to understand their role in AR and NHEJ interaction.

In the models, the parameter for DNA-PKcs binding, k_2, is also an identifiable parameter in both treatment scenarios. The experimental results show that DNA-PKcs activity is reduced by half after ADT, however the modeling results show no significant difference for this parameter. The identifiability analysis has revealed that the parameters k_5, k_6 and k_7 are also identifiable. There is around a 2-fold difference for k6 and 1.5 fold difference for k_7 between the two models, where the dynamics are faster in IR only case. However, k_5 is 1.4 fold slower in IR only case. Further experiments will be required to validate these computational observations and to determine the role of the change of the dynamics of the end ligation by the protein complex XLF/XRCC4/Ligase IV, the release of the repaired DNA and the

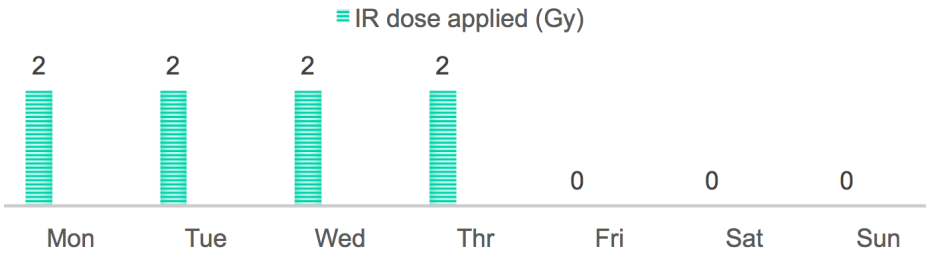

Figure 2.4: Weekly IR Treatment Plan

end processing by Artemis in improved radiosensitivity after ADT.

2.2.5 Quantitative Analysis of the Treatment Outcome

Conventional Fractionated Radiation Treatment Outcome

In [10], in addition to measuring DSB repair kinetics using γH2AX foci, percentage of Sub-G1 cells were also measured post IR+ADT treatment. It is observed that the accumulation of DSBs following an impaired NHEJ repair leads to more Sub-G1 cells.

The IR treatment in a clinical setting will be delivered as smaller doses over a period of multiple days. To simulate the fractional IR treatment with ADT, we use our model with the optimized parameters to simulate the effect of multiple doses of IR that are delivered every 24 hours during a treatment period of one week to mimic the conventional, fractional radiation treatment. We consider the patients receiving IR treatment with the same dose of 2 Gy on the first four days of a week with no treatment for the rest of the week. Since DSB formation process takes much less time than the repair process, we assume that the DSB forms at the time when IR is applied as an impulse function with the absolute value relates to dose density.

We have simulated multiple dose of IR of 2 Gy and use our model to study the repair dynamics of such treatment. Referring to Figure 2.5a, each time IR is applied the DSB will increase instantaneously. We observe that for a one week treatment delivery, the DSBs accumulate more for IR+ADT treatment scenario compared to IR only case. By the end of one week, there are more DSBs remaining for the combination

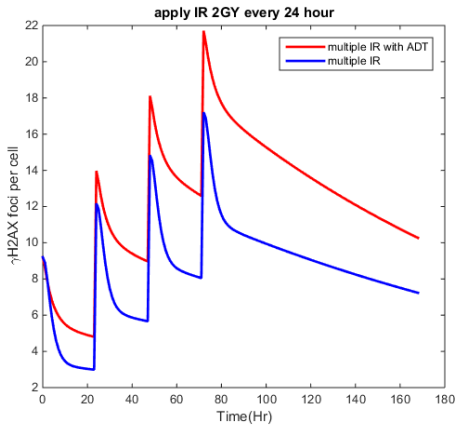

(a) model simulation of averaged DSB amount per cell in a weekly treatment schedule

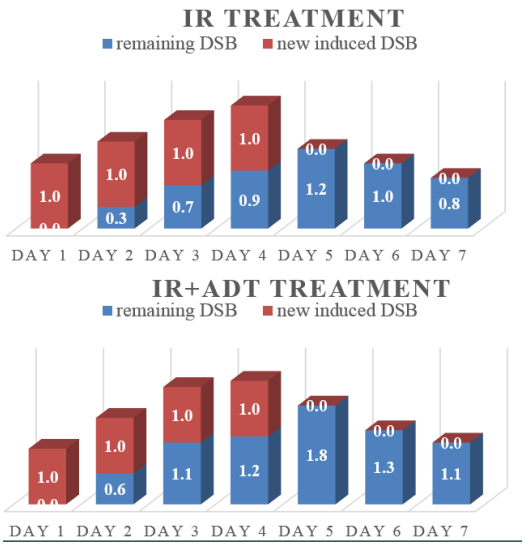

(b) IR induces identical damage amount each day, the remaining damage amount after repair is greater in IR+ADT

Figure 2.5: Averaged DSB per Cell in the Weekly Schedule Treatment Plan

treatment of IR and ADT, showing that cell radiosensitization is increased by adding ADT to IR that leads to inhibition of NHEJ repair pathway.

Variability in Patients Response to Identical Treatment Plans

According to the data in [26], individuals react differently to ADT because of variations in age, tumor size, prostate volume, etc. The measurements using patient samples have shown that castration therapy can lead to decrease of Ku70 and the data is as shown in Figure 2.6. Ku70/80 is the first protein that attaches to the DSB ends, which is also a signal that initiates the NHEJ repair process. Therefore, a decrease in the Ku70 expression can directly slow down the repair process. Tissue samples from 14 patients were analyzed and the data obtained indicating that the levels of Ku70 before and after the castration therapy were different by an average of two fold. It was observed that while the treatment was successful in most of the patients, there were some patients who were unresponsive to castration with unchanged Ku70 levels. For majority of the patients, Ku70 levels dropped resulting in

Figure 2.6: Individual Patient Response to ADT: the Y axis represent relative Ku levels and the X axis indicate patients numbering, different patients have different responses to ADT and the differences are reflected in changes of Ku levels

impaired NHEJ and better radiosensitization. Ku70 intensity levels are implemented as protein level change in our models. It is observed that variations in Ku70 by ADT due to different patients profiles have a positive enhancement on IR treatment. It is also shown in [10] that when ADT is added to IR treatment, the relative number of C4-2 cells are dramatically decreased. Also, the doubling time for C4-2 is twice when having ADT+IR compared to IR treatment. In the meantime, relative Sub-G1 phase cells also show an increased value with ADT treatment together with IR at 24 hours post treatment. Therefore, combining ADT with IR leads to more cell death.

Based on the data in [60], we group the patients described above into three categories by their reaction to ADT with respect to Ku70 levels: very sensitive group, sensitive group, and not sensitive group. All the parameters except Ku are constants in both cases, only changing Ku70/80 protein levels, which corresponds to Ku70 level change after castration. The results are listed in Figure 2.7, Figure 2.8 and Figure 2.9. The variations in ADT responses result in variable radiosensitization improvement. The group that is sensitive to ADT have a significant decrease in Ku70 levels, and as a result, this group has a better outcome for the combination treatment of IR and ADT.

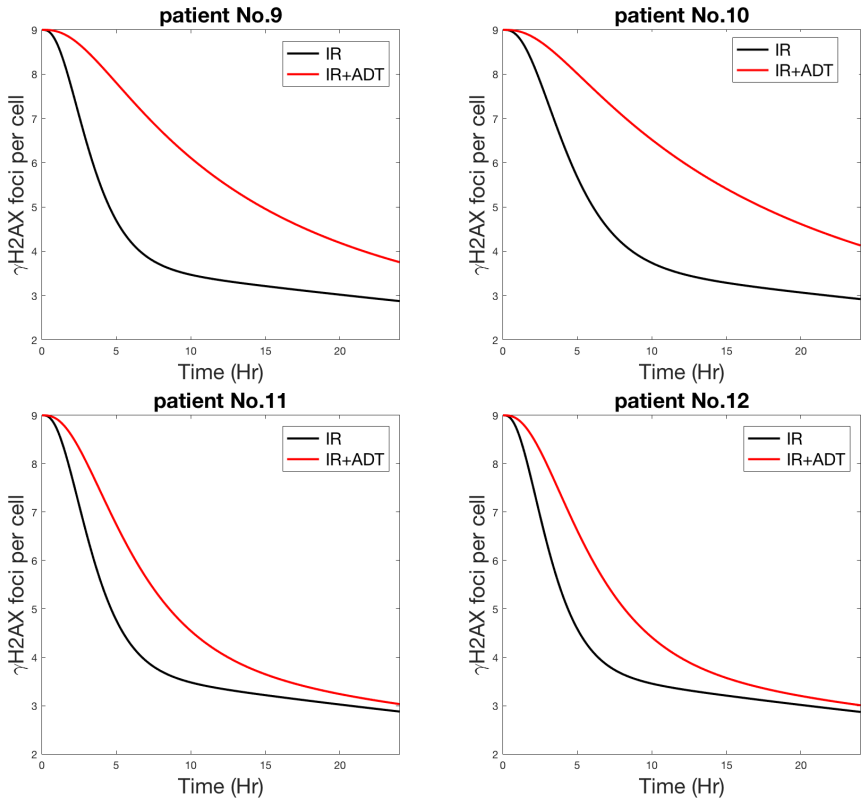

Figure 2.7: Patients Group Sensitive to ADT

2.3 *In Silico* HR Models of Radiotherapy for Prostate Cancer

The purpose of this section is to computationally analyze how the interactions between androgen receptor (AR) and homologous recombination (HR) affect the treatment outcome for ionizing radiation (IR) combined with androgen deprivation therapy (ADT) for prostate cancer (PCa). Combination treatment with radiation and ADT is currently a standard treatment for PCa as demonstrated in previous section. The effectiveness of radiation treatment alone depends on the cells capacity to repair the damage that is mostly in the form of double-strand breaks (DSBs). Two major pathways that repair DSBs are NHEJ and HR. The experimental data in the literature show that AR promotes both NHEJ and HR following IR, and inhibition of AR by ADT impairs both of these pathways in PCa cells leading to either increased

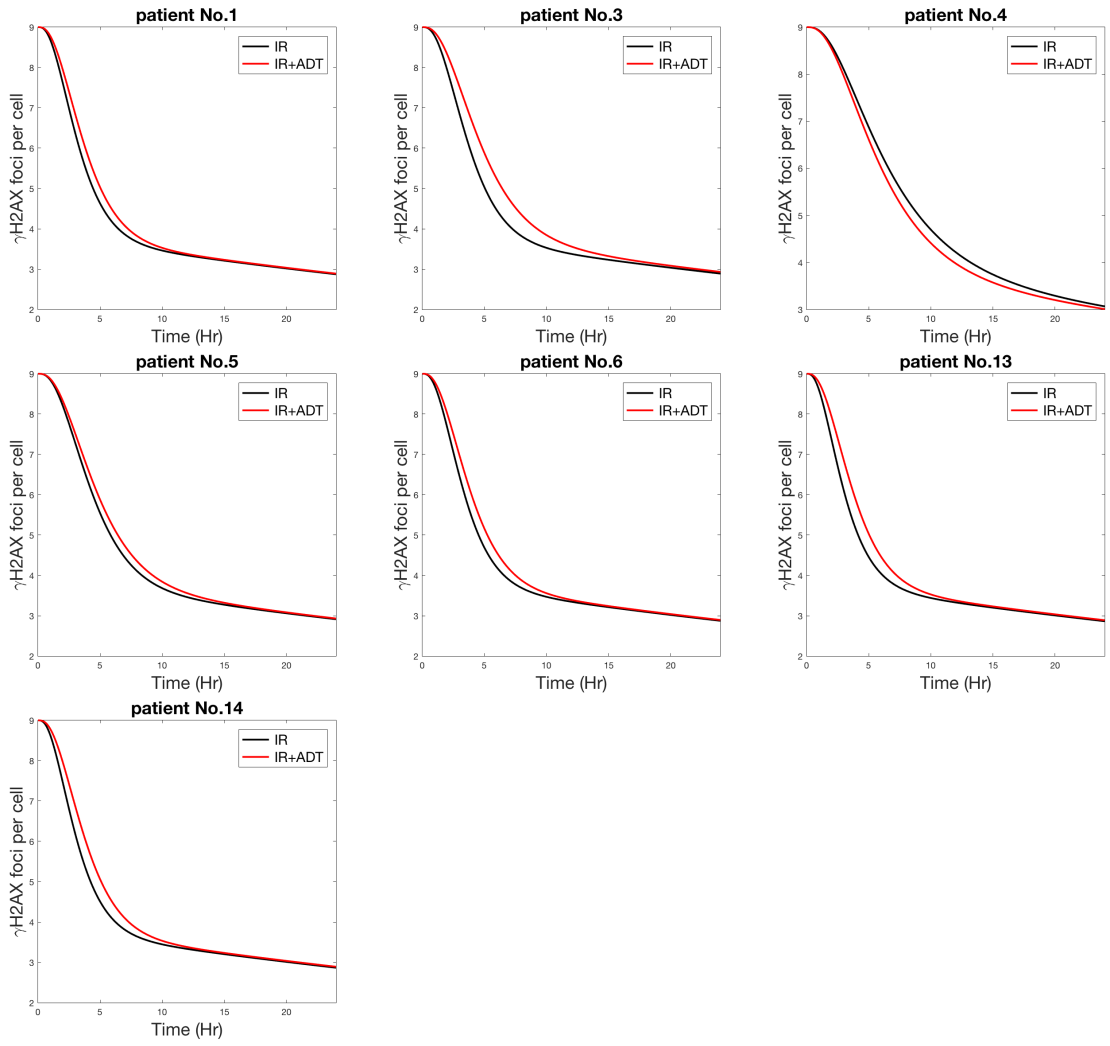

Figure 2.8: Patients Group Less Sensitive to ADT

radiosensitivity or sensitization to PARP inhibitors. In the previous section in this chapter, we developed mathematical models of the NHEJ pathway and in this section, we have developed such models for HR to comprehensively analyze the response of PCa cells to IR combined with ADT. We have modeled HR using a series of ordinary differential equations. The parameters that needed to be estimated are the kinetic rate constants, and we have used the least square estimation to obtain these model parameters. The data sets used in the parameter estimation were obtained from the literature [11] and they were from both *in vitro* experiments as well as clinical data from PCa patients. The experimental data show that AR influences the DNA end

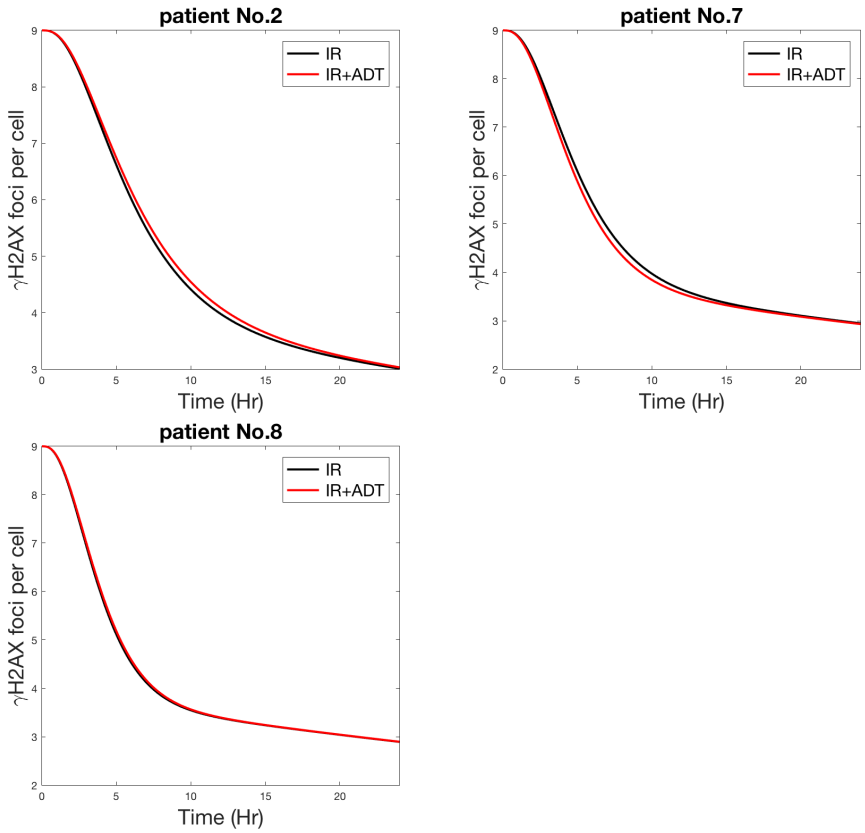

Figure 2.9: Patients Group not Sensitive to ADT

resection that is required for proficient HR and we have computationally included this effect in the kinetics of the models. We have developed models for IR treatment alone or in combination with ADT. We have carried out sensitivity analysis and identifiability tests on all the parameters from both models in order to determine the parameters that are reliably estimated. The outputs from both NHEJ and HR models show that the suppression of AR activity through ADT has the potential to enhance the IR treatment outcomes for PCa patients. The impairment of HR by ADT also opens up an avenue for achieving synthetic lethality using PARP inhibitors as shown in the literature; the HR model is extended for simulating efforts to include the effect of PARP inhibitors on the treatment outcome.

2.3.1 HR Pathway Mechanism

The effectiveness of IR treatment depends on the amount of induced damages and the repair status of the cancer cells. DSBs are the major DNA damages following IR and are repaired by multiple repair pathways. This repair reduces the effectiveness of the treatment leading to resistance to IR. DSBs are repaired by one of the two pathways: NHEJ and HR. NHEJ is the major pathway through the whole cell cycle whereas HR is restricted to S and G2 phases of the cell cycle after DNA replication has been completed. Targeting the DNA repair pathways is effective in modulating the repair efficacy. In the previous section, we have quantitatively studied the role of NHEJ in enhancing the outcome of the combination treatment with ADT and IR for PCa. We analyze the role of HR for the same combination therapy with radiation plus ADT in this section.

The major proteins that are involved in the HR pathway in human cells are: MRN complex, BRCA, Rad51, Rad52, Rad54, RPA, ATM, CtIP and polymerase. [29, 63]. The mechanism of HR is summarized as follows:

i) DSBs detection [64, 65]:

MRE11-Rad50-NBS1 (MRN complex) interacts with each free end of DSB.

MRN interacts with ATM (a kinase) and activates it through autophosphorylation.

ATM phosphorylates H2AX on the serine residue to become γH2AX.

γH2AX recruits checkpoint kinase ChK2 and activates it.

Both ATM and ChK2 phosphorylate p53, p53 further induces expression of proteins involved in repair.

ii) Two-step extended DNA end resection (3-5 by MRN and 5-3 by Exo1 or DNA2) [66, 67]:

MRN component NBS1 then interacts with CtIP.

MRN conformational change activates MRE11 endonuclease activity so that MRE11 is accessible to DNA; then this whole complex will move backwards $5'$ to $3'$ about 100-

200bp (MRE11 endonuclease activity cut at 100-200bp site, and then move forward as exonuclease to trim the DNA from $3'$ to $5'$).

Exo1 or DNA2 continue to resect DNA from $5'$ to $3'$ resulting in about 1000bp overhang.

iii) Formation of Rad51 single stranded DNA nucleofilament [68, 69]:

RPA binds to the single stranded DNA (3 overhang about 1000bp), RPA functions to protect the single stranded DNA, and RPA will be replaced by Rad51.

BRCA2 binds to Rad51 preventing it from binding to double stranded DNA, serves as a nucleation point of Rad51 filament and facilitating the exchange of RPA off and addition of Rad51 to the single strand overhang. This structure is called Rad51 single stranded DNA nucleofilament.

Rad51, ssDNA, ATP form ternary complex.

iv) Strand invasion (homology search) [70, 71]:

Filament invades the template sister chromatid.

Rad54 associates with and stabilizes the Rad51 filament, which targets Rad54 to the pairing site.

D-loop is formed which is stabilized by RPA.

Rad54 also helps to dissociate Rad51 which allows DNA synthesis mainly by DNA polymerase δ or polymerase ϵ.

v) Choice of downstream sub-pathway (depends on D loop stability) [72]:

The downstream sub-pathway includes synthesis-dependent strand annealing (SDSA) (non-crossover repaired DNA) and double strand break repair (DSBR) crossover repaired DNA), and most D loops are repaired by SDSA.

The increased level of HR components result in poor treatment response to IR. For PCa, the hormone level is also a key element that influences the treatment effectiveness. Generally, in most clinical treatment approaches, a combination of ADT and IR is widely used in order to improve patients overall survival probability. AR ac-

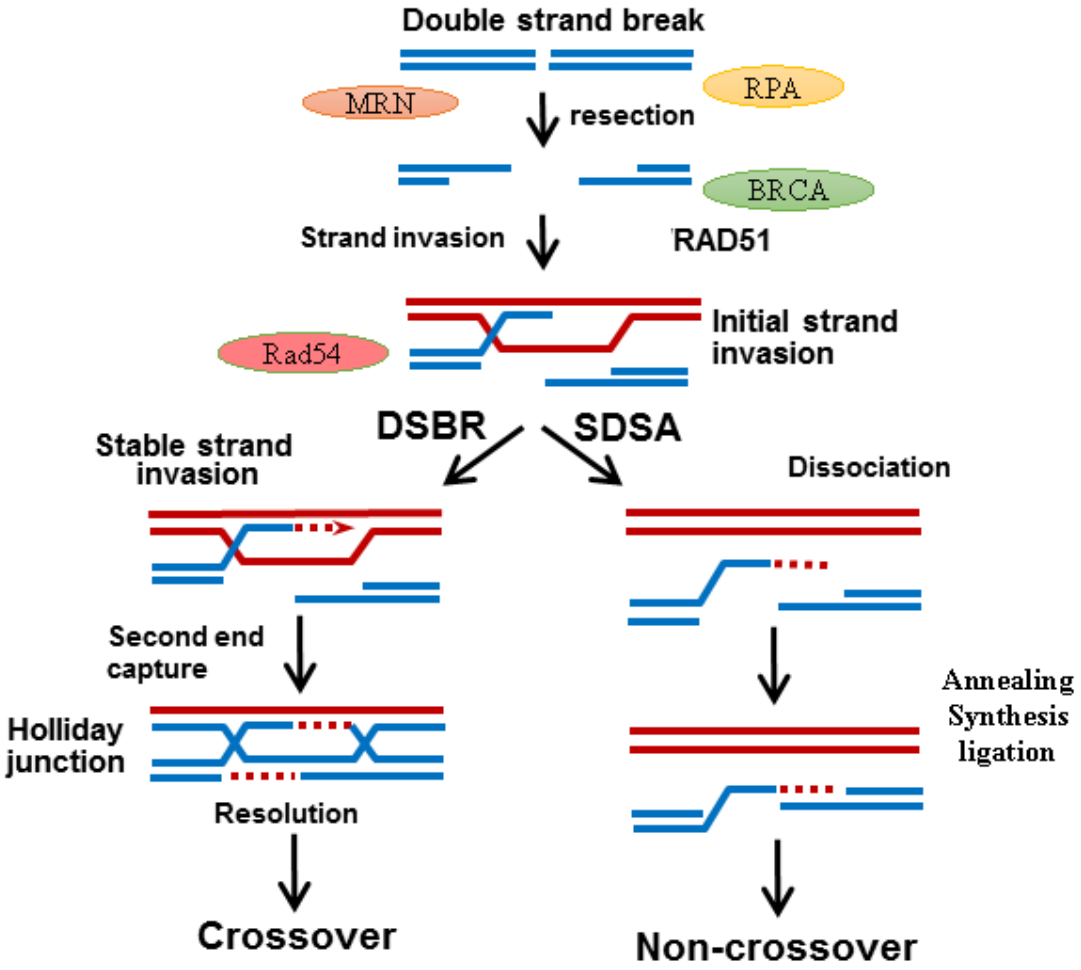

Figure 2.10: Homologous Recombination Mechanism [73]: MRN complex interacts with DSB ends and initiates end resection; RPA binds to DNA damage ends for protection; BRCA binding for facilitating the exchange of RPA off and addition of Rad51 to the single strand overhang; Rad51 filament invades the sister chromatid and starts strand invasion; Rad54 binds, D-loop formation and end capturing; DSBR pathway: second end capturing,Holliday junction formation and resolution, and crossover repaired DNA; and SDSA pathway: dissociation, DNA synthesis, ligation, and non-crossover repaired DNA.

tivities mediate androgen, which is the key factor of prostate cancer progression [74]. Therefore, targeting AR activities is a potential approach to limit tumor growth. AR inhibition by ADT impairs HR and as a result, IR treatment outcome is enhanced [75]. It is demonstrated in [11] that reduced AR signaling activities inhibits HR by down regulating HR proteins including MRE11 (MRN) and Rad51. ADT further

promotes PARP activities in PCa. In addition, PARP inhibitor traps PARP and enhances IR treatment outcome in cells with deficient HR. It is also shown that HR deficiency leads to increased activities of PARP [76]. As reviewed in [77], BRCA mutation results in HR pathway deficiency and in such cancers, base excision repair is entitled as the alternative repair pathway. In this scenario, the use of PARP inhibitor (PARPi) opens up an avenue for synthetic lethality because PARPi inhibits BER leading to DNA damage accumulation. It is shown in [78] that PARPi cause lethal damage to cells with gene mutations of BRCA, ATM and some other HR proteins. It is proposed that PARP inhibitor treatment combined with ADT can have better outcome for cancer patients [11].

In this section, the effect of AR in promoting DNA repair is studied by developing a quantitative model of the HR using the experimental data from [10]. Understanding this mechanism is important for possible enhancement of the treatment of PCa where the growth and progression is AR activity dependent. Here, we quantify the effect of AR and PARPi on the HR pathway. This is an important step in quantitatively analyzing possible treatment scenarios to find the optimal treatment strategies for PCa using the combination treatment of ADT, PARP inhibitors, and IR. HR model is developed in this section for PCa and this model is used to study the effect of AR and PARPi on the repair dynamics after the IR treatment with ADT.

2.3.2 Mathematical Model of HR

The mechanism of HR is simplified with the following steps in the model development as shown in Figure. 2.10:

a) MRN complex interacts with DSB ends and initiates end resection;

b) RPA binds to DNA damage ends for protection;

c) BRCA binds for facilitating the exchange of RPA off and addition of Rad51 to the single strand overhang;

d) Rad51 filament invades the sister chromatid and starts strand invasion;

e) Rad54 binding, D-loop formation and end capturing;

f) DSBR: second end capturing;

g) DSBR: Holliday junction formation and resolution;

h) DSBR: crossover repaired DNA;

i) SDSA: dissociation;

j) SDSA: DNA synthesis, ligation;

k) SDSA: non-crossover repaired DNA.

We have modeled the above activities using the law of mass-action kinetics and the resultant model is given below where Y_i represents the intermediates produced by DSB and enzyme reaction complex; e_i represents the enzyme concentrations which are multiplied with k_i, the enzyme kinetic rate constants, respectively. We assume all concentrations to be equal to each other in the simulations. k_is are the parameters to be estimated in this simulation. Due to the structure of this model from law of mass action, enzymes concentrations and kinetic constants cannot be estimated independently from each other as they are multiplied to each other. The observed affact on rate constants can be considered as a similar effect on the corresponding concentration.

$$\frac{dY_1}{dt} = -k_1 e_{MRN}[Y_1] \tag{2.15}$$

$$\frac{dY_2}{dt} = k_1 e_{MRN}[Y_1] - k_2 e_{RPA}[Y_2] \tag{2.16}$$

$$\frac{dY_3}{dt} = k_2 e_{RPA}[Y_2] - k_3 e_{BRCA}[Y_3] \tag{2.17}$$

$$\frac{dY_4}{dt} = k_3 e_{BRCA}[Y_3] - k_4 e_{Rad51}[Y_4] \tag{2.18}$$

$$\frac{dY_5}{dt} = k_4 e_{Rad51}[Y_4] - k_5 e_{Rad54}[Y_5] \tag{2.19}$$

$$\frac{dY_6}{dt} = k_5 e_{Rad54}[Y_5] - k_6 e_{SDSA}[Y_6] - k_9 e_{DSBR}[Y_6] \tag{2.20}$$

$$\frac{dY_7}{dt} = k_6 e_{SDSA}[Y_6] - k_7 e_{ligation}[Y_7] \tag{2.21}$$

$$\frac{dY_8}{dt} = k_7 e_{ligation}[Y_7] - k_8[Y_8] \tag{2.22}$$

$$\frac{dY_9}{dt} = k_9 e_{DSBR}[Y_6] - k_{10} e_{res}[Y_9] \tag{2.23}$$

$$\frac{dY_{10}}{dt} = k_{10} e_{res}[Y_9] - k_{11}[Y_{10}] \tag{2.24}$$

$$\frac{dY_{11}}{dt} = k_8[Y_8] + k_{11}[Y_{10}] \tag{2.25}$$

The data in [60] show that around 80 percent of DSBs are repaired by NHEJ and the rest (20 percent) are repaired by HR. We have scaled the experimental data in [10] on γH2AX foci by a factor of 0.2 in order to capture the portion of the DSBs that are repaired by HR. The units for k_1-k_7, k_9 and k_{10} are $molecule^{-1}s^{-1}$, for k_8 and k_{11}, units are s^{-1} in Table 2.5. In the optimization, equation 2.13 is used as the objective function of "fmincon" in Matlab (The MathWorks, Inc, Natick, MA) that we used to calculate the optimal results. The parameters are constrained to be all positive as they are the rate constants.

2.3.3 Sensitivity and Identifiability Analysis

Sensitivity Analysis

We investigated how the parameters change, especially how kinetics for MRN complex and Rad51 change, when ADT is added to the treatment. In order to determine if the changes we observe are biologically significant, we have conducted parameter sensitivity analysis. The changes in the parameters in response to different treatments can be considered biologically relevant only for those parameters for which the model is sensitive. We have calculated the sensitivity gain using the equation 2.14.

Identifiability Analysis

An identifiability analysis for HR protein rate constants is performed using the same method as mentioned in NHEJ modeling. The results are presented together with sensitivity gains calculated for all the parameters in Table. 2.6.

2.3.4 Quantitative Analysis of the Role of HR in Response to IR for Prostate Cancer

We have used the data in [10] to estimate the HR model parameters. The experimental data we have used in the parameter estimations are scaled with the factor 20% which is overall HR efficiency for DSB repair.

Modeling Results

We have modeled the experimental observations of AR effect on MRN and Rad51 quantitatively by using the HR models. We have first developed the model for the cells with proficient androgen and estimated the model parameters for the treatment with IR. We have then used the experimental data for the IR combined with ADT treatment case to estimate the model parameters. We have used our original model parameters estimated for the IR only case as our initial parameter set for parameter estimation in the case of IR+ADT treatment. The aim of this approach is to identify which parameters will be affected most after androgen deprivation. Experimentally it is observed that MRN and Rad51 activity is affected from androgen deprivation [11] and in our models this effect is captured as the difference in the rate constants for MRN and Rad51 before and after androgen deprivation. The hypothesized effect is that the expressions of MRN and Rad51 are changing due to androgen deprivation, which would ultimately affect the protein concentrations of MRN and Rad51. In our model, the effect of protein concentration change or kinetic constant change result in

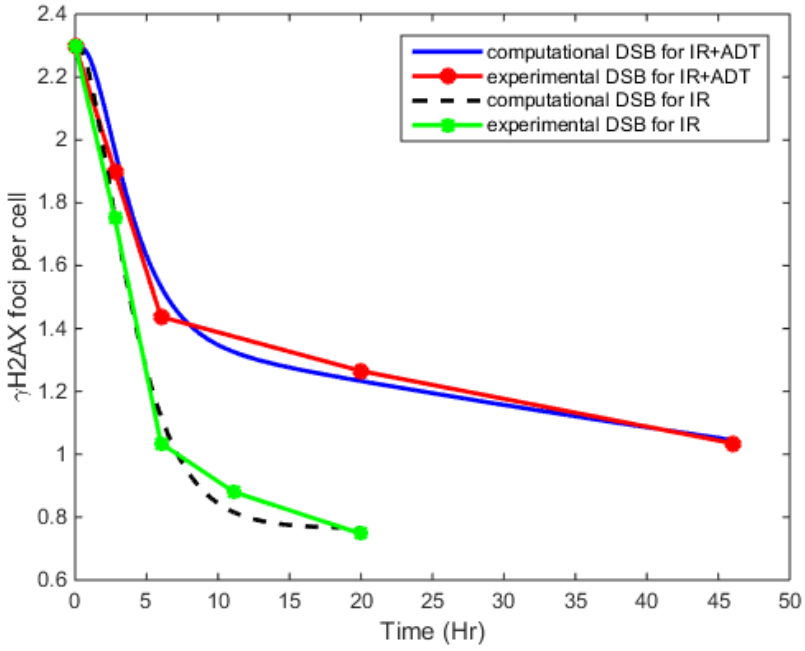

Figure 2.11: HR Model Results with Optimized Parameters for IR and IR+ADT Treatment

the same system output, because they appear in the form of $k_1 e_{MRN}$ and $k_4 e_{Rad51}$. So, any changes we observe in k_1 can also be considered as a change in protein concentration of the same ratio. The model parameters are given in Table 2.5. The modeling results are also given in Figure 2.11 together with the experimental data. The models are successful in capturing the experimentally observed repair dynamics.

Comparing the last two columns in Table 2.5, it is found that k_1 and k_4 values are decreased when ADT is combined with IR. Since k_1 and k_4 are both sensitive and identifiable as tested below, the parameter changes in k_1 and k_4 are biologically significant results. k_1 is the kinetic rate constant for MRN, which is the first protein binds to DSB in HR pathway as an initiator; and k_4 is the kinetic rate constant for Rad51, which is treated as the marker of HR pathway that mediates HR instead of other compensation pathways such as SSA. The interaction of AR with MRN and Rad51 influence DSB repair by HR. When ADT is combined with IR, the suppression

Table 2.5: HR Model Parameters

Name	Description	Value (IR)	Value (IR+ADT)
k_1	MRN	$3.92 * 10^{-9}$	$2.0 * 10^{-9}$
k_2	RPA	$3.48 * 10^{-10}$	$3.48 * 10^{-9}$
k_3	BRCA1/2	$3.37 * 10^{-8}$	$1.16 * 10^{-8}$
k_4	Rad51	$3.68 * 10^{-8}$	$2.15 * 10^{-8}$
k_5	Rad54 end capture	$1.38 * 10^{-4}$	$1.38 * 10^{-4}$
k_6	polymerase	8.7232	1.9555
k_7	gap synthesis	$1.55 * 10^{-3}$	$3.18 * 10^{-10}$
k_8	ligation	$1.28 * 10^{-4}$	$1.89 * 10^{-4}$
k_9	second end capture	4.3554	3.0105
k_{10}	Holliday junction resolution	0.11	0.11
k_{11}	ligation	$3.05 * 10^{-8}$	$1.76 * 10^{-6}$

of AR results in a decrease of the reaction rate of MRN and Rad51, and leads to HR deficiency.

The models developed for IR and IR+ADT are extended to include PARPi effects. The PARPi trapping on DNA results in inhibition of both BER and HR resulting in a large number of unrepaired DSB in HR defective cells. This activity reveals the potential of PARPi in promoting cell death and suppressing tumor growth for patients with a BRCA mutation. Due to this characteristic, it is proposed to have PARPi treatment combined with ADT and IR for enhancing the treatment outcome. PARPi impacts BER activities and the effects and its modeling are to be further discussed in Chapter 4.

Parameter Sensitivity and Identifiability Analyses Results

Referring to Table 2.6, through the calculation of sensitivity gain, it is observed that k_1-k_4, k_6, k_8, k_9 and k_{11} are sensitive parameters under both treatment scenarios, while the models are not sensitive to k_5 and k_{10} regardless of treatment approaches. The model is sensitive to k_7, however it is not a sensitive parameter in the IR model.

The identifiability results are presented in Table 2.6 as well, where + represents

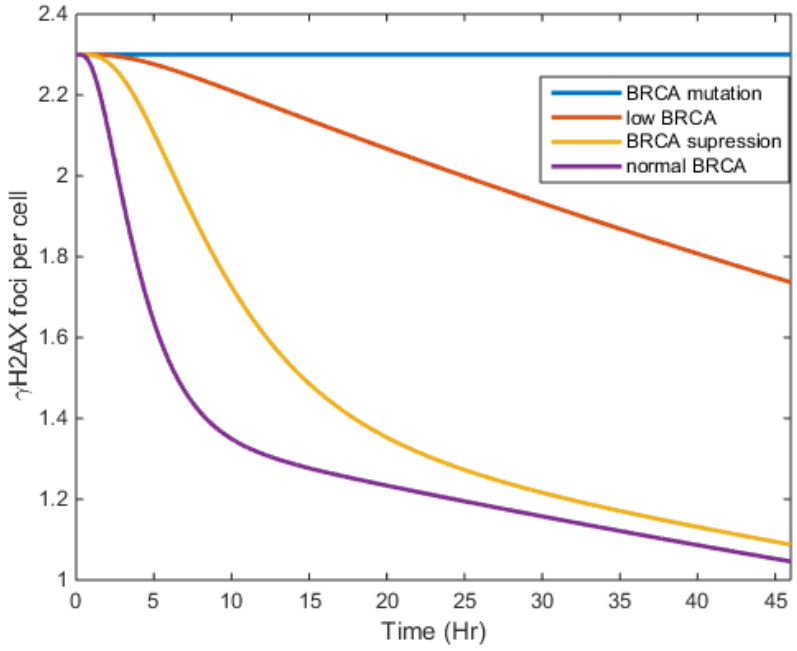

Figure 2.12: HR Efficiency for varying BRCA Protein Concentrations

error increased when the parameters are re-estimated, meaning that the parameter is identifiable. On the contrary, − shows that error remained the same, thus the parameter is non-identifiable. The identifiability test has a similar result as the sensitivity test, k_1-k_4, k_6, k_8, k_9 and k_{11} are not only sensitive parameters but also identifiable under both conditions. It is observed that k_6, the polymerase; k_8, the ligase and k_9, the second end capture in DSBR pathway rates show strong sensitivities in both models while k_1-k_4 are only marginally sensitive. The parameters k_5 and k_{10} are neither sensitive nor identifiable for both treatment scenarios. k_7 is neither sensitive nor identifiable in HR model for IR, however it is highly sensitive and identifiable in the HR model for combination treatment of IR and ADT. A 0.5 fold decrease is observed in MRN enzymes levels and a 0.4 fold decrease is observed for Rad51 under the combination treatment scenario.

Table 2.6: Sensitivity Analysis and Identifiability Test Result for Parameters of HR Gene

	IR		IR+ADT	
Name	Sensitivity Gain	Identifiability	Sensitivity Gain	Identifiability
k_1	0.58	+	1.26	+
k_2	10.71	+	0.70	+
k_3	0.06	+	0.20	+
k_4	0.05	+	0.11	+
k_5	0.00	-	0.00	-
k_6	16.97	+	13.44	+
k_7	0.00	-	6.70	+
k_8	11.59	+	4.91	+
k_9	9.37	+	2.95	+
k_{10}	0.00	-	0.00	-
k_{11}	0.002	+	1.88	+

2.4 Detailed Identifiability Analysis

2.4.1 Strategy I: Data Sampling Technique

In order to analyze the effects of experimental data sampling frequency on parameter estimation and identifiability, a synthetic data generation scheme is developed. A new data sets is generated and the model is rebuilt with the new data set to study the effect of sampling on identifiability. This study tests a potential experimental data measurement method for computational model construction that results in improved identifiability.

Synthetic "experimental" data is generated using the NHEJ model constructed for prostate cancer cells in previous sections.

Improving the identifiability of the parameters is important to be able to use the models to test different mechanistic observations about the interaction between the AR and NHEJ dynamics. In [79], it is recommended to measure additional time points to increase the amount of data used in the parameter estimation. It is also

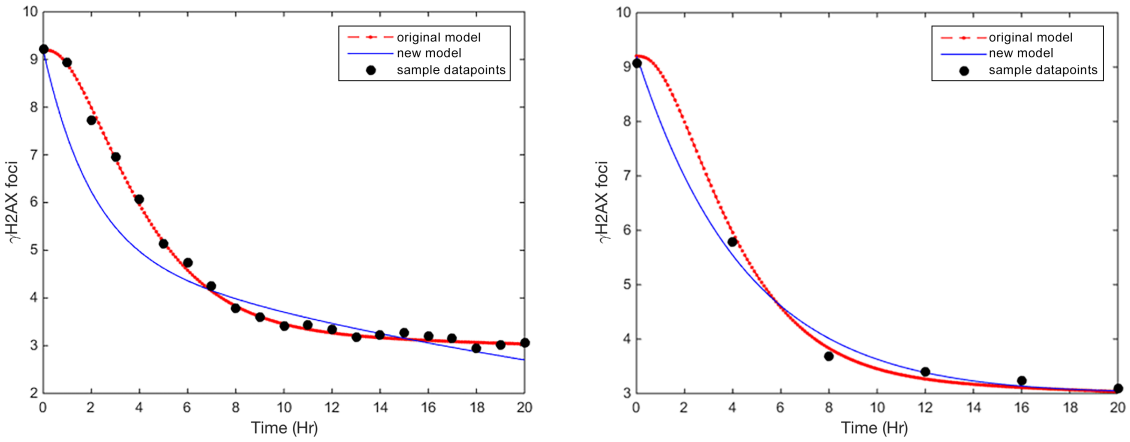

Figure 2.13: Two Sampling Strategies: Panel one has samples every hour, panel two has only six samples. Modeling results show that sampling frequency did not effect model results.

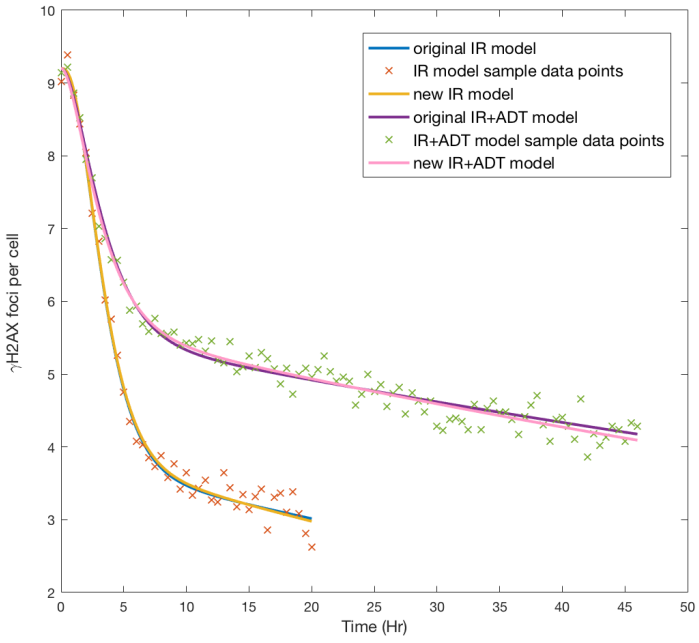

Figure 2.14: Data Sampling Strategies: Sampling with every half hour for IR and IR+ADT models

recommended to measure additional molecular species to overcome the structural non-identifiability.

In order to test the effect of data sampling rate on improving the identifiability

of the rate constants, an experimental strategy is developed. Because of the models ability to capture the experimental repair dynamics successfully as shown in Figure 2.3, these models are assumed to be the underlying experimental models and they are used as toy models to understand the influence of different data sampling schemes on the parameter identifiability. The model outputs are sampled using different scenarios to understand the role of increasing the amount of data on identifiability. In Figure 2.13, the output from original model is sampled every hour and also sparsely, and uniform noise is added. The model outputs taken every half hour are then assumed to be the experimental data and white noise with a signal to noise ratio of 15 is added to the model outputs in order to mimic the experimental variability in Figure. 2.14. These model outputs are then assumed to be the experimental data and the parameter estimation and identifiability analysis are carried out using this data.

The scenarios tested include sampling different number of data points uniformly along the entire time interval during which the original experiments were conducted. In all the different sampling scenarios it is observed that more data points on the final outcome, which is the amount of repaired DSBs, did not improve the identifiability of the parameters. The identifiable parameters remained identifiable with no improvement for the non-identifiable ones. These observations lead to the conclusion that as long as there are data points that capture the entire trend in the outcome, having more points on the same time course does not improve the identifiability.

2.4.2 Strategy II : Model Re-structure Technique

The second strategy that is tested here is to include the intermediate repair product dynamics in the error function for the parameter estimation or alternatively inhibiting the pathway at different reactions and measuring the outcome as the output of an intermediate reaction that becomes the final reaction in the pathway. The following model with the parameters given in Table 2.3 is used to generate the experimental

data on the intermediate product, which in this case is Y_5 representing the amount of DSB bound by DNA-PKcs that has already gone through two auto-phosphorylations.

$$\frac{dY_1}{dt} = \alpha \frac{dDose}{dt} - k_1 e_{Ku}[Y_1] \tag{2.26}$$

$$\frac{dY_2}{dt} = k_1 e_{Ku}[Y_1] - k_2 e_{DNA-Pkcs}[Y_2] \tag{2.27}$$

$$\frac{dY_3}{dt} = k_2 e_{DNA-Pkcs}[Y_2] - k_3[Y_3] \tag{2.28}$$

$$\frac{dY_4}{dt} = k_3[Y_3] - k_4[Y_4] \tag{2.29}$$

$$\frac{dY_5}{dt} = k_4[Y_4] \tag{2.30}$$

This strategy has not improved the identifiability of the unidentifiable parameters. It is concluded that in order to estimate the unidentifiable parameters, an experimental design that includes measuring all the NHEJ repair protein binding time courses using chromatin recruitment assays as presented in [80] would be required to study each protein interaction independently.

2.5 Conclusion

Computational models for the NHEJ repair dynamics in prostate cancer cells are developed in parallel with HR repair modeling to analyze the mechanism of the interaction between AR and NHEJ or between AR and HR, and the role of these interactions in enhancing or reducing the effectiveness of IR treatment. The computational results show that the inhibition of AR activity through ADT inhibits the NHEJ activity by changing the dynamics of the first protein Ku in NHEJ pathway. The radiosensitivity also increases when IR is combined with ADT through inhibition of HR, and this is captured as the changes in Ku and MRN protein dynamics in the models. The sensitivity and identifiability analysis results show the biological

relevance of the observed changes in parameters. The computational results also explain both the experimental and clinical observations presented in the literature. The models and the analysis form the first steps toward developing a combined treatment strategy for better prostate cancer patient outcomes.

Due to variability in patients responses to ADT, there are different Ku70/80 level changes before and after the treatment. Our simulations show that most patients exhibit better radiosensitization due lower Ku70/80 levels after combination treatment. The dose of IR can be adjusted with respect to the level of radiosensitization after ADT on a patient specific level to achieve a desired level of DSBs that will lead to maximum cell death; determining the optimal dose quantitatively will form the basis of the future work.

Chapter 3

Cell Cycle Dependent Modeling of DSB Repair

The effectiveness of IR treatment depends on the amount of induced damages and the DNA damage repair status of the cancer cells. DSBs are repaired by multiple DNA repair pathways and this repair reduces the effectiveness of the treatment, which leads to resistance to IR. Non-homologous end joining (NHEJ) and homologous recombination (HR) are the two pathways that repair DSBs. NHEJ is the major pathway that works throughout the cell cycle, whereas HR is restricted to S or G2/M phases of the cell cycle after DNA replication has been completed.

It has been shown in the literature that the increased levels of NHEJ components result in poor treatment response to IR and cancer has progressed even after the IR treatment [10], and the effectiveness of treatment is often measured by the efficiency of DNA repair pathways. In response to IR induced DSBs, repair pathways are activated. In the meantime, the cell cycle arrest in G1, S and G2 phases are triggered. Our goal is to mathematically model the DSB repair pathways in order to study their role in resistance to IR [81]. The contributions of HR and NHEJ to the repair of DSBs are cell cycle phase dependent, so there is a necessity to identify the differences

in the kinetics of these pathways in different cell cycle phases.

3.1 Cell Cycle Dependent Mathematical Modeling of DSB Repair

3.1.1 Cell Cycle Modeling Background Review

Data driven modeling approaches for the cell cycle focused on using ODEs to model cell cycle protein kinetics have been developed in the literature [82, 83, 84]. In [62], the authors proposed asynchronous probabilistic cell cycle models to quantitatively analyze the relationship between cell cycle dynamics and mismatch repair status during up to two cell population doubling following single agent (IUdR or IR) and combined (IUdR+IR) treatments. Considering the cell cycle system a finite state dynamic system, the states are defined as cell cycle phases (G1, S, G2 and M). The details of the model are described as follows: n1, n2, and n3 are the cells that progress into G1, S, G2/M phases per unit time, f is a probability density function which represents the duration of time of transition from one phase to another, and the states are expressed as below:

$$n_1(t) = 2\int_{-\infty}^{t} n_3(\lambda) f_3(t-\lambda) d\lambda = 2n_3(t) * f_3(t) \tag{3.1}$$

$$n_2(t) = \int_{-\infty}^{t} n_1(\lambda) f_1(t-\lambda) d\lambda = n_1(t) * f_1(t) \tag{3.2}$$

$$n_3(t) = \int_{-\infty}^{t} n_2(\lambda) f_2(t-\lambda) d\lambda = n_2(t) * f_2(t) \tag{3.3}$$

Taking the integration of all the transition per unit time equations, the cell numbers in the three stages are:

$$N_1(t) = \int_{-\infty}^{t} [n_1(\lambda) - n_2(\lambda)] d\lambda \tag{3.4}$$

$$N_2(t) = \int_{-\infty}^{t} [n_2(\lambda) - n_3(\lambda)]d\lambda \tag{3.5}$$

$$N_3(t) = \int_{-\infty}^{t} [n_3(\lambda) - 0.5n_1(\lambda)]d\lambda \tag{3.6}$$

writing in percentages:

$$G_1\% = \frac{N_1}{N_1 + N_2 + N_3} * 100\% \tag{3.7}$$

$$G_1\% = \frac{N_2}{N_1 + N_2 + N_3} * 100\% \tag{3.8}$$

$$G_1\% = \frac{N_3}{N_1 + N_2 + N_3} * 100\% \tag{3.9}$$

Parameters of the probability density functions of transition between each stage need to be estimated every time when there are changes to the system such as a new treatment approach.

In this chapter, we combine the NHEJ pathway and HR pathway models in a cell cycle dependent way to develop comprehensive DSB repair model. The output of this model is represented by cell number or percentages of cells in different stages. Acknowledging that NHEJ is the major pathway through all the phases of cell cycle, and HR is only active during S and G2/M phases, we can use the information on cell cycle phase to determine the accurate repair pathway for DSB repair. A more precise cumulative DSB number after applying IR treatment will be obtained by combining cell cycle model and NHEJ and HR repair models. Parameter estimation for the comprehensive model is performed using experimental data.

It has been shown in the literature that the increased levels of NHEJ components result in poor treatment response to IR and cancer has progressed even after the IR treatment [10]. For PCa, the hormone level is also a key element that influences the treatment effectiveness. Generally, in most clinical treatment approaches, a combination of ADT and IR is widely used in order to improve patients overall survival probability and it is proved to have positive results for PCa patients [26]. The stud-

ies in literature [10, 26] show that AR is activated through IR and that increased AR activity promotes NHEJ repair and increases the radio resistance of the cancer cells. On the contrary, when ADT is applied, there will be less AR activated. Therefore, the tumor cells present less radioresistance, and more DSBs remain compared to IR treatment only. In [26], four human prostate cancer cell lines are under test for studying the phenomenon of AR regulation caused by IR treatment. It shows that with increasing IR dose, there are more AR signaling activities *in vitro* and *in vivo*. Increased AR expression after IR relates to DNA repair pathways through the interactions of DNA repair proteins such as Ku70/80 and DNA-PKcs with AR. Thus the suppression of AR, such as by ADT treatment is a positive approach on enhancing IR treatment to have a better outcome.

In [26], in order to investigate how castration therapy affects NHEJ repair pathway, 14 patient samples are analyzed after castration, Ku 70 and γH2AX foci are tracked for recording. They observed that after castration, Ku70 level is decreased. Ku70, as the first protein that attaches to the DSB end that initiate NHEJ has a key role on the DNA process. The decrease in Ku levels, which increase cancer cells radiosensitivity and IR effectiveness is thus enhanced. [85] also reviews that AR signaling promotes DNA repair and radioresistance in PCa. The treatment option on how to combine IR and ADT for better outcomes is discussed. Other NHEJ targeting drugs are examined for a potential radiosensitization effect

The models for NHEJ and HR are developed in the previous chapter, and the changes in these pathway dynamics after IR/ADT treatment regimens were also captured. In the next section, we will discuss how to apply the model to more specific calculations under the influence of the cell cycle. In particular, the time course and rate of cancer cell proliferation under different treatment plans is examined by combining NHEJ and HR models with the cell cycle model.

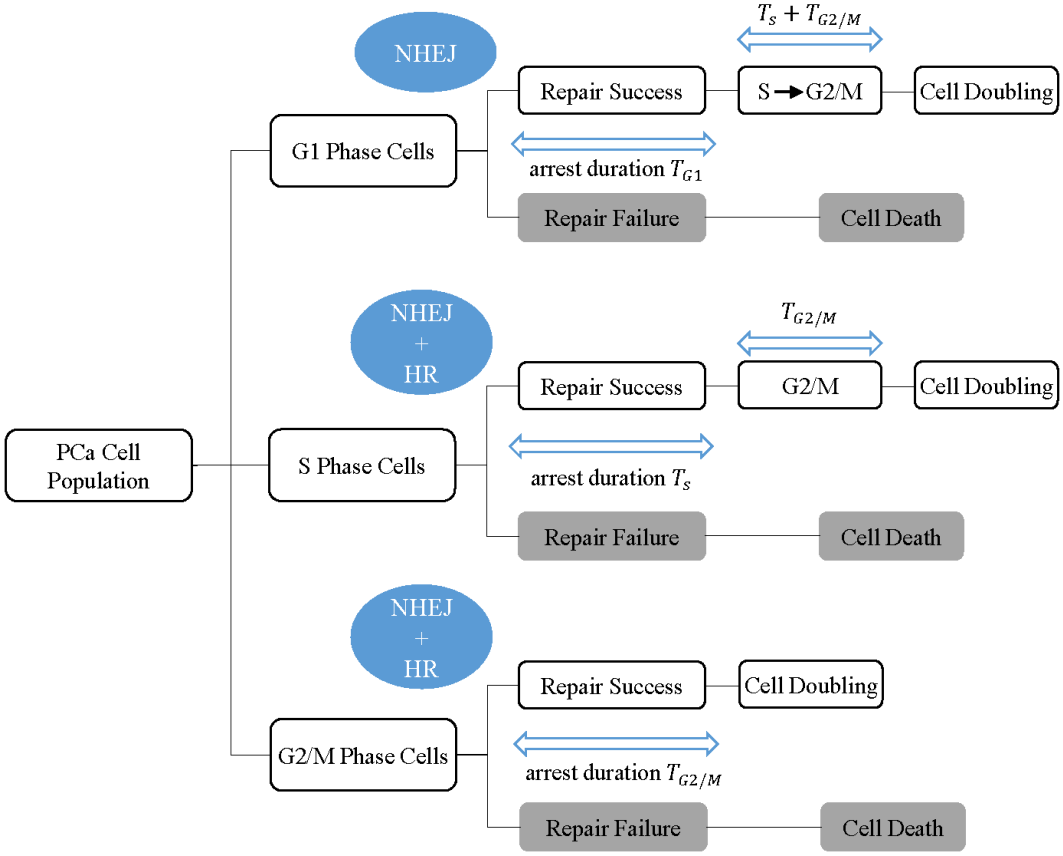

Figure 3.1: DSB Repair Flow in Separate Cell Cycle Phases (G1, S and G2/M)

3.1.2 Modeling Cell Cycle Progression after IR Treatment

The cells in a population are cycling in the asynchronous state under normal conditions. As analysed in [62], G1 phase cells, S phase cells and G2/M phase cells have changes in the dynamics when treated with IR or drugs. After a transition period, the cells reach steady state following the external disturbance. In this work, the changes to the dynamics are analyzed after IR and IR+ADT treatment. The initial assumption is that the average IR induced DSBs are N/M, where N is the number of DSBs and M is the number of cells. G1 phase cells react differently to the same IR dose from S phase cells. The difference also exists in G2/M phase cells. According to [86], there are about 2 fold increase in γH2AX foci detected in average in 40 human

cells for G2 phase cells compared to G1 phase cells under the same condition (15 min post 2Gy IR). The DSBs generated in S phases cells are taken to be around 1.5 fold higher than that of G1 phase cells [30]. A cancer cells population under treatment is grouped into G1, S and G2 phase cells. Using our assumption that the average DSB per cell is N/M, and under steady state conditions where the cell phase distribution is expressed as G1%, S% and G2/M%, then the initial conditions of averaged DNA damage per cell for each group are calculated by the following equations:

$$avg_{G1} = \frac{N/M}{G1\% + 1.5 * S\% + 2 * G2/M\%} \tag{3.10}$$

$$avg_{S} = \frac{1.5 * N/M}{G1\% + 1.5 * S\% + 2 * G2/M\%} \tag{3.11}$$

$$avg_{G2/M} = \frac{2 * N/M}{G1\% + 1.5 * S\% + 2 * G2/M\%} \tag{3.12}$$

When abnormal events occur during cell cycle progression, such as excessive DNA damage or DNA replication blocks, such regulatory mechanisms are activated to interrupt the cell cycle in a timely manner. After the damage is repaired, the cell cycle progression can resume. In the PCa treatment, when IR or other treatment is introduced, cell cycle arrest occurs in response to checkpoints signaling in G1, S, and G2/M phases. As mentioned in [5], the checkpoints arrest cells with damage in the current cell cycle phase until the DNA lesions are repaired or if the damage remains unrepaired, it finally leads to cell death. Cell cycle arrest period length depends on the repair efficiencies. The arrest period is defined from the time of detection of DNA damage accompanied by the onset of cell cycle arrest, to the time when the final repair is completed the cells either continue with cell cycle or die. The duration of this period is determined by many factors, such as damage complexity, repair protein concentration and kinetics, dose intensity, etc. Typically, a total of 24 hours is divided by about 11 hours in G1 phase, 8 hours in S phase and 5 hours in G2/M phase [87].

Table 3.1: C4-2 PCa Cell Doubling Time

control	1	24h
2Gy IR	1.249	30h
2Gy IR + ADT	3.979	95.5h

Because of the wide range of factors that determine cell cycle arrest duration, here we make assumptions about cells that successfully go through DNA damage repairing:

the G1 group has the average cell cycle arrest duration about 60 hours under IR combined with ADT and 15 hours with IR;

the S group has the average cell cycle arrest duration about 44 hours under IR combined with ADT and 11 hours with IR;

the G2/M group has the average cell cycle arrest duration about 28 hours under IR combined with ADT and 7 hours with IR.

In the current model, we preset the cell cycle duration and calculate the number of PCa cells over time. According to [10], the doubling time for C4-2 cells is recorded as listed in Table 3.1, where the first column is the doubling time given as a relative number, and if control is taken 24 hours as a general case, then the doubling time for each treatment is calculated as 30 hours and 95.5 hours. This information provides the constraints for the cell cycle duration time in our model.

The repair pathways involved in DSB repair are NHEJ and HR, which are modeled and parameterized in Chapter 2 for PCa under IR and IR+ADT. In the computational models, because the original experimental data is based on averaged values considering all cell cycle phases and is not measured for individual cell cycle phases, the contributions of NHEJ and HR were not considered in a cell cycle dependent manner. They were modeled separately. Here, we combine both models taking cell cycle phases into account. According to [60], while HR is absent is G1 phase, the efficiencies of the NHEJ and HR are measured as below:

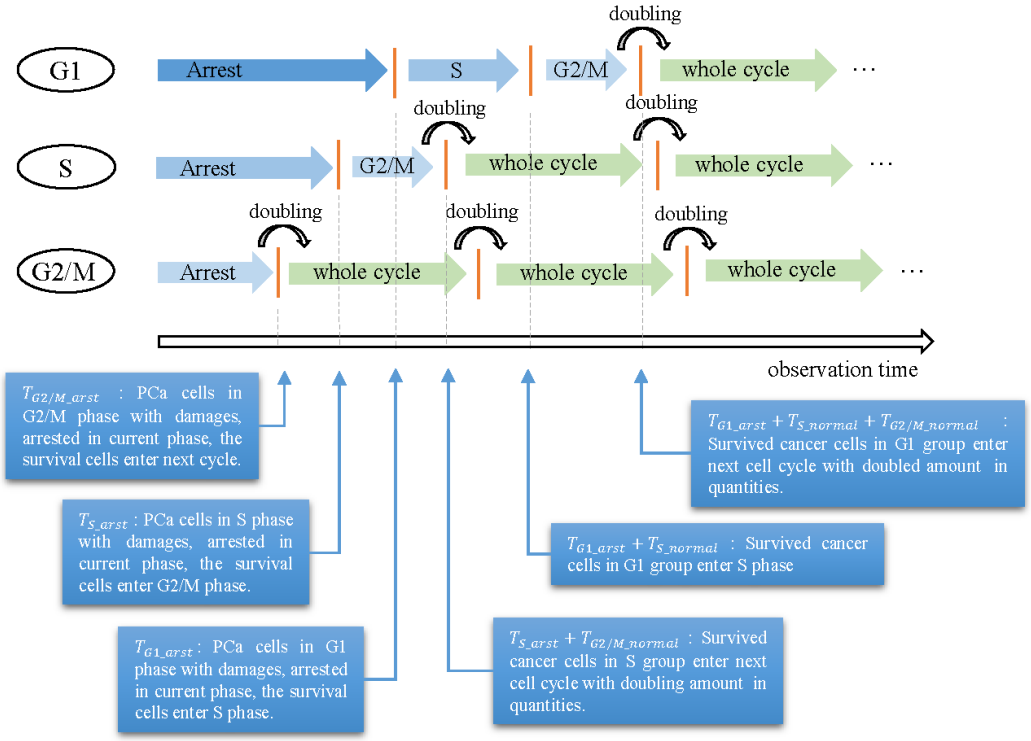

Figure 3.2: Cell Cycle Arrest and Cell Proliferation Timeline

NHEJ efficiency in S phase is 0.686;

NHEJ efficiency in G2/M phase is 0.9275;

HR efficiency in S phase is 0.3145;

HR efficiency in G2/M phase is 0.0625.

Combining all the information above, a survival rate for G1 cells is defined by the formula:

$$ratio_{G1} = \frac{DSB_{NHEJ-repaired}}{avg_{G1}} \tag{3.13}$$

where the repaired DSB number is obtained from the solution of ODEs for NHEJ using a time interval as long as the assumed arrest time for G1. The avg_G1 is given by equation 3.10. The ratio of repaired DSBs to initial DSBs calculated here is used as a surrogate for the survival rate in G1 phase cells. Similarly, for S and G2/M group, the following ratios are obtained, noting that HR is active for both these cell

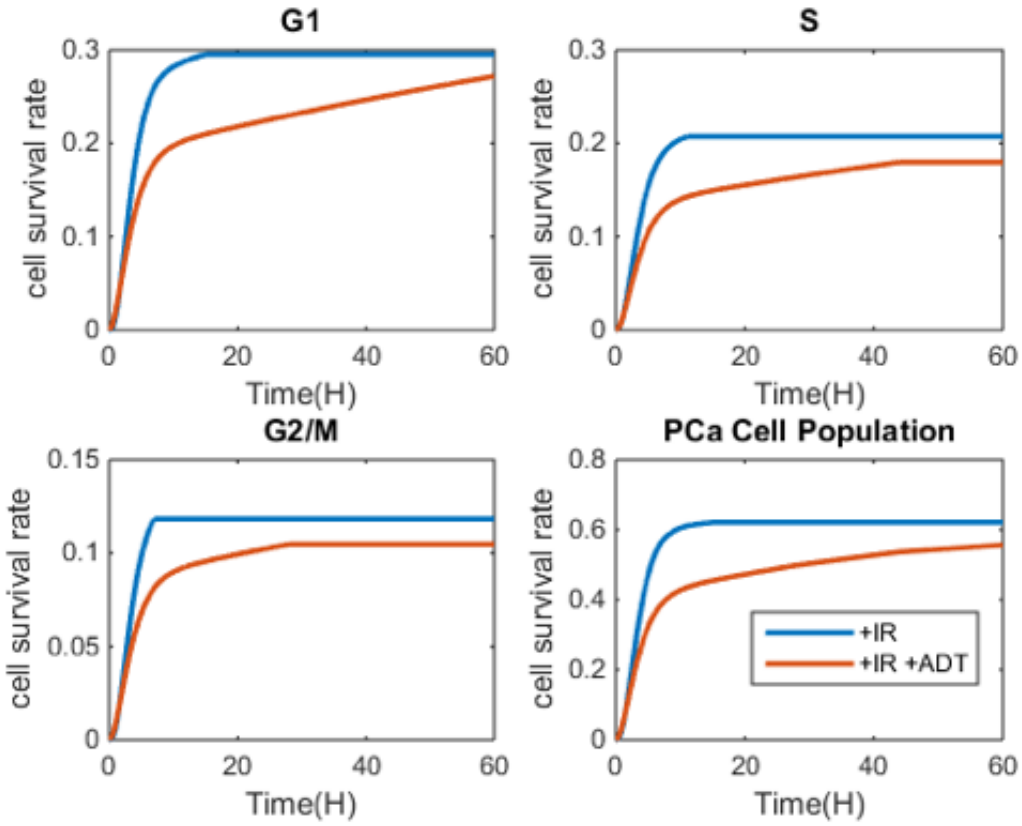

Figure 3.3: Rate of Cell Survival in Cell Cycle

cycle phases:

$$ratio_S = \frac{DSB_{NHEJ-repaired} + DSB_{HR-repaired}}{avg_S} \tag{3.14}$$

$$ratio_{G2/M} = \frac{DSB_{NHEJ-repaired} + DSB_{HR-repaired}}{avg_{G2/M}} \tag{3.15}$$

As for the overall cell population, the cell survival rare is calculated as:

$$P_{survival} = G1\% * ratio_{G1} + S\% * ratio_S + G2/M\% * ratio_{G2/M} \tag{3.16}$$

During the duration of cell cycle arrest, the probability of cell survival is increasing as damage repair progresses as shown in Figure 3.3. In all cell cycle phases, the survival rate of cancer cells is relatively low in the presence of both IR and ADT. A proliferation scheme that is presented in Figure 3.2 is used to study how the damage

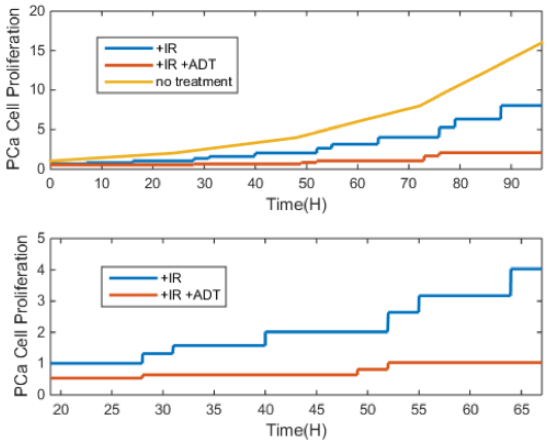

(a)

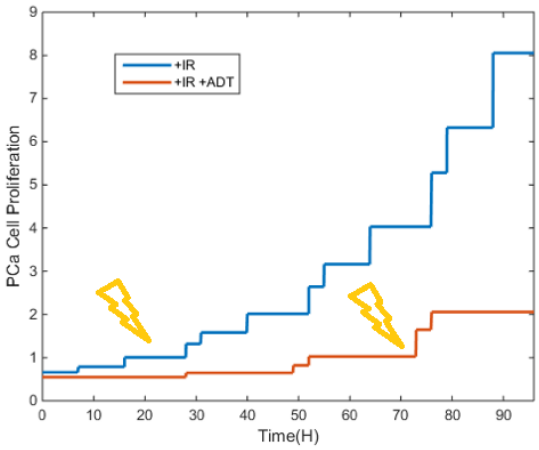

(b)

Figure 3.4: PCa Cell Proliferation

quantity and arrest times will affect cell proliferation and survival.

Proliferation of prostate cancer cells has been significantly inhibited by IR treatment compared with normal cell proliferation rates, and this inhibition is more pronounced under the combined treatment regimen of IR and ADT as shown in Figure 3.4a. Specifically, in the early stages, about 62.1% of the cells survived after the completion of the repair after IR treatment. Compared with the theoretical 24-hour cell doubling, the doubling of the cells is extended to around 40 hours; and under the simultaneous treatment with IR and ADT, the inhibition of cell proliferation is more significant, where about 55.7% PCa cells survive in the early stages together with

Table 3.2: Parameter Used in Cell Proliferation Models

initial conditions		treatment strategy	IR	IR+ADT
DSBs induction	11	G1 Arrest Duration	15h	60h
G1 %	0.46	S Arrest Duration	11h	44h
S %	0.33	G2 Arrest Duration	7h	28h
G2/M %	0.21	dead cell % in G1 grp	0.3574	0.4098
normal G1 duration	11h	dead cell % in S grp	0.3715	0.4548
normal S duration	8h	dead cell % in G2/M grp	0.4361	0.5008
normal G2/M duration	5h	surv cell % from G1 grp	0.2956	0.2719
avg-ini-dsb/G1	7.4	surv cell % from S grp	0.2074	0.1799
avg-ini-dsb/S	11.1	surv cell % from G2M grp	0.1184	0.1048
avg-ini-dsb/G2M	14.8	Total Sur%	0.6214	0.5567
		Total death %	0.3786	0.4433
		doubling time (experimental)	30h	95.5h
		doubling time (computational)	35-45h	85-95h

a longer doubling time about 90 hours. As given in Table 3.2, the doubling times calculated from the models is in good agreement with the experimentally measured times.

Based on the simulation results as presented in Figure 3.4b, it can be concluded that another dose of IR can be delivered might before the cell doubling.

3.2 Detailed Study of DSB Repair by NHEJ During Cell Cycle Post IR

It is the goal of this section to develop the mathematical models of NHEJ pathway in a cell cycle dependent manner using the data from [30]. Specifically, data from [30] show the dynamics of DSB repair for different cell cycle phases for two different IR doses. NHEJ repair models that were developed in Chapter 2 for each cell cycle phase in a data driven way for both IR doses. In the model development, the repair pathway(s) that is / are active for that particular cell cycle phase are taken into account. For

the phases that both pathways are active, we accounted for the contribution of each individual repair pathway. For each model, the sensitivity test and identifiability analysis are performed. For the identifiable parameters, comparison is made between the values of these parameters among the models and a discussion is given on how parameters dynamics determine the performance in different cell cycle phases.

3.2.1 Model Setup and Data Processing

As presented in Chapter 2, biochemical kinetics of NHEJ is modeled using deterministic nonlinear ODE set described in equations 2.3−2.12. In the experimental data, γH2AX foci measurements are used as a marker for repair dynamics. The parameters of the model to be estimated are the rate constants and all the initial conditions are set to be the same as listed in Table 2.1 before parameter estimation as stated in previous chapter in order to have the biologically relevant starting points.

In the literature [30], γH2AX foci in normal human neonatal CCD-34Lu fibroblasts cell are measured in three cell cycle phases for both 0.5Gy and 5Gy; and this IR doses data are used in model development. The remaining DSBs after 5Gy IR are measured in percentages corresponding to G1 and G2 phases under 3 conditions: normal condition, inhibiting HR, inhibiting NHEJ. When calculating γH2AX foci that are repaired by NHEJ, we can take the percentage change under the condition with inhibited HR for different cell cycle phases for each dose accordingly. In order to study the dynamics of NHEJ or HR alone, the other pathways was inhibited. The inhibitor Nu7026 inhibits DNA-PKcs in NHEJ and RI-1 inhibits Rad51 of HR. However, the chemical inhibitors only slow down the reactions but not completely stop the reactions. The inhibition effects are investigated in [30] only during G1 and G2 phases. However, as [60] mentions, the proportion of NHEJ in S is larger than that of G2 phase. On the basis of the existing data, the effect of HR inhibition on S phase could be more significant (about 5 fold) than that of the same inhibition on the G2

Table 3.3: γH2AX Foci With/Without HR Inhibition under 0.5/5Gy IR

γH2AX foci	0.5 Gy				5 Gy			
	0.5h	2h	6h	24h	0.5h	2h	6h	24h
G1 (Control)	145	98	55	5	1400	910	490	210
G1 (-HR)	x	x	x	x	1400	910	570	280
S (Control)	180	145	105	40	1650	1150	700	100
S (-HR)	x	x	x	x	1650	1360	1155	720
G2 (Control)	290	185	125	25	2000	1550	800	250
G2 (-HR)	x	x	x	x	2000	1600	1200	400

phase. Original data discussed above have been shown in Table 3.3 together with the resulting γH2AX foci that are repaired by NHEJ. The numbers are corresponding to G1, G2 and S phases under 5Gy IR. The data described above are used as the experimental data to estimate the kinetic constants of the active proteins. The parameters under each dose corresponding to the cell cycle phase are estimated separately.

In order to determine if the changes we observe are biologically significant, we have conducted parameter sensitivity analysis. The changes in the parameters in response to different treatments can be considered biologically relevant only for those parameters for which the model is sensitive. We have calculated the sensitivity gain using equation 2.14. In our case, the numerator is the percent change in error function and the denominator is the percent change for the parameter itself. We have both increased and decreased the parameters by 10 percent. We calculated the average value of percentage change in M to calculate S. We have also conducted an identifiability analysis as described in Chapter 2 for all the parameters to determine whether the parameters are identifiable in the model. As for a specific parameter that we want to check its identifiability, we kept the estimated result of this parameter as a constant, and estimated all the rest of the parameters by changing the chosen parameter by 10 percent up or down. If the objective function becomes greater, the parameter is identifiable, otherwise, the parameter is non-identifiable when the objective function

Table 3.4: Estimated Protein Kinetics for NHEJ When HR Inhibited

	0.5Gy G1	5Gy G1	5Gy G1(-HR)	5Gy S(-HR)	5Gy G2(-HR)
k_1	$2.69*E^{-8}$	$5.32*E^{-8}$	$2.42*E^{-8}$	$1.86*E^{-8}$	$2.07*E^{-8}$
k_2	$7.16*E^{-8}$	$9.5*E^{-8}$	$4.41*E^{-8}$	$2.74*E^{-8}$	$4.22*E^{-8}$
k_3	0.0105	0.4984	0.0069	0.0024	0.0084
k_4	0.0004	0.5709	0.0002	0.1751	0.2286
k_5	0.0118	0.2357	0.0091	0.0940	0.1769
k_6	0.0035	0.0001	$1.05*E^{-5}$	$7.27*E^{-6}$	$1.69*E^{-5}$
k_7	0.0288	0.1538	0.0106	0.0227	0.0345
k_8	0.0587	0.0563	0.1019	0.0437	0.0748
k_9	$1.38*E^{-8}$	0.0014	0.0157	$6.37*E^{-9}$	$4.33*E^{-9}$
k_{10}	$3.7*E^{-5}$	$1.14*E^{-5}$	0.0068	0.0003	0.0003

remains the same. The results are presented in Table. 3.5

3.2.2 NHEJ Model Parameters for Different Cell Cycle Phases

The kinetics of proteins that are involved in NHEJ under different cell cycle phases are estimated and presented in this section. Resulting values are presented together with the sensitivity test and identifiability test to identify the parameters that are biologically relevant under these circumstances. It is observed from the values on the kinetic rate constants that a potential protein activity change with cell cycle phase change takes place is stated for NHEJ pathway. NHEJ as the major DSB repair pathway, repairs most of the most DSBs through the whole cell cycle. However, proteins behave differently with various doses applied as well as in separate phases during cell cycle.

Parameter Estimation Results

The results for the parameters estimated under each case is listed in Table 3.4 and model outputs together with experimental data are plotted in Figure 3.5. It is shown in the figures that the estimated results are in good agreement with the experimental

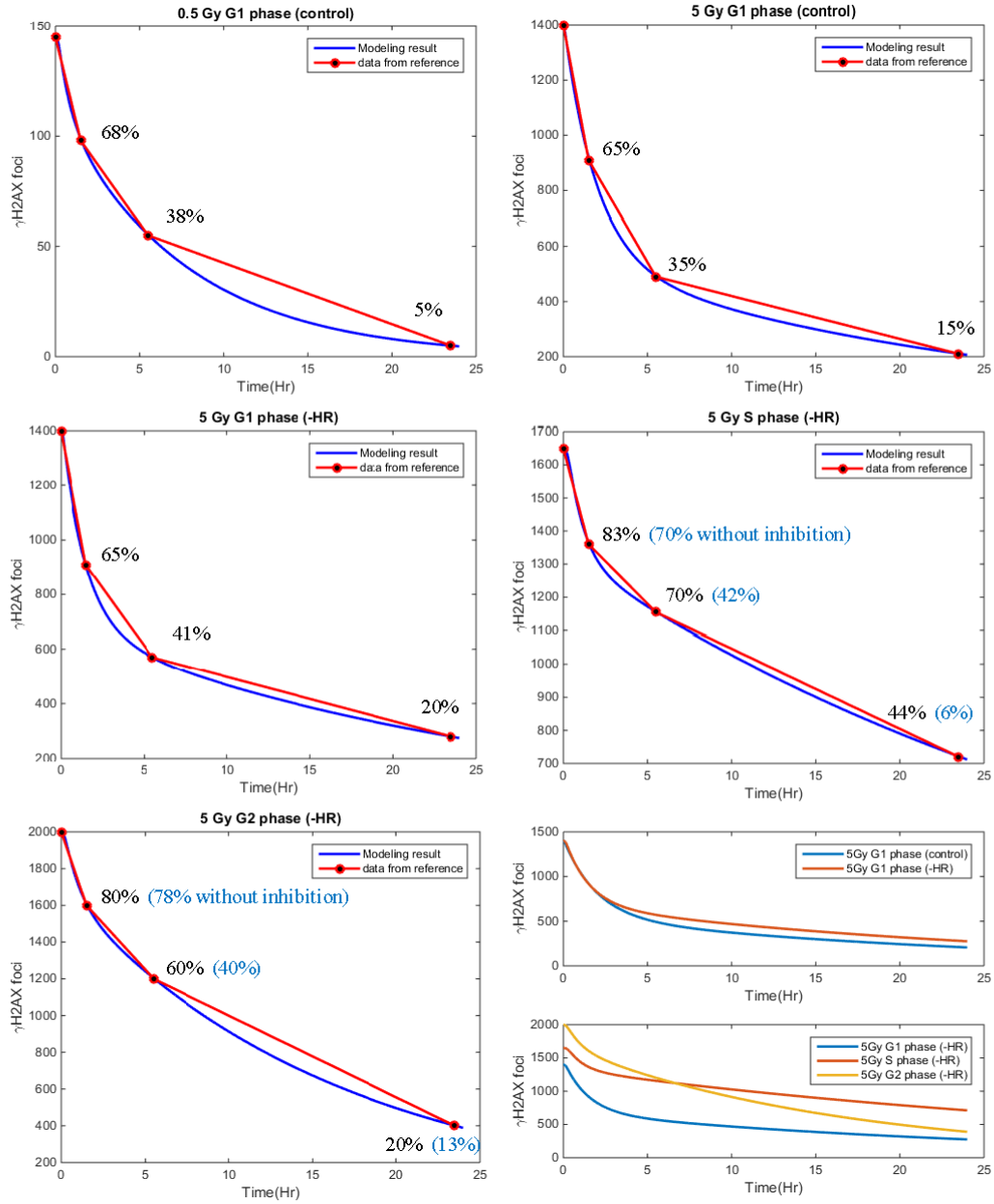

Figure 3.5: Curve Fitting for NHEJ When Inhibiting HR in G1, S and G2 Phase

data. When exposed to 5Gy IR, there are more DSBs generated. G1 phase cells have the greatest overall repaired DSBs in percentage under both low and high IR dose when taking into account the NHEJ and HR pathways. When cells are in G1 phase, only NHEJ is the effective pathway for DSB repair; while in S and G2, NHEJ and HR are both active. Comparing the columns and rows of the Table 3.3 and Table 3.4:

i) G1 phase under 0.5Gy IR *vs.* G1 phase under 5Gy IR: 32% of the damage is repaired within the first 6 hours post 0.5Gy IR. When IR dose is increased, the overall damage amount raises almost 10 fold which is proportional to the fold change in IR dose. However, the repair rate is not influenced much in upstream reactions. The resulting unrepaired damage is higher under 5Gy IR of 15% compared to 5% under 0.5Gy IR. Looking at the experimental data in the first 6 hours post IR, reaction rate is faster to a smaller extent 3% under 5Gy. Faster rate is captured with increase in parameters k_1 (Ku) and k_2 (DNA-PKcs), k_5 and k_7 for ligation and end processing. From 6 hours to 24 hours post IR, G1 phase cells after 0.5Gy are faster in NHEJ rate of repair, the downstream dynamics change with the value of synthesis protein k_{10} dropping with increasing dose.

ii) Normal G1 phase cells *vs.* G1 phase cells with HR inhibition: it is considered that in G1 phase, NHEJ is the only effective pathway for DSB repair. Theoretically, inhibiting Rad51 (HR defect) will not influence outcome for G1 phase cells. However, the experimental data show a slight decrease in the efficiency of NHEJ when an HR inhibitor is applied in G1 phase cells. The overall remaining DSB is about 5% higher under HR restricted condition. This effect suggests that lack of HR repair proteins may also down regulate NHEJ activities and lead to less effective repair. All the significantly sensitive parameters for both cases have decreased values in the current simulation. The comparison here points out to the potential of a Rad51 inhibitor in limiting NHEJ in G1 phase cells to a small extent, but the specific mechanism is not clear.

iii) HR inhibition in G1, S and G2 phase: HR has the largest effect on S phase cells, so inhibiting Rad51 has the greatest impact on S phase, which is reflected in the most unrepaired DSB of about 44% compared to G1 and G2 phase cells of about 20% remaining DSB. Although the change in NHEJ repair rate is not consistent in different cell cycle phases in the case of HR inhibition, overall, HR defect has the

greatest impact on S phase NHEJ DSB repair, followed by G2. Specifically, for the parameters optimally estimated under each scenario, first attached proteins k_1 (Ku) and k_2 (DNA-PKcs) decreases is in G1, G2, and S respectively, a significant decrease of k_5 ligation, k_6 complex releasing and k_7 end processing are observed in S phase cells with HR deficiency.

Sensitivity Test and Identifiability Analysis Results

The analysis of the results shows that k_8 is not sensitive under any scenarios that have been tested. k_5, k_6, and k_7 are parameters that are the most sensitive under all the 5 conditions. k_1, k_2, and k_3 show sensitivities but not as significant as k_5-k_7. For the rest of the parameters, they present different sensitivities under different scenarios. k_4 is a sensitive parameter in 0.5Gy G1 phase cells and 5Gy S phase cells with HR inhibition. k_9 shows insensitivity in 5 Gy G1 phase cell with/without HR inhibition, but is sensitive in the rest simulations. k_{10} is only less sensitive in HR defective G1 phase cells and sensitive to the model in the other simulations especially for normal G1 phase cells. According to the dynamics that the k's represented, a conclusion is drawn from the current model that: end ligation, Artemis end processing and complex release have an important role in the dynamics of NHEJ activities in different cell cycle phases. k_1 and k_2 show biological relevance of Ku and DNA-PKcs activities. The result of identifiability test is in consistent with sensitivity test. The non-sensitive parameters are not identifiable either. The parameters discussed in the results above for comparisons have been tested to be both sensitive and identifiable.

Table 3.5: NHEJ Parameter Sensitivity and Identifiability Results in G1, S, G2

sensitivity gain		k_1	k_2	k_3	k_4	k_5	k_6	k_7	k_8	k_9	k_{10}
0.5Gy	G1 (control)	1.5622	0.9759	1.5556	130.0471	237.4031	2.1674	126.1766	0	1.8396	404.9995
5Gy	G1 (control)	1.9747	0.5157	0.3403	0.5034	1115.3488	1229.4442	811.4800	0	0	509.6185
	G1 (-HR)	1.2117	0.3479	2.2921	233.9394	212.9499	115.6769	335.8142	0	0	1.8505
	S (-HR)	1.5463	0.8554	5.6582	0.0479	216.2557	560.3451	298.0195	0	3.6159	61.0402
	G2 (-HR)	1.6685	0.8040	1.6611	0.0565	91.1649	937.1740	171.3480	0	4.5180	43.5363
Identifiability		k_1	k_2	k_3	k_4	k_5	k_6	k_7	k_8	k_9	k_{10}
0.5Gy	G1 (control)	Y	Y	Y	Y	Y	Y	Y	N	Y	Y
5Gy	G1 (control)	Y	Y	Y	Y	Y	Y	Y	N	N	Y
	G1 (-HR)	Y	Y	Y	Y	Y	Y	Y	N	N	Y
	S (-HR)	Y	Y	Y	N	Y	Y	Y	N	Y	Y
	G2 (-HR)	Y	Y	Y	N	Y	Y	Y	N	Y	Y

Chapter 4

Computational Modeling of Base Excision Repair

The purpose of this work is to computationally analyze the effect of inhibition of base excision repair (BER) on improving the response to treatment with 5-fluorodeoxyuridine. 5-fluorouracil (5-FU) and its metabolite 5-fluorodeoxyuridine (5-FdU) are standard treatments for different solid tumors and especially for colon cancer. In the literature, it is shown that the depletion of uracil DNA glycosylase (UDG), one of the enzymes that initiate the BER pathway, enhanced the cytotoxicity of 5-FdU, making DNA glycosylase a potential target to enhance efficacy of chemotherapeutic agents. It is also shown that the activity of DNA glycosylase is significantly higher in colon cancer cells compared to normal tissues. We have developed a computational model of the BER pathway to capture the BER dynamics in colon cancer cell lines after treatment with 5-FdU. The model is composed of a series of ordinary differential equations where the parameters are the kinetic rate constants and the enzyme concentrations. The data from the literature is used to initially parameterize the models. Then the least square estimation method is used to find the parameters that could capture the BER time course for colon cancer cells after 5-FU treatment using the experimental

data from the literature. We have performed sensitivity and identifiability analyses to determine the parameters that are reliably estimated. The experimental data from the literature show that the depletion of UDG resulted in incorporation of uracil and 5-FU in the DNA. We have computationally replicated this effect by decreasing the protein concentration of UDG in the models and simulating the amount of remaining DNA damages after BER with reduced activity has taken place. We have studied the depletion effect for different protein concentrations of UDG and the results have shown that the accumulation of 5-FU in these colon cancer cells correlate with the level of UDG. The suppression of UDG activity has the potential to enhance the outcome of treatment with 5FdU. It is also shown in literature that poly ADP ribose polymerase inhibitor (PARPi) could enhance the toxicity of 5FU. We also successfully replicated this effect in our model. We incorporate the effect of the lack of adenomatous polyposis coli (APC) that leads to 5-FU treatment failure in our model. The results from the model are in agreement with the experimental results from the literature. The computational models developed can be used to quantitatively optimize the 5FU treatment in the future work.

4.1 Introduction

In this section, we will examine the role of BER in enhancing the chemotherapy. 5-FU and its metabolite 5-FdU are common and standard chemotherapy and are widely used in various solid tumor treatments especially for colon cancer [88]. Referring to Figure 4.1 [89, 90], the mechanism of 5-FU metabolism and how it induces DNA toxicity can be summarized as: 5-FU and 5-FdUrd metabolism results in accumulation of 5-FdUMP. The target of 5-FU and 5-FdUrd is thymidylate synthase (TS), which is the enzyme that converts dUMP to dTMP, Therefore, the suppression of TS prevents dUMP from becoming dTMP and the ratio of dUMP and dTMP is increased

and resulting in incorporation of the false base uracil(U) and 5-FU into DNA during DNA replication. The DNA damage that is caused by the incorporation of an incorrect base is repaired by DNA repair pathways and BER is the major pathway that deals with this kind of DNA lesions. Referring to Figure 4.2 [90, 21, 91], BER is initiated by DNA glycosylase removing the incorrect base. There are different types of DNA glycosylases depending on the specific damages detected[92, 93]. Monofunctional DNA glycosylase targets the damaged base and N-glycosidic bond hydrolysis generates apurinic/apyrimidinic (AP) sites[94]. Then, the DNA with AP sites reacts with the enzyme APE1, which results in gaped DNA with 5dRP [95]. 5dRP is removed by the activities of the polymerase, and downstream BER includes short-patch and long-patch BER which is decided by the 5dRP terminus status[96, 97, 98]. In the short-patch pathway, polymerase β removes dRP and the final step is ligation by Ligase3α/XRCC1 for the damage to be finally repaired; while in the long-patch pathway, dRP is removed and DNA is repaired by polymerase δ, FEN1, and ligase I to complete the DNA repair[99, 100, 101].

It is demonstrated in [102] that incorporation of 5-FU into DNA leads to FU paring with A or G and these lesions are mainly targeted by uracil-Nglycosylase 1(UNG1) and uracil-Nglycosylase 2 (UNG2) both *in vitro* and *in vivo*. This suggests that knockdown of DNA glycosylase as the initiator would influence the BER process, which makes DNA glycosylase a potential target to enhance drug effect in cancer treatment. Different lesions caused by 5-FU and U incorporation into DNA are studied in [89] *in vitro* and the kinetics of different DNA glycosylases (including UNG, SMUG and TDG) are measured and compared. UNG is the major DNA glycosylase that works for all lesions regardless of substrate types. The experimental data shows that down regulating or inhibiting UNG, BER could be slowed down leading to DNA damage accumulation. In [103], two different DNA glycosylases were studied and the results show that the sensitivity to 5-FU increased by 2 fold if SMUG was in-

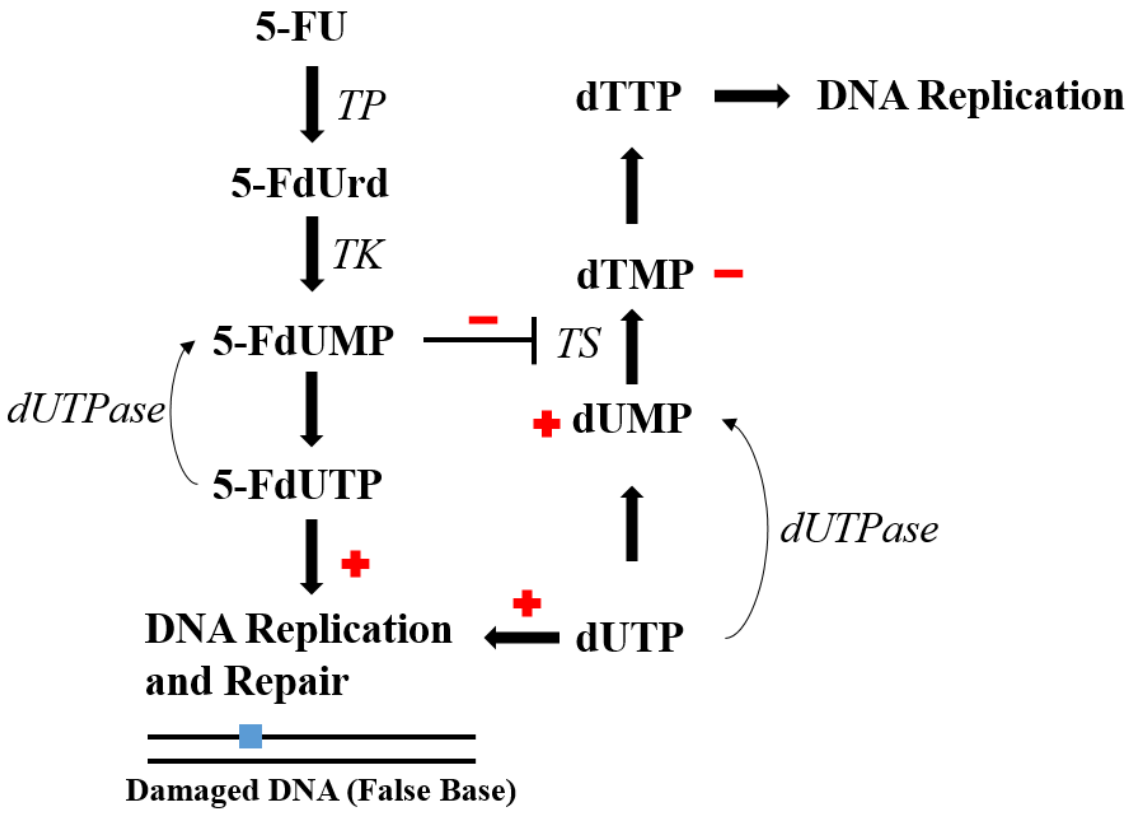

Figure 4.1: 5-FU Cytotoxicity to DNA

hibited instead of UNG, which also suggest a specific DNA glycosylase as a potential target to increase drug toxicity. DNA glycosylase depletion causes cell cycle arrest in G1 and S phase of the cell cycle and sub G1 cells are accumulating which indicates increasing cell death. It is shown in the experiments that UDG depletion enhance 5-FdU cytotoxicity [104].

The treatment outcome of 5-FU can also be influenced by factors other than inhibited UDG. 5-FU, as the major treatment for colorectal cancer, loses its cytotoxicity when APC is muted, because APC has interactions with polymerase β and FEN1, which are key proteins involved in long-patch BER [105]. It is shown in [106] that a combination treatment with 5-FU and PARP inhibitor enhances the outcome of 5-FU. PARP inhibitor is known to enhance cancer treatment outcome when DNA double strand break proteins are deficient including BRCA1/2 and PTEN in homol-

ogous recombination [107], but the mechanism in PARPi for increasing toxicity of 5-FU and BER need further investigation. The results in [108] show the evidence that PARP is actively involved in BER by interacting with polymerase β, and the efficiency of especially short-patch pathway, which is considered the major BER pathway, is down regulated by about half fold and long-patch is severely influenced when PARP is inhibited. In recent years, studies also suggest that PARP is not directly involved in BER, but rather has impact on this repair pathway when PARPi is used. PARPi arrests PARP on the repair intermediates during BER thus disturbing the repair process by preventing the intermediates from proceeding to ligation step [109].

In this section, we study the effect of 5-FU induced DNA damages repaired by BER by developing a quantitative model of the pathway including short-patch pathway and long-patch pathway using data of SW480 and HeLa cell lines from [91]. The BER models will be used to analyze the possible enhancement of 5-FU treatment through inhibition of BER pathway quantitatively.The computational model makes it possible to analyze different scenarios for the optimal treatment strategies when chemotherapy is combined with other adjuvant treatments such as PARP inhibitors [106].

Mathematical modeling of BER have been developed in [21, 22, 23, 24, 25] using stochastic method or deterministic modeling approaches. The process of BER post chemotherapy is modeled by using nonlinear differential equations deterministically as in [21]. We use the data on FU:G measurements on SW480 and HeLa cell line [91] to quantitatively analyze DNA glycosylase activities and kinetics of the rest of the BER enzymes. By determining the relative enzyme levels, we are able to study the effects that are caused by mutation or down regulation of certain enzymes on the BER efficiency.

4.2 Quantitative Base Excision Repair Model

4.2.1 Mathematical Model of BER

As illustrated in Figure 4.2 [90, 21, 91], the pathway can be described according to the following steps: initial lesion is targeted by UDG followed by APE1 reaction before branching into short-patch and long patch pathway. Gapped DNA with dRP reacts with polymerase β and the product either reacts with polymerase β and ligase3α/XRCC1 to have the repair completed or reacts with polymerase δ, FEN1 and ligase1 for the final steps in BER [110]. We have modeled the BER pathway actions step by step using a set of nonlinear differential equations that is similar to [21]. The equations follow Michealis-Menten kinetics and the resultant model is given below. In this model, Yi denotes to the concentration of the initial amount of damaged bases, all repair intermediates and the repaired base damages as results. The enzyme concentrations are denoted by e's, the catalytic rate constants (kcat) are denoted by ki's (s^{-1}) and the Michaelis constants (Km) are denoted by Ki's (nM):

$$\frac{dY_1}{dt} = -\frac{k_1 e_u [Y_1]}{K_1 + [Y_1]} \tag{4.1}$$

$$\frac{dY_2}{dt} = \frac{k_1 e_u [Y_1]}{K_1 + [Y_1]} - \frac{k_2 e_a [Y_2]}{K_2 + [Y_2]} \tag{4.2}$$

$$\frac{dY_3}{dt} = \frac{k_2 e_a [Y_2]}{K_2 + [Y_2]} - \frac{k_3 e_{pbg} [Y_3]}{K_3 + [Y_3]} \tag{4.3}$$

$$\frac{dY_4}{dt} = \frac{k_3 e_{pbg} [Y_3]}{K_3 + [Y_3]} - \frac{k_4 e_{pbl} [Y_4]}{K_4 + [Y_4]} - \frac{k_6 e_{pd} [Y_4]}{K_6 + [Y_4]} \tag{4.4}$$

$$\frac{dY_5}{dt} = \frac{k_4 e_{pbl} [Y_4]}{K_4 + [Y_4]} - \frac{k_5 e_{l3} [Y_5]}{K_5 + [Y_5]} \tag{4.5}$$

$$\frac{dY_6}{dt} = \frac{k_5 e_{l3} [Y_5]}{K_5 + [Y_5]} \tag{4.6}$$

$$\frac{dY_7}{dt} = \frac{k_6 e_{pd} [Y4]}{K_6 + [Y4]} - \frac{k_7 e_f [Y7]}{K_7 + [Y7]} \tag{4.7}$$

$$\frac{dY_8}{dt} = \frac{k_7 e_f [Y7]}{K_7 + [Y7]} - \frac{k_8 e_{l1} [Y8]}{K_8 + [Y8]} \tag{4.8}$$

$$\frac{dY_9}{dt} = \frac{k_8 e_{l1} [Y8]}{K_8 + [Y8]} \tag{4.9}$$

The repair time course data from [91] is given in Table 4.1 and is used in parameter estimation. The data is measured from SW480 and HeLa cell lines and are presented as the percentage of the repaired F:G lesions over time. In the simulations, in order to be in consistence with the enzyme concentrations that are predefined with unit nM, we set the total lesion number to be 100 nM as initial conditions for calculations. We defined all the enzyme concentrations according to the literature [21] and the values are listed in Table 4.2. Note that the system output through short-patch pathway is calculated by Y_6 and Y_9 is the result of repaired damaged bases through long-patch pathway which enable to quantitatively analyze the efficiencies of the two sub-pathways under various scenarios. The final repair outcome is the summation of Y_6 and Y_9 that will be compared with the experimental data during the parameter estimation. We have used fmincon function of Matlab (The MathWorks, Inc, Natick, MA) for parameter optimization for the kinetics constants and "ode15s" for solving the ordinary differential equation set. The parameters are constrained such that they are all positive to avoid negative reaction rates. We have used the following cost objective function where Ym is the model output, in our case is $Y_6 + Y_9$ and Ye is the experimental data at a particular experimental time point and we sum all the squared errors over all the time points:

$$Err = \sum (Y_6 + Y_9 - Y_e)^2 \tag{4.10}$$

In [105], it is shown that APC mutation can lead to 5-FU insensitivity and the mechanism for this treatment failure is explained through the interaction of APC with FEN1 and polymerase β. If APC is muted, FEN1 and polymerase β us up-regulated

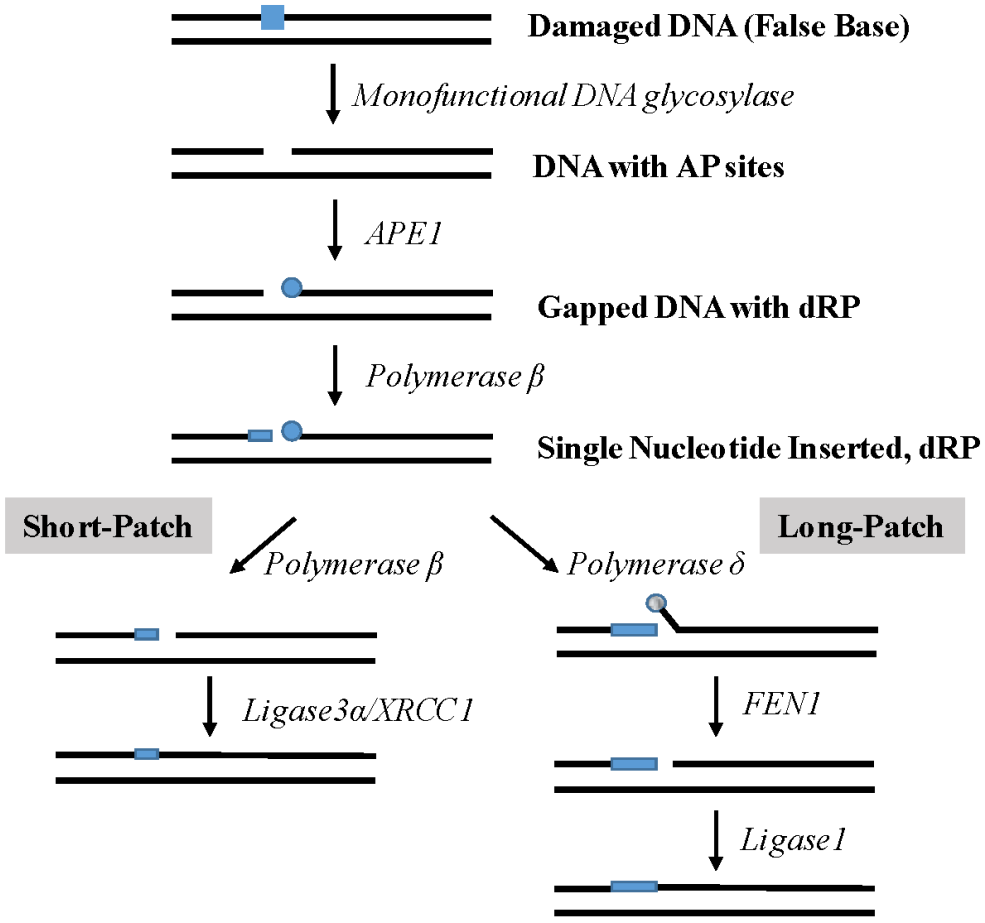

Figure 4.2: BER Pathway Mechanism

making BER more effective thus decreasing the cytotoxicity of 5-FU. The observations in [105] are summarized in Table 4.4. We use our BER models developed above for the simulation of the APC mutation effects on BER in colon cancer cell lines. The fold changes observed experimentally for FEN1 and polymerase β are incorporated in our model to study BER outcome. We also use this model to simulate the effects of PARPi blocking ligation step of the BER intermediates by trapping PARP using the data provided in [109]. The data is converted to relative numbers for the accumulating intermediates when ligation step in inhibited after PARPi is involved as listed in Table 4.5. The deficiency in ligase is studied individually as well as its combination with

Table 4.1: Number of Repaired FU:G Lesions in Percentage

Time(min)	0	15	30	45	60
SW480	0	75%	88%	90%	90%
Hela	0	65%	75%	83%	85%

Table 4.2: Enzyme Concentrations Used in the Model

e_u	DNA glycosylase	70.6nM
e_a	APE1	117.7nM
e_{pbg}	polymerase β gap filling	19.8nM
e_{pbl}	polymerase β dRP remove	19.8nM
e_{pd}	polymerase δ	19.8nM
e_{l3}	ligase3α	11.9nM
e_f	FEN1	19.8nM
e_{l1}	ligase1	1.98nM

PARPi to obtain the combined effect on BER dynamics.

4.2.2 Sensitivity Analysis

One important goal of our studies is to observe how the parameters react under different treatment scenarios, particularly, those parameters which are sensitive in this model making the corresponding enzymes potential targets to inhibit BER repair and enhance the treatment effect, such as drug toxicity for chemotherapy with 5-FU. Therefore, we conduct sensitivity analysis to investigate biological relevance of the parameters in the mathematical model to experimental phenomena. DNA glycosylase, as the initiator of the BER process, is a potential target and the efficiency of short and long patch pathways can also be determined individually from the computational models. Sensitivity gain indicates whether the model is sensitive to a certain parameter and the degree of the sensitivity. The sensitivity gain is calculated using the same method as described in equation 2.14, where M is the BER system output.

The results are presented in the next section.

4.2.3 Identifiability Analysis

We have conducted an identifiability analysis for all the parameters to determine whether the parameters are identifiable in the BER model parameterized for 5-FU treatment in colon cancer cell lines. Due to the structure of the model where the catalytic rate constants are multiplied with the enzyme concentrations, we only take the catalytic rate constants into account and we set the enzyme concentrations to be constants. The identifiability test is generated for all the parameters one by one applying previously stated method for NHEJ modeling and HR modeling as described in [62]. The results are presented in the next section.

4.3 Role of Base Excision Repair in Sensitization of Cancer Cells to Chemotherapy

4.3.1 BER Parameters in the Modeling Results

We use the data from experimental measurements and estimate the parameters k_{cat} and K_M for all the enzymes that are involved in the BER process. The results are listed in Table 4.3, and when these parameters are used in the model, the model output is in good agreement with the experimental data as shown in Figure 4.3. We observe that it takes about 60 minutes to complete BER when base damage is detected, in our case the damage is FU:G lesions. The overall repair efficiency is dependent on the cell type and the enzyme kinetics for the different cell types. In the experimental data, SW480 cells present a better repair rate as well as total repair percentage compared to HeLa cells. In both cell types, BER goes on fast for the first 30 minutes and becomes gradually steady at 40 minute post exposure to chemical

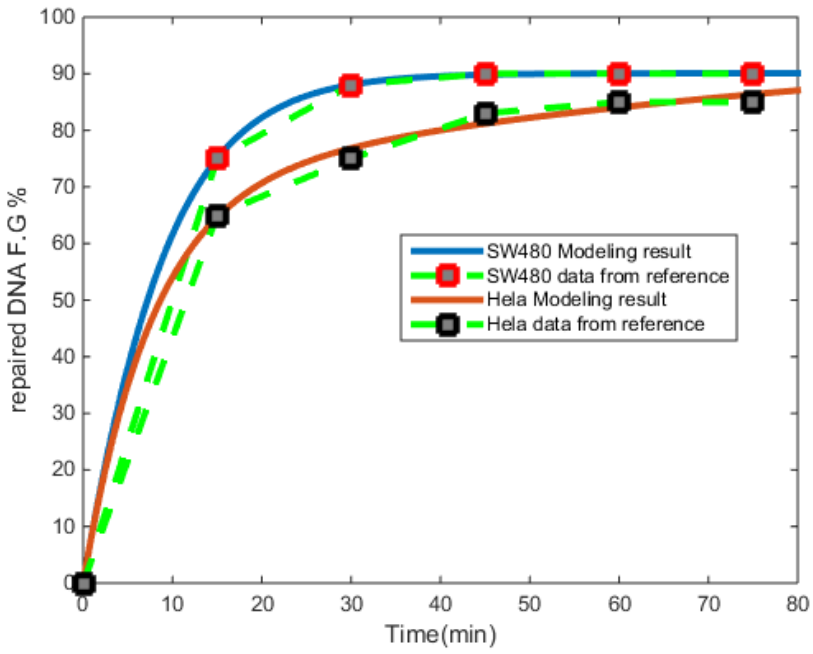

Figure 4.3: BER Model Results compared with Experimental Data for SW480 and HeLa Cell Lines

intervention. In HeLa cells, it takes longer to reach a steady state and these cells are more sensitive to 5-FU. SW480 cells have less 5-FU toxicity. Starting with the same amount of base damage, SW480 cells have a faster overall repair rate and better efficiency than HeLa cells. When the resultant parameters for these two cell lines are compared, we find that the parameters show very different enzyme kinetics for different cell lines.

4.3.2 DNA Glycosylase Depletion Enhances 5-FU Effect

We have used the model for HeLa cells to study the effect of DNA glycosylase depletion on 5-FU treatment outcome and BER efficiency. In Figure 4.4, the model for HeLa cells as shown in Figure 4.3 is used as the control set, for which the parameters are as listed in the last column of Table 4.3. In this model, we decrease DNA glycosylase concentration by 0.8 fold, 0.5 fold, 0.1 fold and 0.01 fold. We observe that, with decreasing DNA glycosylase concentrations, the repaired damage amount is decreased

Table 4.3: Parameters Fitted in Experimental Data: the unit of k_i is s^{-1} and the unit of K_m is nM

Name in Eqn	description	SW480	Hela
k_1	DNA glycosylase k_{cat}	0.6	0.0325
K_1	DNA glycosylase K_m	41.4	1000
k_2	APE1 k_{cat}	37.1	861.2
K_2	APE1 K_m	24.0	97.6
k_3	polymerase β gap filling k_{cat}	1.8	604.3
K_3	polymerase β gap filling K_m	78.2	790
k_4	polymerase β dRP remove k_{cat}	31.5	367.5
K_4	polymerase β dRP remove K_m	41.1	927.4
k_5	ligase3α k_{cat}	$4.8E^{-5}$	0.015
K_5	ligase3α K_m	165.1	1000
k_6	polymerase δ k_{cat}	36.3	832.9
K_6	polymerase δ K_m	5.3	805.0
k_7	FEN1 k_{cat}	0.03	916.9
K_7	FEN1 K_m	208.7	716.1
k_8	ligase1 k_{cat}	41.1	932.6
K_8	ligase1 K_m	70.0	137.3

over time. The overall efficiency within a certain time range has a considerable drop. The repair percentages are 82.5%, 81%, 42% and 8% corresponding to the decreasing DNA glycosylase concentrations. Especially when DNA glycosylase concentration is decreased to 0.01 fold, only about 8% of damaged is repaired within 60 minutes compared to around 83% when there is no DNA glycosylase depletion.

Suppression of DNA glycosylase concentration leads to not only a slower BER rate but also a drop in overall repaired damage amount. When BER is suppressed by down regulating DNA glycosylase, 5-FU caused base damages are repaired less thus 5-FU toxicity is enhanced. In this simulation, we successfully capture the dynamics of depletion of DNA glycosylase as a potential approach to enhancing 5-FU treatment outcome.

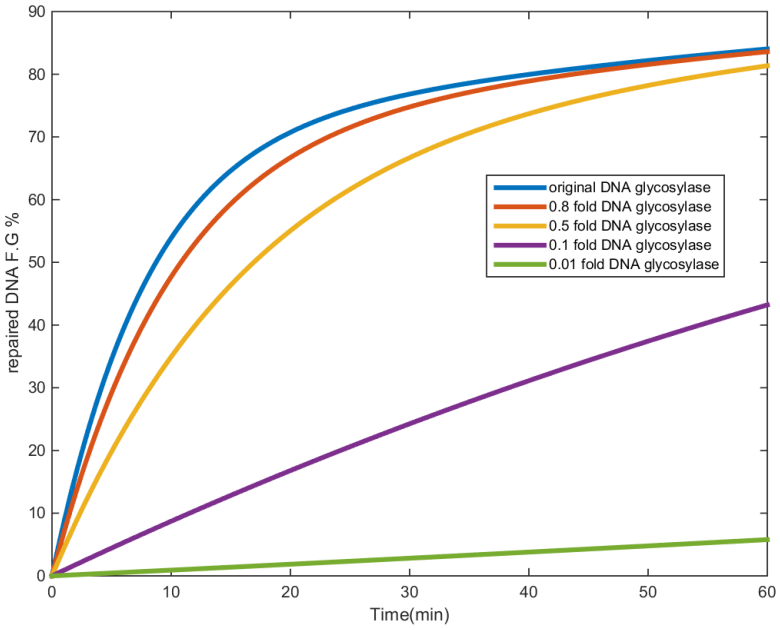

Figure 4.4: DNA Glycosylase Depletion and BER Outcome

4.3.3 APC Mutation Decreases 5-FU Cytotoxicity

We have used the model for SW480 cells to study BER dynamics for treatment scenarios with different levels of APC expression, as the experimental data is on colon cancer cells and SW480 is also another colon colon cancer cell line. As given in Table 4.4, there are three types of colon cancer cells to be examined: HCT-116 cells with high APC expression; HT-29 cells with medium APC expression; and LOVO cells with low APC expression (APC mutation). APC's interaction with FEN1 and polymerase β is displayed as fold change in the enzyme concentrations. With respect to each cell line, the fold changes in FEN1 and polymerase β levels are measured from low to high dose of 5-FU for dose levels 2.5μM, 5μM and 10μM. The fold change is implemented as multiplying the original model enzyme concentrations with the fold change to simulate the effects.

For both high APC and medium APC expressing cells, with increasing 5-FU dose, FEN1 decreased significantly and the decrease in medium APC cells is more significant

Table 4.4: APC Mutation's Effect on Enzymes

cell type APC expression	HCT-116 High	HT-29 Medium	LOVO Low
No 5-FU FEN1 No 5-FU polymerase β	1 1	1 1	1 1
2.5μM 5-FU FEN1 2.5μM 5-FU polymerase β	0.55 0.97	0.5 0.83	NA NA
5μM 5-FU FEN1 5μM 5-FU polymerase β	0.33 0.93	0.02 0.9	NA NA
10μM 5-FU FEN1 10μM polymerase β	0.08 0.85	0.0 0.9	1.04 1.04

than high APC cells. While there is also a slight decrease in polymerase β it is not as significant as in FEN1. Low APC cells don't show changes in enzymes concentrations with varying 5-FU doses. For 5-FU dose at 10μM, APC mutated cells have higher levels of FEN1 and polymerase β compared to high and medium APC expressing cells. As shown in Figure 4.5, APC mutated cells (LOVO) have the most damage repaired because FEN1 and polymerase β concentrations are the highest compared to non APC mutated cells. Figure 4.6 shows damage repair dynamics for different cell types under varying 5-FU doses. HT-29 cells are more sensitive to the dose change compared to HCT-116 cells. As for the same cell line, when there is a higher 5-FU dose applied, less FEN1 concentration is detected, and regarding the same level of damage concentration, BER is slower in rate and repaired number of damages are lower. In both HCT-116 and HT-29 cells, 10μM 5FU scenario has the lowest BER efficiency, and the scenario with 5-FU at 2.5μM has the most damaged DNA repaired. Higher levels of 5-FU are more toxic due to BER suppression.

4.3.4 PARPi and Ligase Enzyme Deficiency Inhibit BER

In Table 4.5, the experimental data from [109] in term of the number of SSB accumulation fold change with time is shown up to 60 minutes post PARPi treatment. PARPi

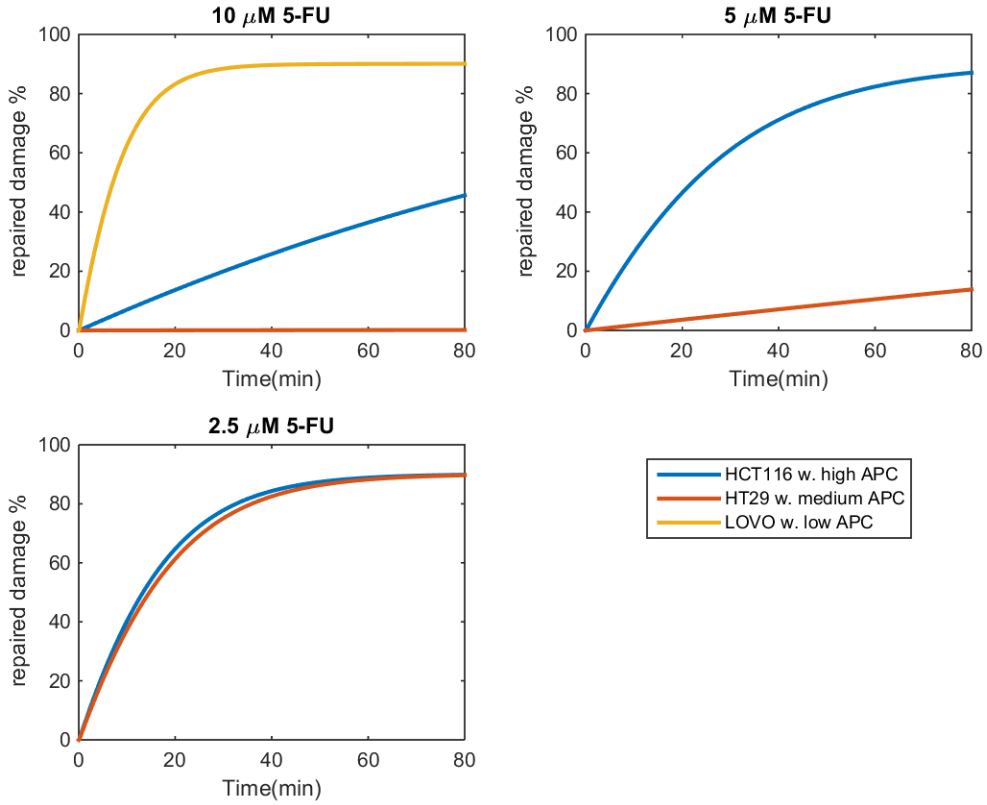

Figure 4.5: Repaired Damage for Different APC Expression Cells

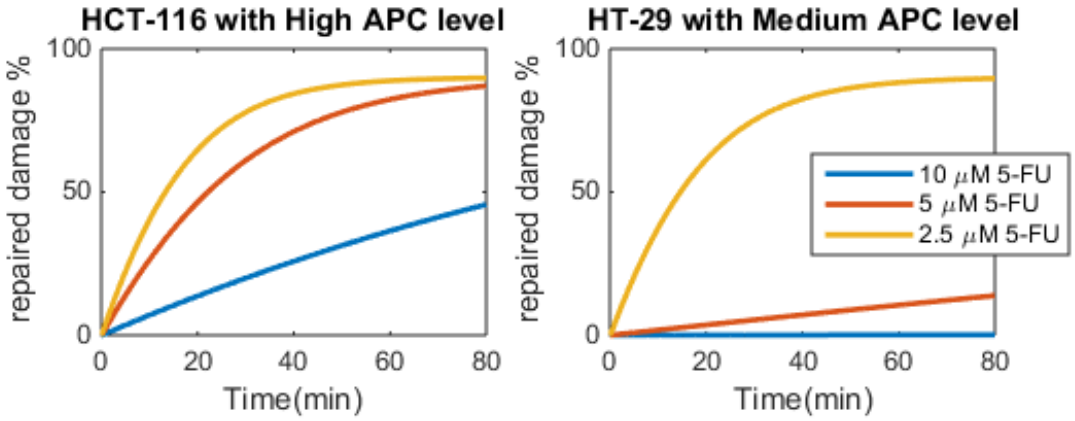

Figure 4.6: Repair in Cells with Different APC Levels for Varying 5-Fu Doses

traps PARP, which is not directly involved in BER, onto the BER intermediates one step before the final ligation step. Therefore, the ligation step is inhibited,which

Table 4.5: Intermediates Accumulating +PARPi

Time(min)	0	10	20	40	60
EM9-V cell	1	1	1	1	1
EM9-V cell +PARPi	1.2	1.2	1.9	1.5	1.4

leads to failure of BER repair of the damage induced by 5-FU. The averaged fold change is used to generate the experimental data for PARPi effects by multiplying the repair kinetics data with the corresponding fold change. The parameter estimation is performed using this new repair kinetics data set. Figure 4.7 a shows an increase in number of accumulation of base damage when there is PARPi added to the simulation. Table 4.6 lists the parameter kinetics that have changed after PARPi treatment.

The remaining damage is calculated in our model for different treatment scenarios. As shown in Figure 4.7 b and c. The control in this case is normal BER dynamics when repair is not inhibited by PARPi or ligase deficiency. We study the effect of PARPi on BER kinetics and the results are given in Figure 4.7 b and Table 4.6 Among the parameters that are re-estimated for BER with PARPi, DNA glycosylase and ligase show decreases in value as shown in Table 4.6. To simulate the case when there is ligase deficiency, we decreased the enzyme concentration of ligase in the model simulations and this results in similar increase in remaining DNA damages for both cell lines. In Figure 4.7 d, the increasing amount of remaining damages are displayed after individual application of PARPi and ligase deficiency. The combination of PARPi and ligase deficiency shows an enhancement compared to individual intervention by either PARPi or ligase in terms of remaining unrepaired damages. Due to the synthetic lethality of PARPi and BRCA mutation, the results analyzed for adding PARPi into treatment leads to damage enhancement only when the DSB formed by replication fork collapse cannot be resolved by HR due to BRCA mutation. Otherwise, the

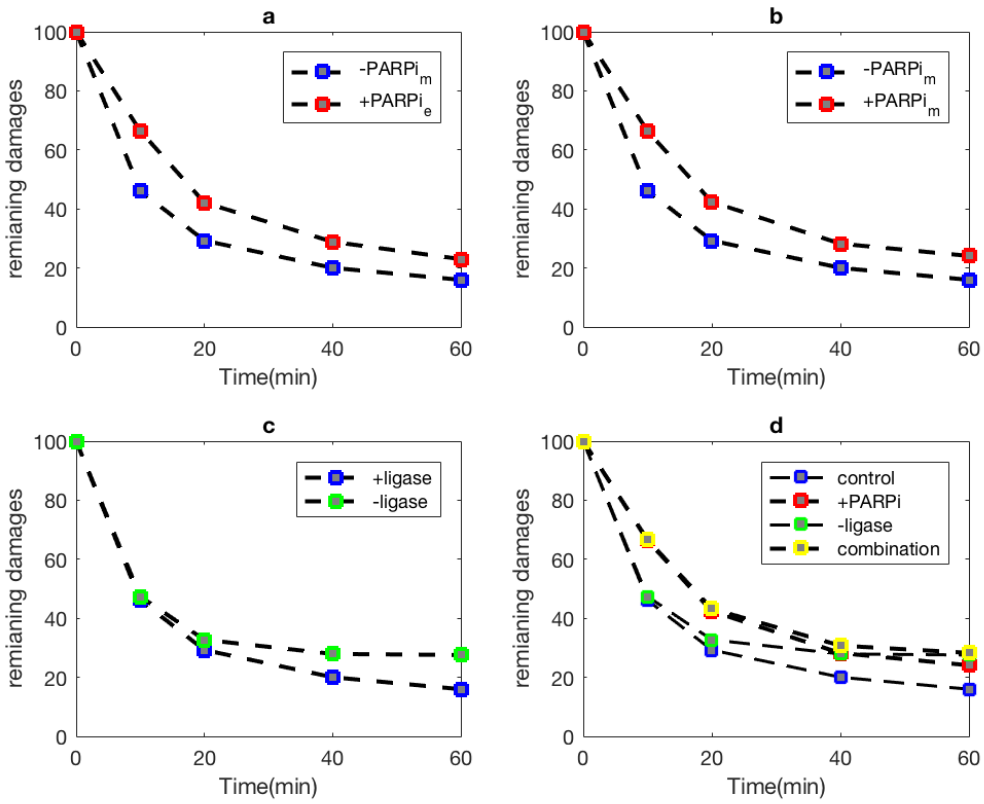

Figure 4.7: a. Experimental data without PARPi and the data set generated from this experimental data with PARPi effects included; b.BER kinetics change after PARPi; c. BER kinetics change after inhibition of ligase; d. PARPi and ligase inhibition on BER kinetics.

damages can be repaired by HR.

4.3.5 Sensitivity Analysis Results

We calculate the sensitivity gain using the method as described in equation 2.14 for the parameters estimated in Table 4.3 and the results are presented in Table 4.7. We predefined the enzyme concentrations to be constants in our model and we don't estimate the enzyme concentrations in our parameter estimation. Enzyme concentration changes under the various scenarios created for 5-FU treatment and BER can similarly be considered as the changes on enzyme rate constants because of

Table 4.6: Altered Parameters in BER with PARPi (I: identifiable SGain: Sensitivity Gain)

description	-PARPi	SGain	I	+PARPi	SGain	I
DNA glycosylase k_{cat}	0.0325	10.95	+	0.0194	28.13	+
ligase3α k_{cat}	0.015	4.19	+	0.004	4.63	+

the structure of the model. The enzyme concentration e is multiplied with k_{cat}, if k_{cat} is tested to be sensitive then the model is sensitive to the corresponding multiplier e.

The sensitivity analysis results for the model parameters that are estimated for SW480 cells can be summarized as follows: the model is most sensitive to k_7, k_8, and k_{11}-k_{14} for the kinetics of to polymerase β for dRP removal, polymerase δ and FEN1, correspondingly. The model shows less sensitivity to the rest of the parameters with low sensitivity gains. Varying levels of APC expression has different degrees of regulation on FEN1 and polymerase β and FEN1 is tested to be a sensitive parameter of this model. We successfully captured loss of 5-FU toxicity when APC is mutated by tuning the parameters for polymerase β and FEN1 according to the fold changes of enzyme kinetics in the literature.

We also perform sensitivity analysis for HeLa cell model, which has a distinct parameter set: sensitivity results show that k_1, k_2, and k_7-k_{10} are most sensitive parameters for this model and the rest are less sensitive with a very low sensitivity gain. The sensitive parameters correspond to DNA glycosylase, polymerase β for dRP removal, ligase 3α/XRCC1 and polymerase δ kinetics respectively. We use this model to study DNA glycosylase depletion, PARPi and ligase inhibition effects on BER kinetics. As for the former, we down regulated DNA glycosylase concentration and obtained lower repair by BER; for the later, PARPi cause accumulation of SSB and ligase enzyme concentration decrease further enhances this effect on inhibition of BER kinetics. It is observed that PARPi effect is further enhanced by the action of ligase regulation. The sensitivity test provide biological relevance of the parameters

Table 4.7: Sensitivity and Identifiability Test Results

description	SW480		Hela	
	SGain	Iden	SGain	Iden
DNA glycosylase k_{cat}	0.92	+	10.95	+
DNA glycosylase K_m	0.30	+	7.02	+
APE1 k_{cat}	0.32	+	0.006	+
APE1 K_m	0.23	+	0.006	+
Polymerase β gap filling k_{cat}	0.19	+	0.006	+
Polymerase β gap filling K_m	0.28	+	0.007	+
Polymerase β dRP remove k_{cat}	821.5	+	15.0	+
Polymerase β dRP remove K_m	662.3	+	17.3	+
ligase3α k_{cat}	0.29	+	4.19	+
ligase3α K_m	0.14	+	4.68	+
Polymerase δ k_{cat}	678.9	+	17.31	+
Polymerase δ K_m	814.1	+	15.0	+
FEN1 k_{cat}	1688	+	0.006	+
FEN1 K_m	1515	+	0.007	+
ligase1 k_{cat}	0.19	+	0.007	+
ligase1 K_m	0.48	+	0.006	+

we estimated in these studies.

4.3.6 Identifiability Test Results

The identifiability results for both SW480 cells and HeLa cells are presented together with sensitivity results in Table 4.7. In the table, + indicates that the parameter is identifiable. If the parameter is not identifiable, it is indicated with a − sign as listed in the table.

There are some parameters which show low sensitivity gain, however, in the identifiability test, all the parameters are tested and are found to be identifiable. In the case of SW480 cells, k_7, k_8, and k_{11}-k_{14} have high sensitivity gains, and the rest of the parameters show low sensitivity gains; in the identifiability test, all the parameters are found to be identifiable. For HeLa cells, k_1, k_2 and k_7-k_{10} have high sensitivity gains, and the rest parameters show low sensitivity gains; in the identifiability test, all the

parameters are found to be identifiable parameters. The identifiability results show that the observed effects in our model are in consistent with the experimental data under various scenarios created for enhancement and inhibition of 5-FU treatment outcome.

4.4 Conclusion on BER and 5-FU Chemotoxicity

We have successfully constructed a mathematical model for BER and conducted parameter estimation for the model. We found that the quantitative model is in a good agreement with the experimental data with sensitive and identifiable parameters. Thus our parameters optimized in the model are considered to be biologically relevant. By decreasing DNA glycosylase concentrations, we generate a set of models that mimic the repair kinetics after various levels of depletion of DNA glycosylase. With decreasing values of DNA glycosylase concentration, BER process slows down leading to accumulation of 5-FU in cancer cells. Therefore, the suppression of DNA glycosylase has a potential to enhance the outcome of treatment with 5-FdU. We successfully simulated the negative impact of APC mutation on the effectiveness of 5-FU treatment by leading to increases in FEN1 and polymerase β concentrations. The simulation is developed for varying doses of 5FU among distinct cell lines with high, medium and low APC expressions. In our model, cells with low APC expression shows most drug resistance to 5-FU. We have also performed simulations using our model of PARPi effects on accumulating BER intermediates and successfully captured the enhanced effect on treatment toxicity by combining ligation enzyme deficiencies and PARPi. 5-FU leads to incorporation of U and FU into DNA therefore causes base damages. BER is the major pathway for the repair of these damages. Many factors can have a positive or negative impact on the repair process. In our case we simulate the enhancement of 5-FU outcome by DNA glycosylase depletion, 5-FU failure

by APC mutation and the effect of combining PARP inhibitor and ligase deficiency on BER kinetics. In future work, this model can be further used to quantitatively optimize these effects as well as other potential factors for better treatment outcome or combination treatment in cancer therapy.

Chapter 5

Conclusions

In this work, DNA damage induced by cancer treatment and the corresponding DDR have been studied. Specifically, novel computational models of NHEJ, HR, and BER are developed to quantitatively analyze the role of DNA repair in the treatment outcome for PCa. A computational model of NHEJ has been successfully parameterized for PCa under IR treatment and a combination treatment of IR and ADT. The suppression of AR signaling activities through ADT which then leads to inhibition of NHEJ through Ku down regulation is successfully captured in the model dynamics. NHEJ models were used to capture the individual differences to ADT toxicity among patient profiles, which indicate patients responsiveness to ADT through Ku depletion. On the other hand, AR activities not only impact NHEJ proteins but also regulate HR proteins including MRN and Rad51. Computational HR model is also built for PCa using the same experimental data as NHEJ for consistency. Suppression of AR activities through ADT also impairs HR, thus contributing further to IR outcome enhancement. Kinetics of MRN, the HR initiator; Rad51, the HR marker; and how BRCA mutation effect HR are validated in this model.

In SSB repair, BER and HR are compensating repair pathways and possible targets for synthetic lethality through PARPi in cancer that have deficient HR due to

BRCA mutations. BER modeling of damage repair after 5-FU treatment is developed. The quantitative analysis shows that DNA glycosylase is a potential target for BER inhibition that will enhance 5-FU treatment outcome. Gene mutation of APC in some patients results in drug resistance to 5-FU due to BER kinetics changes. In addition, PARPi trapping PARP leads to ligation failure and accumulation of SSB thus enhancing the treatment outcome, especially for the defective cancers due to synthetic lethality.

The computational models are developed using ordinary differential equations that model reaction steps in the repair pathways and least squares method is used for parameter estimation. Model reliability is determined by sensitivity and identifiability analysis. The model results are considered biologically relevant when the model parameters are found to be sensitive and identifiable. Different methods were introduced such as data sampling enhancement or using repair intermediates in the error function to improve identifiability. The results did not improve with these methods. As a result, it is suggested to deal with non-identifiable parameters with independent experimental design that measures individual reaction kinetics.

NHEJ efficiencies in different cell cycle phases have been. The consistency between the results in the computational model and the experimental data are reflected in the drop in protein kinetics during the cell cycle phases when NHEJ is less efficient. The integration of the cell cycle with NHEJ and HR shows the cell proliferation under IR treatment and combination treatment of IR and ADT for PCa patients. The overall cancer cell survival rate and cell propagation are computationally studied for PCa after IR and IR+ADT. The models show that IR limits the PCa cell proliferation, and this effect is more significant when combined with ADT.

A framework of major DNA damage repair pathways, especially a framework for DSB repair pathways are developed by taking into account cell cycle efficiencies for PCa under different treatment plans (IR, ADT, and drugs in chemotherapy). It is

displayed quantitatively in this dissertation that IR therapy is enhanced by ADT. In addition to ADT enhancement on IR, PARPi mechanism is integrated in the computation models for BER to analyze the ability of PARPi in improving treatment efficacy. This dissertation systematically summarizes the basic framework of DDR and describes and simulates the determinate mechanisms. For more comprehensive analysis, the individual repair pathway models are combined in a cell cycle dependent manners. The models make computational experiments possible and thee computational analysis allow for detailed study of DDR that might not be feasible through lab experiments. The presented integration of models are the initial steps in quantitatively analyzing possible scenarios to find the optimal personalized treatment strategies for PCa patients using IR, hormone therapy, and chemotherapy. Furthermore, the models developed in this dissertation and the model construction methods can be applied to other cancer types treatments for quantitative analysis.

Chapter 6

Suggested Future Work

In the current model, although the role of cell cycle for repair efficiency is fully considered, the role of checkpoint activities is only macroscopically quantified. In fact, checkpoints' mechanism is a very complex process that triggers cell cycle arrest to allow for DNA repair. It is suggested to add checkpoints signaling mechanism into the current computational model, that will allow a more detailed analysis of the relationship between cell death and DNA damage repair in a quantitative manner for PCa. The major lesions studied in this work were DSBs after IR and SB after 5-FU incorporation into DNA. In the future, other lesion types and the corresponding repair pathways can be added to obtain more comprehensive DDR models. As [111] and [112] mentions, PARPi clinical trials have been designed for PCa patients together with chemotherapy, IR, ADT, targeted agents and immunotherapy. The combination treatment with chemotherapy and PARPi shows some positive results especially for BRCA mutation patients. But the potential mechanisms of PARP-1 (the most abundant member in PARP family) in DDR remains unclear. PARP-1 is reported to be actively involved in BER for promoting BER genes. Therefore, the role of PARPi in treatment enhancement is most likely through increasing DSB by SSBR/BER inhibition. In addition to PARPi inhibiting PARP-mediated recruitment of proteins in

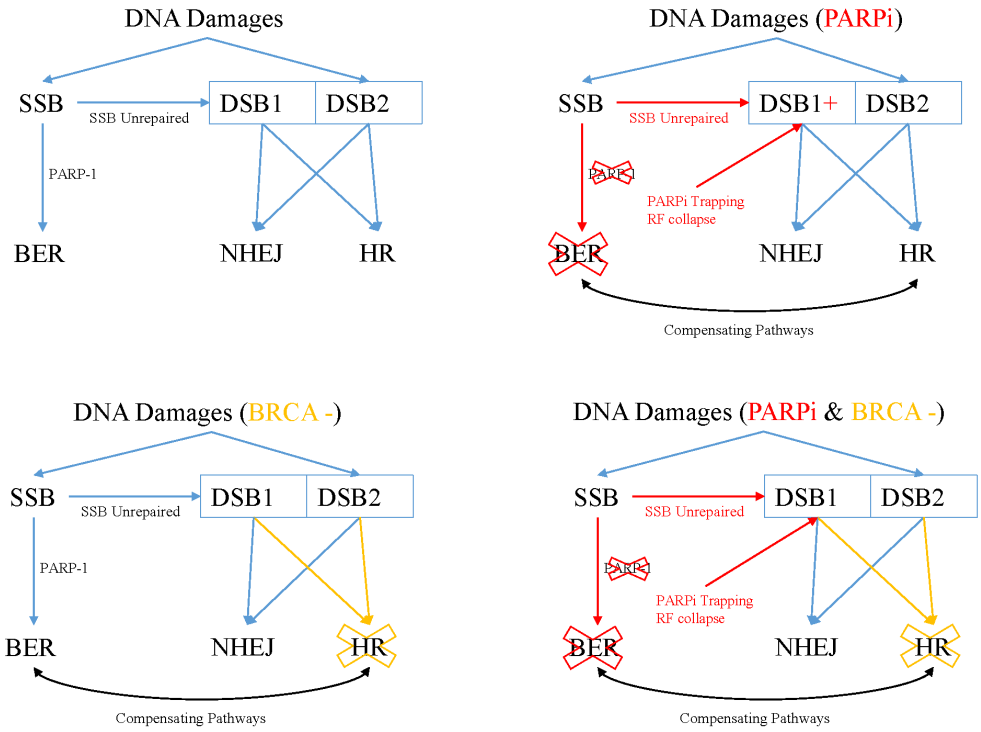

Figure 6.1: Synthetic Lethality of PARPi and BRCA Mutation

BER, PARPi is also reported to trap PARP onto SSB ends and to accumulate DSB due to replication fork collapse. Besides, due to the compensating character of BER and HR as shown in Figure 6.1, the most lethal role of PARPi is on the synthetic lethality with BRCA mutation. PARP activities and PARPi activities with the DDR proteins dynamics will be studied in the future and incorporated into the models.

In addition, more scenarios will be created and compared for PCa patients for an optimized treatment plan. In designing a treatment plan, there are multiple optimization objectives such as IR dose calculations, IR dose timing, surgery and drug decision. This current model enables quantitative study of multiple treatment scenarios and makes predictions about overall treatment outcomes.

Bibliography

[1] Freddie Bray, Jacques Ferlay, Isabelle Soerjomataram, Rebecca L Siegel, Lindsey A Torre, and Ahmedin Jemal. Global cancer statistics 2018: Globocan estimates of incidence and mortality worldwide for 36 cancers in 185 countries. *CA: a cancer journal for clinicians*, 68(6):394–424, 2018.

[2] Mark J OConnor. Targeting the dna damage response in cancer. *Molecular cell*, 60(4):547–560, 2015.

[3] The beginning of the end for cancer chemotherapy? `https://www.genomicseducation.hee.nhs.uk/news/item/174-the-beginning-of-the-end-for-cancer-chemotherapy/`.

[4] External beam radiation therapy for cancer. `https://www.cancer.gov/about-cancer/treatment/types/radiation-therapy/external-beam`.

[5] Dana Branzei and Marco Foiani. Regulation of dna repair throughout the cell cycle. *Nature reviews Molecular cell biology*, 9(4):297, 2008.

[6] Giuseppina Giglia-Mari, Angelika Zotter, and Wim Vermeulen. Dna damage response. *Cold Spring Harbor perspectives in biology*, 3(1):a000745, 2011.

[7] Thomas Helleday, Eva Petermann, Cecilia Lundin, Ben Hodgson, and Ricky A Sharma. Dna repair pathways as targets for cancer therapy. *Nature Reviews Cancer*, 8(3):193, 2008.

[8] Thomas Helleday. The underlying mechanism for the parp and brca synthetic lethality: clearing up the misunderstandings. *Molecular oncology*, 5(4):387–393, 2011.

[9] Zhongsheng You and Julie M Bailis. Dna damage and decisions: Ctip coordinates dna repair and cell cycle checkpoints. *Trends in cell biology*, 20(7):402–409, 2010.

[10] Jonathan F Goodwin, Matthew J Schiewer, Jeffry L Dean, Randy S Schrecengost, Renée de Leeuw, Sumin Han, Teng Ma, Robert B Den, Adam P Dicker, Felix Y Feng, et al. A hormone–dna repair circuit governs the response to genotoxic insult. *Cancer discovery*, 3(11):1254–1271, 2013.

[11] Mohammad Asim, Firas Tarish, Heather I Zecchini, Kumar Sanjiv, Eleni Gelali, Charles E Massie, Ajoeb Baridi, Anne Y Warren, Wanfeng Zhao, Christoph Ogris, et al. Synthetic lethality between androgen receptor signalling and the parp pathway in prostate cancer. *Nature communications*, 8(1):374, 2017.

[12] Yongfeng Li and Francis A Cucinotta. Modeling non-homologous end joining. *Journal of theoretical biology*, 283(1):122–135, 2011.

[13] Yongfeng Li, Pamela Reynolds, Peter O'Neill, and Francis A Cucinotta. Modeling damage complexity-dependent non-homologous end-joining repair pathway. *PloS one*, 9(2):e85816, 2014.

[14] Reza Taleei and Hooshang Nikjoo. The non-homologous end-joining (nhej) pathway for the repair of dna double-strand breaks: I. a mathematical model. *Radiation research*, 179(5):530–539, 2013.

[15] Reza Taleei, Peter M Girard, Krishnaswami Sankaranarayanan, and Hooshang Nikjoo. The non-homologous end-joining (nhej) mathematical model for the

repair of double-strand breaks: Ii. application to damage induced by ultrasoft x rays and low-energy electrons. *Radiation research*, 179(5):540–548, 2013.

[16] Werner Friedland, Peter Jacob, and Pavel Kundrát. Stochastic simulation of dna double-strand break repair by non-homologous end joining based on track structure calculations. *Radiation research*, 173(5):677–688, 2010.

[17] Werner Friedland, Pavel Kundrát, and Peter Jacob. Stochastic modelling of dsb repair after photon and ion irradiation. *International journal of radiation biology*, 88(1-2):129–136, 2012.

[18] Oleg V Belov, Eugene A Krasavin, Marina S Lyashko, Munkhbaatar Batmunkh, and Nasser H Sweilam. A quantitative model of the major pathways for radiation-induced dna double-strand break repair. *Journal of theoretical biology*, 366:115–130, 2015.

[19] Reza Taleei and Hooshang Nikjoo. Biochemical dsb-repair model for mammalian cells in g1 and early s phases of the cell cycle. *Mutation Research/Genetic Toxicology and Environmental Mutagenesis*, 756(1-2):206–212, 2013.

[20] Reza Taleei, Michael Weinfeld, and Hooshang Nikjoo. A kinetic model of single-strand annealing for the repair of dna double-strand breaks. *Radiation protection dosimetry*, 143(2-4):191–195, 2010.

[21] Evren Gurkan-Cavusoglu, Sriya Avadhani, Lili Liu, Timothy J Kinsella, and Kenneth A Loparo. Developing an in silico model of the modulation of base excision repair using methoxyamine for more targeted cancer therapeutics. *IET systems biology*, 7(2):27–37, 2013.

[22] Bahrad A Sokhansanj, Garry R Rodrigue, J Patrick Fitch, and David M Wilson III. A quantitative model of human dna base excision repair. i. mechanistic insights. *Nucleic acids research*, 30(8):1817–1825, 2002.

[23] Philip S Crooke and Fritz F Parl. A mathematical model for dna damage and repair. *Journal of nucleic acids*, 2010, 2010.

[24] VA Semenenko, Robert D Stewart, and Eric J Ackerman. Monte carlo simulation of base and nucleotide excision repair of clustered dna damage sites. i. model properties and predicted trends. *Radiation research*, 164(2):180–193, 2005.

[25] VA Semenenko and RD Stewart. Monte carlo simulation of base and nucleotide excision repair of clustered dna damage sites. ii. comparisons of model predictions to measured data. *Radiation research*, 164(2):194–201, 2005.

[26] Firas LT Al-Ubaidi, Niklas Schultz, Olga Loseva, Lars Egevad, Torvald Granfors, and Thomas Helleday. Castration therapy results in decreased ku70 levels in prostate cancer. *Clinical Cancer Research*, 19(6):1547–1556, 2013.

[27] Keegan E Hines, Thomas R Middendorf, and Richard W Aldrich. Determination of parameter identifiability in nonlinear biophysical models: A bayesian approach. *The Journal of general physiology*, 143(3):401–416, 2014.

[28] Inger Brandsma and Dik C van Gent. Pathway choice in dna double strand break repair: observations of a balancing act. *Genome integrity*, 3(1):9, 2012.

[29] Joseph San Filippo, Patrick Sung, and Hannah Klein. Mechanism of eukaryotic homologous recombination. *Annu. Rev. Biochem.*, 77:229–257, 2008.

[30] Leonardo Bee, Sonia Fabris, Roberto Cherubini, Maddalena Mognato, and Lucia Celotti. The efficiency of homologous recombination and non-homologous end joining systems in repairing double-strand breaks during cell cycle progression. *PloS one*, 8(7):e69061, 2013.

[31] David WP Dolan, Anze Zupanic, Glyn Nelson, Philip Hall, Satomi Miwa, Thomas BL Kirkwood, and Daryl P Shanley. Integrated stochastic model of dna damage repair by non-homologous end joining and p53/p21-mediated early senescence signalling. *PLoS computational biology*, 11(5):e1004246, 2015.

[32] Nasrollah Saleh-Gohari and Thomas Helleday. Conservative homologous recombination preferentially repairs dna double-strand breaks in the s phase of the cell cycle in human cells. *Nucleic acids research*, 32(12):3683–3688, 2004.

[33] Yun Wu, Noriko Kantake, Tomohiko Sugiyama, and Stephen C Kowalczykowski. Rad51 protein controls rad52-mediated dna annealing. *Journal of Biological Chemistry*, 283(21):14883–14892, 2008.

[34] Zhiyong Mao, Michael Bozzella, Andrei Seluanov, and Vera Gorbunova. Comparison of nonhomologous end joining and homologous recombination in human cells. *DNA repair*, 7(10):1765–1771, 2008.

[35] Michael R Lieber, Yunmei Ma, Ulrich Pannicke, and Klaus Schwarz. Mechanism and regulation of human non-homologous dna end-joining. *Nature reviews Molecular cell biology*, 4(9):712, 2003.

[36] Robert B West, Mariana Yaneva, and Michael R Lieber. Productive and non-productive complexes of ku and dna-dependent protein kinase at dna termini. *Molecular and cellular biology*, 18(10):5908–5920, 1998.

[37] Huichen Wang, Zhao-Chong Zeng, Ange R Perrault, Xinbo Cheng, Wei Qin, and George Iliakis. Genetic evidence for the involvement of dna ligase iv in the dna-pk-dependent pathway of non-homologous end joining in mammalian cells. *Nucleic acids research*, 29(8):1653–1660, 2001.

[38] Doug W Chan and Susan P Lees-Miller. The dna-dependent protein kinase is inactivated by autophosphorylation of the catalytic subunit. *Journal of Biological Chemistry*, 271(15):8936–8941, 1996.

[39] Ulf Grawunder, David Zimmer, Peter Kulesza, and Michael R Lieber. Requirement for an interaction of xrcc4 with dna ligase iv for wild-type v (d) j recombination and dna double-strand break repairin vivo. *Journal of Biological Chemistry*, 273(38):24708–24714, 1998.

[40] Mauro Modesti, Joanne E Hesse, and Martin Gellert. Dna binding of xrcc4 protein is associated with v (d) j recombination but not with stimulation of dna ligase iv activity. *The EMBO journal*, 18(7):2008–2018, 1999.

[41] Jonathan Tang, Walter Georgescu, Thomas Deschamps, Steven M Yannone, and Sylvain V Costes. Mathematical modeling for dna repair, carcinogenesis and cancer detection. In *Genomic instability and cancer metastasis*, pages 75–93. Springer, 2015.

[42] Ryosuke Mori, Yusuke Matsuya, Yuji Yoshii, and Hiroyuki Date. Estimation of the radiation-induced dna double-strand breaks number by considering cell cycle and absorbed dose per cell nucleus. *Journal of radiation research*, 59(3):253–260, 2018.

[43] SH MacPhail, JP Banath, TY Yu, EHM Chu, H Lambur, and PL Olive. Expression of phosphorylated histone h2ax in cultured cell lines following exposure to x-rays. *International journal of radiation biology*, 79(5):351–359, 2003.

[44] Soheil Rastgou Talemi, Gabriel Kollarovic, Anastasiya Lapytsko, and Jörg Schaber. Development of a robust dna damage model including persistent telomere-associated damage with application to secondary cancer risk assessment. *Scientific reports*, 5:13540, 2015.

[45] Aida Muslimovic, Pegah Johansson, and Ola Hammarsten. Measurement of h2ax phosphorylation as a marker of ionizing radiation induced cell damage. In *Current topics in ionizing radiation research*. IntechOpen, 2012.

[46] Arishya Sharma, Kamini Singh, and Alexandru Almasan. Histone h2ax phosphorylation: a marker for dna damage. In *DNA repair protocols*, pages 613–626. Springer, 2012.

[47] Jens Karschau, Camila De Almeida, Morgiane C Richard, Samantha Miller, Ian R Booth, Celso Grebogi, and Alessandro PS De Moura. A matter of life or death: modeling dna damage and repair in bacteria. *Biophysical journal*, 100(4):814–821, 2011.

[48] Teresa Neumaier, Joel Swenson, Christopher Pham, Aris Polyzos, Alvin T Lo, PoAn Yang, Jane Dyball, Aroumougame Asaithamby, David J Chen, Mina J Bissell, et al. Evidence for formation of dna repair centers and dose-response nonlinearity in human cells. *Proceedings of the National Academy of Sciences*, 109(2):443–448, 2012.

[49] JF Ward. The yield of dna double-strand breaks produced intracellularly by ionizing radiation: a review. *International journal of radiation biology*, 57(6):1141–1150, 1990.

[50] Zacharenia Nikitaki, Vladimir Nikolov, Ifigeneia V Mavragani, Emil Mladenov, Anastasios Mangelis, Danae A Laskaratou, Georgios I Fragkoulis, Christine E Hellweg, Olga A Martin, Dimitris Emfietzoglou, et al. Measurement of complex dna damage induction and repair in human cellular systems after exposure to ionizing radiations of varying linear energy transfer (let). *Free radical research*, 50(sup1):S64–S78, 2016.

[51] Shaun Moore, Fintan KT Stanley, and Aaron A Goodarzi. The repair of environmentally relevant dna double strand breaks caused by high linear energy transfer irradiation–no simple task. *DNA repair*, 17:64–73, 2014.

[52] Mengdi Qian, Alexandru Almasan, and Evren Gurkan-Cavusoglu. Computational analysis of androgen receptor dependent radiosensitivity in prostate cancer. In *2016 38th Annual International Conference of the IEEE Engineering in Medicine and Biology Society (EMBC)*, pages 1426–1429. IEEE, 2016.

[53] Andreas Raue, Johan Karlsson, Maria Pia Saccomani, Mats Jirstrand, and Jens Timmer. Comparison of approaches for parameter identifiability analysis of biological systems. *Bioinformatics*, 30(10):1440–1448, 2014.

[54] Lijian Shao, Wei Feng, Kyung-Jong Lee, Benjamin PC Chen, and Daohong Zhou. A sensitive and quantitative polymerase chain reaction-based cell free in vitro non-homologous end joining assay for hematopoietic stem cells. *PLoS One*, 7(3):e33499, 2012.

[55] Naoya Uematsu, Eric Weterings, Ken-ichi Yano, Keiko Morotomi-Yano, Burkhard Jakob, Gisela Taucher-Scholz, Pierre-Olivier Mari, Dik C van Gent, Benjamin PC Chen, and David J Chen. Autophosphorylation of dna-pkcs regulates its dynamics at dna double-strand breaks. *The Journal of cell biology*, 177(2):219–229, 2007.

[56] Ken-ichi Yano and David J Chen. Live cell imaging of xlf and xrcc4 reveals a novel view of protein assembly in the non-homologous end-joining pathway. *Cell cycle*, 7(10):1321–1325, 2008.

[57] Tracey A Dobbs, Philip Palmer, Zoitsa Maniou, Martine E Lomax, and Peter ONeill. Interplay of two major repair pathways in the processing of complex double-strand dna breaks. *DNA repair*, 7(8):1372–1383, 2008.

[58] Shay Covo, Jean-Pierre de Villartay, Penny A Jeggo, and Zvi Livneh. Translesion dna synthesis-assisted non-homologous end-joining of complex double-strand breaks prevents loss of dna sequences in mammalian cells. *Nucleic acids research*, 37(20):6737–6745, 2009.

[59] Emad A Ahmed, Peter de Boer, Marielle EP Philippens, Henk B Kal, and Dirk G de Rooij. Parp1–xrcc1 and the repair of dna double strand breaks in mouse round spermatids. *Mutation Research/Fundamental and Molecular Mechanisms of Mutagenesis*, 683(1-2):84–90, 2010.

[60] Zhiyong Mao, Michael Bozzella, Andrei Seluanov, and Vera Gorbunova. Dna repair by nonhomologous end joining and homologous recombination during cell cycle in human cells. *Cell cycle*, 7(18):2902–2906, 2008.

[61] Kwang-Hyun Cho, Sung-Young Shin, Walter Kolch, and Olaf Wolkenhauer. Experimental design in systems biology, based on parameter sensitivity analysis using a monte carlo method: A case study for the tnfα-mediated nf-κ b signal transduction pathway. *Simulation*, 79(12):726–739, 2003.

[62] Evren Gurkan-Cavusoglu, Jane E Schupp, Timothy J Kinsella, and Kenneth A Loparo. Quantitative analysis of the effects of iododeoxyuridine and ionising radiation treatment on the cell cycle dynamics of dna mismatch repair deficient human colorectal cancer cells. *IET systems biology*, 7(4):114–124, 2013.

[63] Alessandro A Sartori, Claudia Lukas, Julia Coates, Martin Mistrik, Shuang Fu, Jiri Bartek, Richard Baer, Jiri Lukas, and Stephen P Jackson. Human ctip promotes dna end resection. *Nature*, 450(7169):509, 2007.

[64] Shunichi Takeda, Kyoko Nakamura, Yoshihito Taniguchi, and Tanya T Paull. Ctp1/ctip and the mrn complex collaborate in the initial steps of homologous recombination. *Molecular cell*, 28(3):351–352, 2007.

[65] Toshiki Tanaka, Xuan Huang, Ellen Jorgensen, Diana Gietl, Frank Traganos, Zbigniew Darzynkiewicz, and Anthony P Albino. Atm activation accompanies histone h2ax phosphorylation in a549 cells upon exposure to tobacco smoke. *BMC Cell Biology*, 8(1):26, 2007.

[66] Zhu Zhu, Woo-Hyun Chung, Eun Yong Shim, Sang Eun Lee, and Grzegorz Ira. Sgs1 helicase and two nucleases dna2 and exo1 resect dna double-strand break ends. *Cell*, 134(6):981–994, 2008.

[67] Amiram Ronen and Barry W Glickman. Human dna repair genes. *Environmental and molecular mutagenesis*, 37(3):241–283, 2001.

[68] Maria Jasin. Homologous repair of dna damage and tumorigenesis: the brca connection. *Oncogene*, 21(58):8981, 2002.

[69] Xuan Wang and James E Haber. Role of saccharomyces single-stranded dna-binding protein rpa in the strand invasion step of double-strand break repair. *PLoS biology*, 2(1):e21, 2004.

[70] Lumir Krejci, Veronika Altmannova, Mario Spirek, and Xiaolan Zhao. Homologous recombination and its regulation. *Nucleic acids research*, 40(13):5795–5818, 2012.

[71] Gerard Mazón, Eleni P Mimitou, and Lorraine S Symington. Snapshot: Homologous recombination in dna double-strand break repair. *Cell*, 142(4):648–e1, 2010.

[72] Dmitry V Bugreev, Roberto J Pezza, Olga M Mazina, Oleg N Voloshin, R Daniel Camerini-Otero, and Alexander V Mazin. The resistance of dmc1 d-loops to dissociation may account for the dmc1 requirement in meiosis. *Nature structural & molecular biology*, 18(1):56, 2011.

[73] The homologous recombination pathway. https://pezza.omrf.org/research-interests/the-homologous-recombination-pathway/.

[74] Kerry L Burnstein. Regulation of androgen receptor levels: implications for prostate cancer progression and therapy. *Journal of cellular biochemistry*, 95(4):657–669, 2005.

[75] David T Miyamoto, Richard J Lee, Shannon L Stott, David T Ting, Ben S Wittner, Matthew Ulman, Malgorzata E Smas, Jenna B Lord, Brian W Brannigan, Julie Trautwein, et al. Androgen receptor signaling in circulating tumor cells as a marker of hormonally responsive prostate cancer. *Cancer discovery*, 2(11):995–1003, 2012.

[76] Helen E Bryant, Niklas Schultz, Huw D Thomas, Kayan M Parker, Dan Flower, Elena Lopez, Suzanne Kyle, Mark Meuth, Nicola J Curtin, and Thomas Helleday. Specific killing of brca2-deficient tumours with inhibitors of poly (adp-ribose) polymerase. *Nature*, 434(7035):913, 2005.

[77] Anshul Bhalla and Muhammad Wasif Saif. Parp-inhibitors in brca-associated pancreatic cancer. *JOP. Journal of the Pancreas*, 15(4):340–343, 2014.

[78] Heather H Cheng, Colin C Pritchard, Thomas Boyd, Peter S Nelson, and Bruce Montgomery. Biallelic inactivation of brca2 in platinum-sensitive metastatic castration-resistant prostate cancer. *European urology*, 69(6):992–995, 2016.

[79] A Raue, C Kreutz, T Maiwald, U Klingmüller, and J Timmer. Addressing parameter identifiability by model-based experimentation. *IET systems biology*, 5(2):120–130, 2011.

[80] Payel Chatterjee, Gaurav S Choudhary, Turkeyah Alswillah, Xiahui Xiong, Warren D Heston, Cristina Magi-Galluzzi, Junran Zhang, Eric A Klein, and

Alexandru Almasan. The tmprss2–erg gene fusion blocks xrcc4-mediated non-homologous end-joining repair and radiosensitizes prostate cancer cells to parp inhibition. *Molecular cancer therapeutics*, 14(8):1896–1906, 2015.

[81] Lei Li, Michael Story, and Randy J Legerski. Cellular responses to ionizing radiation damage. *International Journal of Radiation Oncology* Biology* Physics*, 49(4):1157–1162, 2001.

[82] Michael C Weis, Jayant Avva, James W Jacobberger, and Sree N Sreenath. A data-driven, mathematical model of mammalian cell cycle regulation. *PLoS One*, 9(5):e97130, 2014.

[83] Jill C Sible and John J Tyson. Mathematical modeling as a tool for investigating cell cycle control networks. *Methods*, 41(2):238–247, 2007.

[84] James E Ferrell Jr, Tony Yu-Chen Tsai, and Qiong Yang. Modeling the cell cycle: why do certain circuits oscillate? *Cell*, 144(6):874–885, 2011.

[85] Jiri Bartek, Martin Mistrik, and Jirina Bartkova. Androgen receptor signaling fuels dna repair and radioresistance in prostate cancer. *Cancer discovery*, 3(11):1222–1224, 2013.

[86] Markus Löbrich, Atsushi Shibata, Andrea Beucher, Anna Fisher, Michael Ensminger, Aaron A Goodarzi, Olivia Barton, and Penny A Jeggo. γh2ax foci analysis for monitoring dna double-strand break repair: strengths, limitations and optimization. *Cell cycle*, 9(4):662–669, 2010.

[87] Cooper GM. *The Cell: A Molecular Approach.* Sunderland (MA): Sinauer Associates, 2000.

[88] Daniel B Longley, D Paul Harkin, and Patrick G Johnston. 5-fluorouracil: mechanisms of action and clinical strategies. *Nature reviews cancer*, 3(5):330, 2003.

[89] Breeana C Grogan, Jared B Parker, Amy F Guminski, and James T Stivers. Effect of the thymidylate synthase inhibitors on dutp and ttp pool levels and the activities of dna repair glycosylases on uracil and 5-fluorouracil in dna. *Biochemistry*, 50(5):618–627, 2011.

[90] Michael D Wyatt and DM 3rd Wilson. Participation of dna repair in the response to 5-fluorouracil. *Cellular and molecular life sciences*, 66(5):788–799, 2009.

[91] Hans E Krokan and Magnar Bjørås. Base excision repair. *Cold Spring Harbor perspectives in biology*, 5(4):a012583, 2013.

[92] Paola Fortini, Eleonora Parlanti, Olga M Sidorkina, Jacques Laval, and Eugenia Dogliotti. The type of dna glycosylase determines the base excision repair pathway in mammalian cells. *Journal of Biological Chemistry*, 274(21):15230–15236, 1999.

[93] James T Stivers. Site-specific dna damage recognition by enzyme-induced base flipping. In *Progress in nucleic acid research and molecular biology*, pages 37–65. 2004.

[94] Natalia A Lebedeva, Nadejda I Rechkunova, and Olga I Lavrik. Ap-site cleavage activity of tyrosyl-dna phosphodiesterase 1. *FEBS letters*, 585(4):683–686, 2011.

[95] Shweta Thakur, Bibekananda Sarkar, Ravi P Cholia, Nandini Gautam, Monisha Dhiman, and Anil K Mantha. Ape1/ref-1 as an emerging therapeutic target for various human diseases: phytochemical modulation of its functions. *Experimental & molecular medicine*, 46(7):e106, 2014.

[96] Grigory L Dianov, Rajendra Prasad, Samuel H Wilson, and Vilhelm A Bohr. Role of dna polymerase β in the excision step of long patch mammalian base excision repair. *Journal of Biological Chemistry*, 274(20):13741–13743, 1999.

[97] Julie K Horton, Mary Watson, Donna F Stefanick, Daniel T Shaughnessy, Jack A Taylor, and Samuel H Wilson. Xrcc1 and dna polymerase β in cellular protection against cytotoxic dna single-strand breaks. *Cell research*, 18(1):48, 2008.

[98] Luc Leyns and Laetitia Gonzalez. Genomic integrity of mouse embryonic stem cells. In *Embryogenesis*. IntechOpen, 2012.

[99] AB Robertson, A Klungland, T Rognes, and I Leiros. Dna repair in mammalian cells. *Cellular and molecular life sciences*, 66(6):981–993, 2009.

[100] Ulrike Sattler, Philippe Frit, Bernard Salles, and Patrick Calsou. Long-patch dna repair synthesis during base excision repair in mammalian cells. *EMBO reports*, 4(4):363–367, 2003.

[101] Paola Fortini, Barbara Pascucci, Eleonora Parlanti, Robert W Sobol, Samuel H Wilson, and Eugenia Dogliotti. Different dna polymerases are involved in the short-and long-patch base excision repair in mammalian cells. *Biochemistry*, 37(11):3575–3580, 1998.

[102] Henrik Sahlin Pettersen, Torkild Visnes, Cathrine Broberg Vågbø, Eva K Svaasand, Berit Doseth, Geir Slupphaug, Bodil Kavli, and Hans E Krokan. Ung-initiated base excision repair is the major repair route for 5-fluorouracil in dna, but 5-fluorouracil cytotoxicity depends mainly on rna incorporation. *Nucleic acids research*, 39(19):8430–8444, 2011.

[103] Pratik Nagaria, David Svilar, Ashley R Brown, Xiao-hong Wang, Robert W Sobol, and Michael D Wyatt. Smug1 but not ung dna glycosylase contributes to

the cellular response to recovery from 5-fluorouracil induced replication stress. *Mutation Research/Fundamental and Molecular Mechanisms of Mutagenesis*, 743:26–32, 2013.

[104] Yan Yan, Xiangzi Han, Yulan Qing, Allison G Condie, Shashank Gorityala, Shuming Yang, Yan Xu, Youwei Zhang, and Stanton L Gerson. Inhibition of uracil dna glycosylase sensitizes cancer cells to 5-fluorodeoxyuridine through replication fork collapse-induced dna damage. *Oncotarget*, 7(37):59299, 2016.

[105] Dipon Das, Ranjan Preet, Purusottam Mohapatra, Shakti Ranjan Satapathy, Sumit Siddharth, Tigist Tamir, Vaibhav Jain, Prasad V Bharatam, Michael D Wyatt, and Chanakya Nath Kundu. 5-fluorouracil mediated anti-cancer activity in colon cancer cells is through the induction of adenomatous polyposis coli: Implication of the long-patch base excision repair pathway. *DNA repair*, 24:15–25, 2014.

[106] Maria Vittoria Verga Falzacappa, Chiara Ronchini, Mario Faretta, Ilaria Iacobucci, Andrea Ghelli Luserna Di Rorà, Giovanni Martinelli, Lüder Hinrich Meyer, Klaus-Michael Debatin, Stefania Orecchioni, Francesco Bertolini, et al. The combination of the parp inhibitor rucaparib and 5fu is an effective strategy for treating acute leukemias. *Molecular cancer therapeutics*, 14(4):889–898, 2015.

[107] Peter C Fong, David S Boss, Timothy A Yap, Andrew Tutt, Peijun Wu, Marja Mergui-Roelvink, Peter Mortimer, Helen Swaisland, Alan Lau, Mark J O'connor, et al. Inhibition of poly (adp-ribose) polymerase in tumors from brca mutation carriers. *New England Journal of Medicine*, 361(2):123–134, 2009.

[108] Françoise Dantzer, Guadelupe de la Rubia, Josiane Ménissier-de Murcia, Zdenek Hostomsky, Gilbert de Murcia, and Valérie Schreiber. Base excision

repair is impaired in mammalian cells lacking poly (adp-ribose) polymerase-1. *Biochemistry*, 39(25):7559–7569, 2000.

[109] Cecilia E Strom, Fredrik Johansson, Mathias Uhlen, CA Szigyarto, Klaus Erixon, and Thomas Helleday. Poly (adp-ribose) polymerase (parp) is not involved in base excision repair but parp inhibition traps a single-strand intermediate. *Nucleic Acids Res*, 39(8):3166–3175, 2011.

[110] Jung-Suk Sung and Bruce Demple. Roles of base excision repair subpathways in correcting oxidized abasic sites in dna. *The FEBS journal*, 273(8):1620–1629, 2006.

[111] Ciara C O'Sullivan, Dominic H Moon, Elise Kohn, and Jung-Min Lee. Beyond breast and ovarian cancers: Parp inhibitors for brca mutation-associated and brca-like solid tumors. *Frontiers in oncology*, 4:42, 2014.

[112] Praveen Ramakrishnan Geethakumari, Matthew J Schiewer, Karen E Knudsen, and Wm Kevin Kelly. Parp inhibitors in prostate cancer. *Current Treatment Options in Oncology*, 18(6):37, 2017.